ESSIAL

Deliverable D 3.3
Magneto-mechanical dynamic modeling

WP3: Physical studies
Date of Delivery: 30/04/2021 (3rd update)
Lead Beneficiary: UPJV - Amiens
Type: Report
Dissemination Level: Public
Version: 4.3

ESSIAL has received funding from the European Union's Horizon 2020 research and innovation program under grant agreement No 766437.

Document identifier: ESSIAL-WP3 – D3.3

Deliverable leader	ESIEE - Amiens
Deliverable contributors	UPJV, ESIEE Amiens
Related work package	WP3
Author(s)	SALLOUM Elias PANIER Stéphane MALOBERTI Olivier
Due date of deliverable	30/04/2021 (Update 3)
Actual submission date	30/04/2021 (Update 3)
Approved by	PANIER Stéphane MALOBERTI Olivier
Dissemination level	Public
Call	H2020-FoF-06-2017
Project number	766437
Instrument	Research & Innovation Actions
Start date of project	01/11/2017
Duration	54 months

Revision history log

Version number	Date of release	Author	Summary of changes
4.1	31/01/2021	SALLOUM Elias	New parts: 2.2: Magnetic static behavior 3.4, 3.5: Magneto-Mechanical static 3.6, 3.7: Magneto-Elasticity study 4.5: Laser Effect on the Magnetization and the Magnetostriction
4.2	27/04/2021	MALOBERTI Olivier	Approval
4.3	28/04/2021	GUILLOTEAU Lucie	Editing
3.1	14/06/2019	SALLOUM Elias	Redaction
3.2	25/06/2019	MALOBERTI Olivier	Corrections
3.3	08/07/2019	SALLOUM Elias	Corrections
3.4	18/07/2019	BERSANS Paul	Editing
3.5	31/07/2019	SALLOUM Elias	Final Version, submission on 31/07/2019 (2nd update)
2.1	09/11/2018	SALLOUM Elias	Redaction
2.2	23/11/2018	MALOBERTI Olivier	Correction
2.3	28/11/2018	SALLOUM Elias	Correction
2.4	29/11/2018	BERSANS Paul	Editing
2.5	30/11/2018	SALLOUM Elias	Final Version, submission on 30/11/2018 (1st update found after page 24 of the 2nd update)
1.1	28/02/2017	SALLOUM Elias	Chapter 1: State of art
1.2	06/04/2018	MALOBERTI Olivier	State of art correction and adding
1.3	20/04/2018	SALLOUM Elias	Chapter 2-3: Theory and first simulations
1.4	25/04/2018	PANIER Stéphane	Corrections
1.5	27/04/2018	SALLOUM Elias	Final Version, submission on 30/04/2018 (Initial deliverable found after page 20 of the 1st update)

Table of contents (3rd update)

List of Figures

List of Tables

Summary

The report aims at developing the physical study and the modeling techniques that define the magneto-mechanical properties. First, a state of the art is presented in Chapter 1 for the different magnetic and magneto-mechanical modeling techniques adopted by researchers.
Then, the magnetic modeling performed in Chapter 2 is then presented, starting from the microscopic study at the domains scales, where the magnetic propeties are defined and then homogenized at the mesoscopic scale. The macroscopic scale is then presented, where the magnetic model is conceived in a way to be adapted to the experimental setup, using the magnetic diffusion model.
Similarly, magneto-mechanical modeling is developed in Chapter 3 by analyzing the microscopic behavior, then the mesoscopic homogenized properties and finally the macroscopic mechanical model adapted with the measurements and based on a dynamic vibrational model. The magneto-mechanical modeling also includes the magnetic modeling performed in the previous chapter, specially the magnetic diffusion phenomenon. The magneto-mechanical modeling constitutes a basis for the vibration and noise analysis.
Finally, the different models, from the microscopic to the macroscopic scale are investigated in order to study of the laser treatment on the magnetic and the magneto-mechanical behavior, and eventuelly the losses and the vibrations. For this purpose, a presentatioon of the laser treatment technology and its theoretical effect on the behavior is presented in Chapter 4.

Chapter 1

State of the Art

1.1 Introduction

The main challenge of the project is to improve the magnetic and the magneto-mechanical performances of electrical steels inside electrical and magnetic components. This includes the enhancement of the permeability, the decrease of iron losses and reduction of vibration and noise. Therefore, understanding the static and the dynamic magnetic and magneto-mechanical behavior at different scales is a must. A litterature review of the modeling techniques of the magnetization and the induced magneto-mechanical behavior at different scales is presented in this chapter. Based on previous researches, specific models are selected and developed in order to describe the coupled magneto-mechanical behavior in the magnetic structure, and then to understand the role played by laser treatments on this behavior.
The microscopic phenomena related to the domain structure from energetic point of view are first presented. Then the scale transition is described between the microscopic to the mesoscopic scale. The phenomenological models that reveal the global apparent behavior, first from a purely magnetic point of view, then from the magneto-mechanical point of view are finally discussed. The presented models are described in static and dynamic approaches, depending on the application.

1.2 The Microscopic Behavior

In this section, the microscopic origin of the magnetization and the magnetic induced deformation is explained based on the energy minimization for the magnetic structure.

1.2.1 Static Energy Contributions

Steels are constituted of grains divided into magnetic domains separated by walls. Each domain is already magnetized and oriented by a cosine vector α. The domains are distributed and oriented in a way to minimized the total internal energy of the material. The arrangement of the localized magnetic moments is determined by various kinds of energies (expressed in $J.m^{-3}$): the exchange energy, the magnetostatic energy, the magnetocrystalline anisotropy and the magnetoelastic energy [18].

- **Magnetocrystalline anisotropy energy** E_K: Each domain initially magnetized to saturation is oriented in a specific direction called easy direction. The magnetocrystalline anisotropy energy tends to direct the magnetization in the easy direction's domains.

$$E_K = K_1(\alpha_1^2\alpha_2^2 + \alpha_2^2\alpha_3^2 + \alpha_3^2\alpha_1^2) + K_2(\alpha_1^2\alpha_2^2\alpha_3^2) \tag{1.1}$$

Where K_1 and K_2 are the anisotropic constants (in J.m^{-3}) and $\alpha = [\alpha_1, \alpha_2, \alpha_3]$ is the cosine vector of the domain orientation.

- **Exchange energy** E_{ex}: It results from the interaction between the electrons of the nearby atoms. It decreases with higher distance between the atoms.

$$E_{ex} = A_{ex}(grad\alpha)^2 \tag{1.2}$$

where A_{ex} is the exchange constant (in J.m^{-3}).

- **Magnetostatic energy** W_{mag}: It is due to the application of a magnetic field (Zeeman energy) and to the demagnetizing field $\mathbf{H}_d$. The Zeeman energy tends to align the magnetization $\mathbf{M}$ in the magnetic field orientation $\mathbf{H}_0$. It is also minimal when they are already parallel. As for the demagnetizing energy, it is due to the interaction between the distant atoms in order to cancel the global magnetization.

$$W_{mag} = \mu_0 \mathbf{M}^T \mathbf{H}_0 + \frac{1}{2}\mu_0 \mathbf{M}^T \mathbf{H}_d \tag{1.3}$$

- **Elastic Energy** E_{el}: It is related to the mechanical elasticity of the material. $\mathbf{C}$ is the stiffness matrix, characteristic of the material. This energy generates a strain ε.

$$E_{el} = \frac{1}{2}\varepsilon^T \mathbf{C} \varepsilon \tag{1.4}$$

- **Magnetoelastic energy** E_{me}: It results from the interaction between the magnetization direction and the deformation direction of the crystal. It is a coupling energy between the magnetization process and the mechanical deformation of the magnetic domain. This energy is the source of magnetostriction generation.

$$E_{me} = \mathbf{b}\varepsilon \tag{1.5}$$

ε is the strain vector and $\mathbf{b}$ is a magneto-elastic coupling vector (in J.m^{-3}).

- **Stress-Induced Energy** W_{mech}: It is due to the application of a mechanical stress vector σ in a specific direction.

$$W_{mech} = \sigma^T \varepsilon \tag{1.6}$$

1.2.2 Magnetization Process

Based on the energy approach described in the previous section based on Brissoneau [18] and Alves [1], the material tends to minimize the global energy by creating a specific domain structure that considers the different energy contributions. In the initial state before magnetization, each domain is already magnetized at a saturation magnetization M_s but each in a different orientation. The total magnetization vector sum is equal to zero. When a magnetic field is applied, the global magnetization appears using two mechanisms: the walls displacement and the rotation of the magnetic moments. These mechanisms occur in a way to minimize the internal energy as explained before by taking into consideration the exchange between the atoms, the easy direction magnetization due to the anisotropy energy, the direction of the applied magnetic field, the demagnetization process due to the magnetostatic energy, the elastic behavior presented by the magnetoelastic energy and the application of a mechanical stress. The material magnetizes gradually with higher magnetic fields till reaching the saturation.
The effect of the domain structure on the internal energy is explained using the different

examples in Fig. 1.1. Configuration (a) has minimal exchange and anisotropy energy, but an important magnetostatic energy due to the importance of the ratio between the surface of each magnetic pole and the distance between the two poles. As for configuration (b), the magnetostatic energy decreases due to the decrease of surface of each magnetic pole. The walls energy (sum of the anisotropy and exchange energy inside walls) rises due to the increase of the walls' number. In this case, closure domains of type spike can be obtained. Finally, in the configuration (c), closure domains are introduced (90° orientation), magneto-elastic energy is introduced and the material is deformed in the magnetization direction.

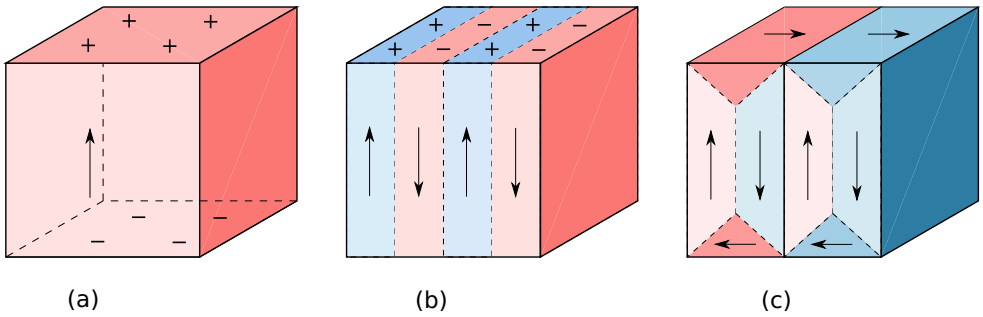

Fig. 1.1 (a) Uniform magnetization; (b) Magnetization of antiparallel domains; (c) Magnetization of antiparallel domains with closure domains. [1]

Different other configurations can be obtained such as the single and the double spike domains and the echelon structure. In this microcsopic study, closure domains with 90° orientation are considered for analysis. They are representative of the magnetization and at the same time the magnetostriction phenomenon, conserving a simple structure. The other structures give different results but with the same spirit of the considered structure. An optimal magnetic structure is obtained due to the energy minimization, which modifies the magnetic behavior as schematically explained in Fig. 1.2. In fact, the application of a mechanical stress modifies the domains structure in way to increase or decrease the fraction volume of domains oriented in the same orientation of the applied stress. As for the field application, the domain structure is also modified in a way to increase the fraction of domains oriented in the same direction of the magnetic field.

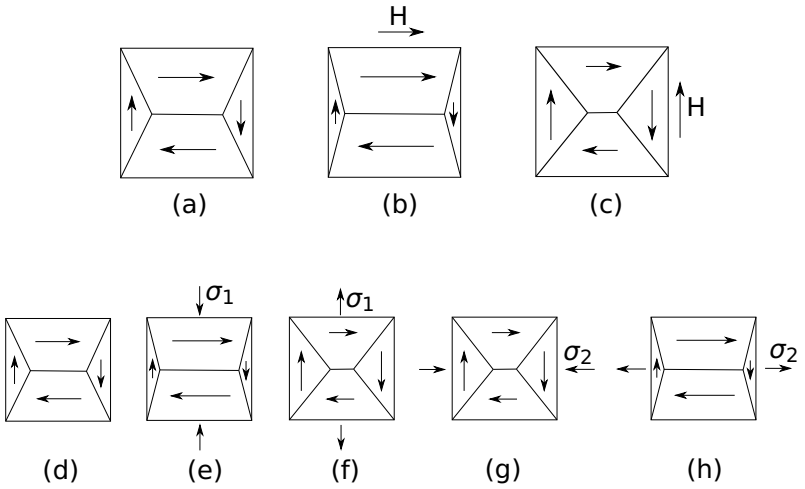

Fig. 1.2 Magnetic Domains for a positive magnetostriction (a,d) Free case; (b) Longitudinal magnetic field; (c) Transverse magnetic field; (e) Compressive stress (direction 1); (f) Tensile stress (direction 1); (g) Compressive stress (direction 2); (h) Tensile stress (direction 2). [2]

The whole magnetization and deformation processes are illustrated in **Fig. 1.3** for a specific configuration. The application of magnetic field modifies initially the domains structure without changing the domains orientation (easy axis magnetization) by only changing the domains sizes and the volume fraction of each domain based on their initial orientation. In fact, the size of domains that have an orientation close to that of the magnetic field increases and the other ones decrease. This phenomenon is called **walls displacement**, providing a linear behavior: the magnetization is proportional to the applied magnetic field.
For a higher magnetic field, the size decreasing domains begin to disappear gradually and the walls are merged. In this case, the walls displacement phenomenon ends and the domains rotation is triggered, trying to reach the magnetic field's direction. This behavior called the **domains rotation** is non-linear and the magnetization reaches the saturation: the application of magnetic field cannot magnetize the material anymore.

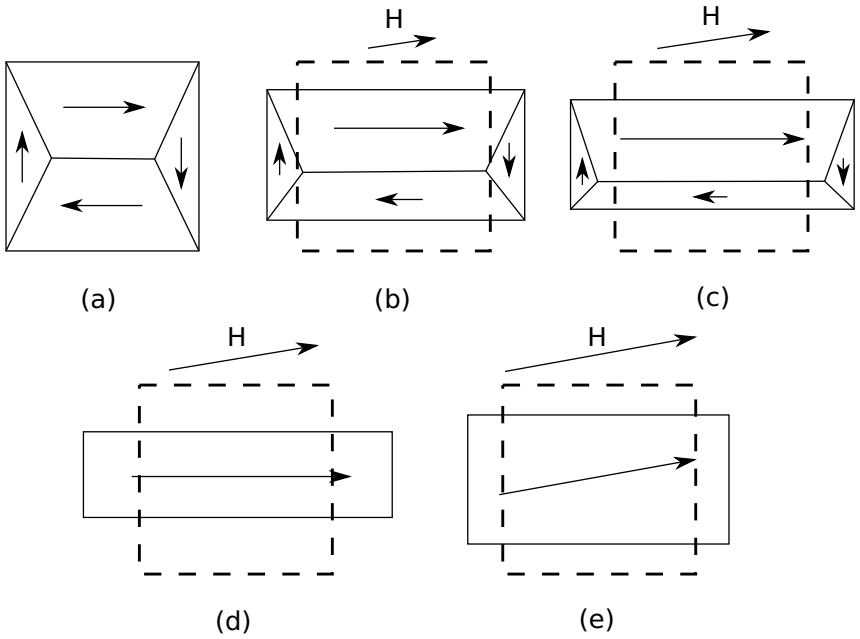

Fig. 1.3 Magnetization and positive magnetostriction processes (a) Free case; (b) Low walls displacement; (c) High walls displacement; (e) Maximal walls displacement; (f) Domains rotation. [3] (—— New deformation, - - - - Initial deformation.)

1.2.3 Magnetic Induced Strain Process

As mentioned before, the magnetization process induces a deformation related to the magnetoelastic energy and the elastic property of the material. The phenomenon is called **magnetostriction**, providing a deformation in the presence of a magnetic field [19]. The application of a low magnetic field induces a magnetic strain with a volume conservation. The strain can be either positive or negative depending on the presence of a mechanical stress that modifies not only the magnetization process, but also the mechanical behavior.

1.2.4 Energy Minimization

The total microscopic energy E_T is calculated by summing up each energy contribution and minimizing with respect to the strain ε.

$$E_T(\alpha,\varepsilon) = E_K(\alpha) + E_{ex}(\alpha) + E_{me}(\alpha,\varepsilon) + E_{el}(\varepsilon) - W_{mag}(\alpha) - W_{mech}(\varepsilon) \tag{1.7}$$

$$\frac{\partial E_T(\alpha,\varepsilon)}{\partial \varepsilon} = 0 \tag{1.8}$$

The total energy becomes:

$$\begin{aligned} E_T(\alpha) = A_{ex}(grad\alpha)^2 + \left[K_1\left(\alpha_1^2\alpha_2^2 + \alpha_2^2\alpha_3^2 + \alpha_3^2\alpha_1^2\right) + K_2\left(\alpha_1^2\alpha_2^2\alpha_3^2\right)\right] \\ + \frac{1}{2}\varepsilon^T\mathbf{C}\varepsilon + \{-\frac{3}{2}\lambda_{100}[\sigma_{11}\left(\alpha_1^2 - \frac{1}{3}\right) + \sigma_{22}\left(\alpha_2^2 - \frac{1}{3}\right) + \sigma_{33}\left(\alpha_3^2 - \frac{1}{3}\right)] \\ -3\lambda_{111}\left(\sigma_{12}\alpha_1\alpha_2 + \sigma_{13}\alpha_1\alpha_3 + \sigma_{32}\alpha_3\alpha_2\right)\} - [\mu_0 M_s(\alpha_1 H_{01} + \alpha_2 H_{02} + \alpha_3 H_{03})] \end{aligned} \tag{1.9}$$

with $\alpha = \begin{bmatrix}\alpha_1 & \alpha_2 & \alpha_3\end{bmatrix}^T$, H_{01}, H_{02} and H_{03} are the components of the locally applied magnetic field vector $\mathbf{H}_0 = \begin{bmatrix}H_{01} & H_{02} & H_{03}\end{bmatrix}^T$, σ_{11}, σ_{22}, σ_{33}, σ_{12}, σ_{13} and σ_{32} are the components of the stress tensor $[\sigma]$ and λ_{100} and λ_{111} are the magnetostriction coefficients. The energy optimum gives the following magnetization vector and strain tensor:

$$\mathbf{M}(\alpha) = M_s\begin{bmatrix}\alpha_1 & \alpha_2 & \alpha_3\end{bmatrix}^T \tag{1.10}$$

$$[\varepsilon]^{\mu} = \frac{3}{2}\begin{bmatrix}\lambda_{100}\left(\alpha_1^2 - \frac{1}{3}\right) & \lambda_{111}\alpha_1\alpha_2 & \lambda_{111}\alpha_1\alpha_3 \\ \lambda_{111}\alpha_2\alpha_1 & \lambda_{100}\left(\alpha_2^2 - \frac{1}{3}\right) & \lambda_{111}\alpha_2\alpha_3 \\ \lambda_{111}\alpha_3\alpha_1 & \lambda_{111}\alpha_3\alpha_2 & \lambda_{100}\left(\alpha_3^2 - \frac{1}{3}\right)\end{bmatrix} \tag{1.11}$$

The different characteristics for the electrical steel FeSi 3% including the saturation magnetization M_s, the anisotropy constants K_1 and K_2, the magnetostriction constants λ_{100}, λ_{111} and the Young Moduli in the directions [100], [110] and [111], are given in **Table 1.1**.

Table 1.1 Electrical Steel *FeSi* single crystal characteristics [3].

Constant	Value
M_s	(1.59, 1.61) × 10^6 A/m
(K_1, K_2)	(35;0)(38;0) kJ/m^3
$(\lambda_{100}, \lambda_{111})$	(27; -5)(23; -4.5) × 10^{-6}
$(E_{100}, E_{110}, E_{111})$	(238, 142, 232) GPa

The magnetostriction depends on the domain's orientation in a crystal. It is only uniform inside the domain. When working with polycrystals, the magnetostriction varies between one grain to another. In this case, the magnetostriction modeling becomes more complex and requires the knowledge of material's texture. It can also be modeled using mesoscopic and macroscopic models at higher scales.

1.3 Multiscale Approach

The multiscale model is studied by Daniel et al. [3] considering the interaction between the grains of polycrystals. Successive calculations and scale changes between the macroscopic and the mesoscopic scale are performed as shown in **Fig. 1.4**. The macroscopic applied stress and field are the system's magnetic and mechanical excitations. The macroscopic magnetization and magnetostriction are the system's output. The transition is performed by using the method of localisation inside a homogeneous medium (from macro to micro), a physical study in the microscopic scale and then a homogenization (from micro to macro) [21]. The localisation and the homogenization are performed in a way to take into account the materials microstructure and domains distribution.
Multiscale transition is a good technique that explains and interprets the macroscopic behavior based on microstructural observations of the material's texture. However, it requires very high computational power and time consumption. In this study, this technique is presented for a simple case as an illustrative method, in order to understand the effect of the domain structure on the magnetization and the magnetostriction. Therefore, several domain structures for which we compare the magneto-mechanical response under the application of a magnetic field are considered.

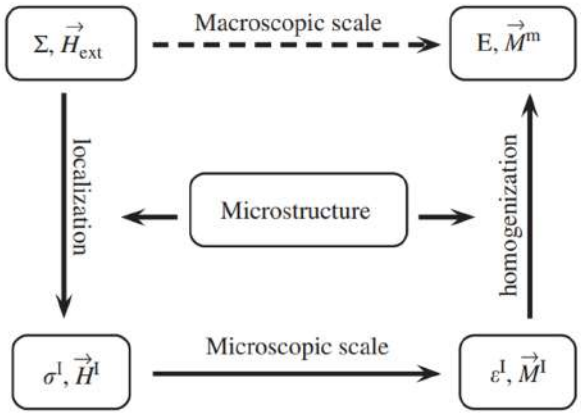

Fig. 1.4 Multiscale approach [3].

1.4 Static Magneto-Mechanical Models

1.4.1 Description

In this section, we present the static magnetic behavior that can be observed at the macroscopic scale. Once the material is magnetized, and especially after the application of a high magnetic field, the magnetization cancelation requires the application of an opposite magnetic field called the coercive field H_c. Otherwise, if the initial magnetic field is removed without adding the coercive field, a residual magnetization appears due to the presence of imperfections and impurities (pinning). We note that H_c is low for soft magnetic materials, hence the designation **soft magnetic material**. The irreversible static mechanism described in this part is the origin of the so called static losses and the static hysteresis P_{stat}. **Fig. 1.5** plots the loop that presents the magnetic flux density B in Tesla (T) as function of the applied magnetic field H. $B = \mu_0(H + M)$ where M is the magnetization and $\mu_0 = 4\pi.10^{-7}$ H.m^{-1} the vacuum permeability. It shows the initial magnetization curve and the static hysteresis loop where static energy losses per cycle corresponding to the loop's area are observed. The plot also shows the coercive field $H_c = H(B = 0)$ and the remanent induction $B_r = B(H = 0)$. As shown, the anhysteretic curve is not linear, this is due to the domains rotation at high magnetic field where the curve's slop decreases, reaching saturation at very high field. In this section, we present the static magnetization behavior with irreversibilies using the Jiles-Atherton model with static parameters that describe the magnetization process.

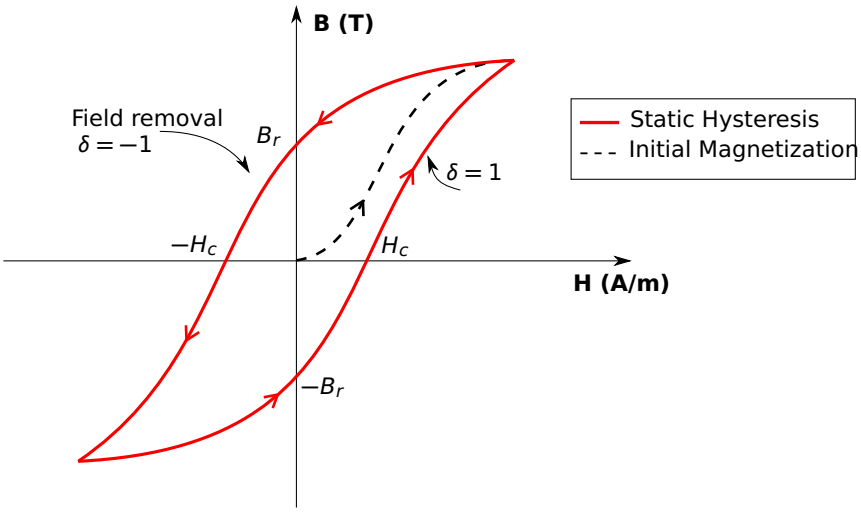

Fig. 1.5 Hysteresis loop of the static magnetization. [4]

1.4.2 The Jiles-Atherton Model

The static behavior's identification at a specific induction magnitude is presented based on the Jiles-Atherton model [22]. Considering a static magnetic field H and magnetization M, we define the effective magnetizing field $H_{\text{eff}} = H + \alpha M$, where α denotes the inter-domain coupling. The anhysteretic magnetization M_{an} is expressed by the Langevin function that contains a linear behavior at low field and a magnetization saturation at high field:

$$M_{\text{an}} = M_s \left[\coth\left(\frac{H_{\text{eff}}}{a}\right) - \frac{a}{H_{\text{eff}}} \right] \tag{1.12}$$

M_s is the saturation magnetization and a is a thermodynamic factor that represents the ratio between the thermal energy and the Zeeman energy. It is expressed by $a = k_B T/\mu_0 m_1$ where k_B is the Boltzmann constant, T is the temperature and m_1 is the mean effective domain size [23]. In the Jiles-Atherton's model, the irreversibility process is modeled by the irreversibility magnetization M_{irr}:

$$\frac{dM_{\text{irr}}}{dH_{\text{eff}}} = \frac{M_{\text{an}} - M_{\text{irr}}}{k\delta} \tag{1.13}$$

k is a factor of proportionality between the wasted energy when a domain wall crosses a pinning site and the variation of the sample's magnetization. δ parameter is:

$$\delta = \begin{cases} 1, & \text{if } \frac{dH}{dt} > 0 \\ -1, & \text{if } \frac{dH}{dt} < 0 \end{cases} \tag{1.14}$$

The contribution of the reversibility and irreversility phenomena is represented by the magnetization reversibility coefficient c, and described as follows:

$$M = (1-c)M_{\text{irr}} + cM_{\text{an}} \tag{1.15}$$

The magnetization, the induction and the magnetic field are correlated with the permeability of vacuum μ_0 by:

$$B = \mu_0(H + M) \tag{1.16}$$

1.4.3 Magnetostriction Model with Local Maximum

Szewczyk [5] developed a magnetostriction model directly related to the walls displacement and the domains rotation in $Mn_{0.70}Zn_{0.24}Fe_{2.06}O_4$ ferrite. The model considers the transition between the two mechanisms (walls displacement and domains rotation) quantified by the Maxwell-Boltzmann statistical distribution. It also includes the magnetostrictive hysteresis loop.
The walls movement magnetostriction λ_{mov} is an even function of the induction with a parabola shape:

$$\frac{d\lambda_{mov}}{dB} = 2a_1 B \tag{1.17}$$

However, the domain rotation magnetostriction from the easy to the hard axis has a linear dependence with the induction

$$\frac{d\lambda_{rot}}{dB} = a_2 \tag{1.18}$$

The transition between both mechanisms is quantified using the Maxwell-Boltzmann statistical distribution:

$$W(B) = \text{erf}\left(\frac{B - B_{sw}}{k_b\sqrt{2}}\right) - \sqrt{2}\pi\frac{(B - B_{sw})e^{-(B-B_{sw})/(2k_b^2)}}{k} \tag{1.19}$$

where B_{sw} is the induction value when the magnetization starts to change from the walls movement to the domain rotation. The hysteresis loop $B(H)$ and the $W(B)$ distribution are shown in **Fig. 1.6**. A first region with low magnetic field and a linear behavior corresponds to the walls movement and a $W(B) \sim 0$. In the transitional region, a non-linear behavior appears with an intervention of both the walls movement and the domains rotation, $W(B)$ highly increases. Finally at very high field region, only the domains rotation occurs and $W(B) \sim 1$.

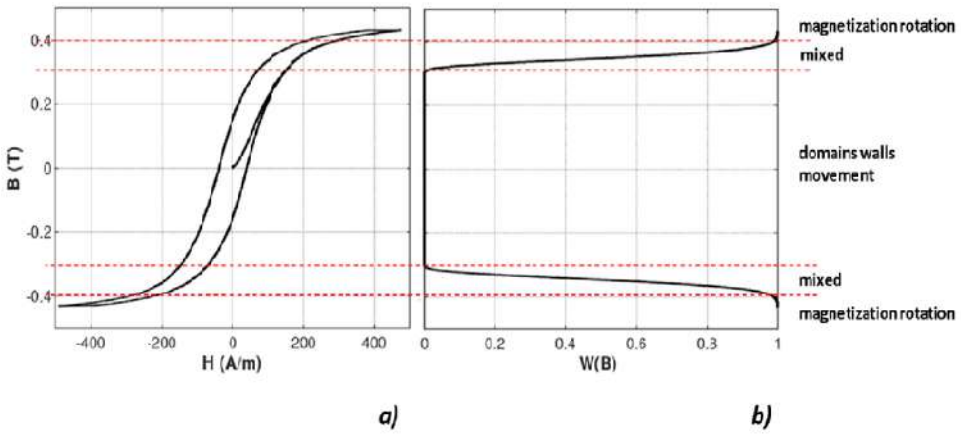

Fig. 1.6 Changes in magnetization mechanisms (a) Hysteresis loop; (b) Statistical distribution [5].

Based on the global statistic distribution, the global anhysteretic magnetostriction variation with the induction is given by:

$$\frac{d\lambda_{anhyst}}{dB} = \frac{d\lambda_{mov}}{dB}(1 - W(B)) + \frac{d\lambda_{rot}}{dB}W(B) \tag{1.20}$$

Eq. 1.20 result is presented in **Fig. 1.7**. In the walls movement region, the magnetostriction increases with the induction with an even function (linear $\lambda_{anhyst} \propto B^2$). As for the transitional

region, a local magnetostriction maximum is created due to the coexistence of both magnetization mechanisms. Finally in the domains rotation region, the magnetostriction decreases linearly with the induction ($\alpha_2 < 0$).

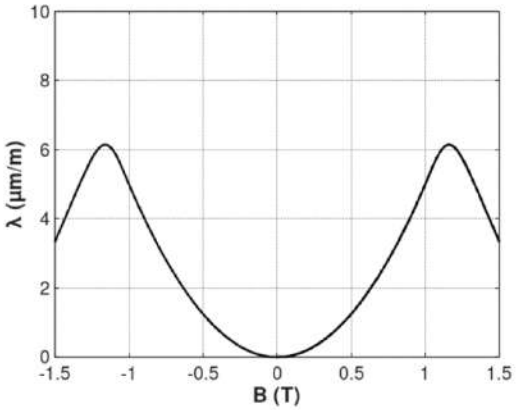

Fig. 1.7 Anhysteretic magnetostriction dependence on the induction [5].

1.4.4 Phenomenological Static Model

This modeling technique uses empirical equations that describe the macroscopic behavior based on obtained experimental observations. One of these approaches is the Helmholtz free energy that describes the magneto-mechanical behavior at the macroscopic scale. It shows a very good agreement with the measurements. A free energy density ψ is considered, it depends on the magnetic flux density vector $\mathbf{B}$ and the total strain tensor ε. Six scalar invariants are obtained:

$$I_1 = tr(\varepsilon), I_2 = \frac{1}{2}tr(\varepsilon^2), I_3 = det(\varepsilon), I_4 = \mathbf{B}.\mathbf{B}, I_5 = \mathbf{B}.(\varepsilon.\mathbf{B}), I_6 = \mathbf{B}.(\varepsilon^2.\mathbf{B}) \tag{1.21}$$

I_1, I_2 and I_3 are mechanical invariant, I_4 describes the magnetization and I_5 and I_6 correspond to magneto-mechanical coupling. The Helmholtz free density ψ is written as [24, 25, 26, 27, 6]:

$$\psi = \frac{1}{2}\lambda_L I_1^2 + 2GI_2 + \sum_{i=0}^{4}\frac{g_i(I_1)}{i+1}I_4^{i+1} + \frac{1}{2}\alpha_5 I_5 + \frac{1}{2}\alpha_6 I_6 \tag{1.22}$$

The function $g_i(I_1)$ is given by:

$$g_i(I_1) = \alpha_i \exp\left(\frac{4(i+1)}{3}I_1\right) - \begin{cases} \frac{1}{8\mu_0}, & \text{if } i = 0 \\ 0, & \text{if } i > 0 \end{cases} \tag{1.23}$$

λ_L and G are material's elastic constants (Lamé) and α_i, β_i and γ_i are fitting parameters to be identified with the measurements. The magnetization vector $\mathbf{M}$ and the stress tensor σ_{me} are partial derivative of ψ and are expressed as:

$$\mathbf{M}(\mathbf{B}, \varepsilon) = -\frac{\partial\psi(\mathbf{B}, \varepsilon)}{\partial\mathbf{B}} \text{ and } [\sigma_{me}](\mathbf{B}, \varepsilon) = \frac{\partial\psi(\mathbf{B}, \varepsilon)}{\varepsilon} \tag{1.24}$$

Fig. 1.8 illustrates the anhysteretic magnetization and magnetostriction results obtained by Aydin et al. [6] using the Helmholtz free energy (HE) model and under uniaxial stress. Results show a good fitting between the model and the experiment. The application of an increasing

stress modifies the permeability and the magnetostriction peak in the opposite direction: an increase of the permeability and a decrease of the magnetostriction is obtained between σ =-30 MPa to σ =10 MPa then a decrease of the permeability and a negative magnetostriction with an increasing peak value.

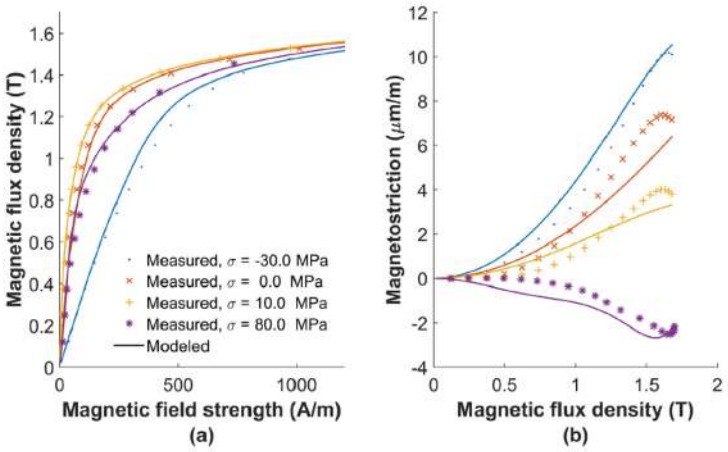

Fig. 1.8 Comparison of measured uniaxial stress dependent anhysteretic magnetization and magnetostriction with modeled results from the HE model (a) Anhysteretic magnetization; (b) Anhysteretic magnetostriction results [6].

The magnetostriction strain tensor can be expressed as an even function of the components of the induction vector $\mathbf{B} = \begin{bmatrix} B_1 & B_2 & B_3 \end{bmatrix}^T$, similar to the Maxwell tensor [28]:

$$[\varepsilon] = \sum_{n=0}^{N} \beta_n ||\mathbf{B}||^{2n} \begin{bmatrix} B_1^2 - \frac{1}{2}B_2^2 - \frac{1}{2}B_3^2 & \frac{3}{2}B_1B_2 & \frac{3}{2}B_1B_3 \\ \frac{3}{2}B_1B_2 & B_2^2 - \frac{1}{2}B_1^2 - \frac{1}{2}B_3^2 & \frac{3}{2}B_2B_3 \\ \frac{3}{2}B_1B_3 & \frac{3}{2}B_2B_3 & B_3^2 - \frac{1}{2}B_1^2 - \frac{1}{2}B_2^2 \end{bmatrix} \tag{1.25}$$

The parameters β_n can be identified using experimental measurements and the least squared method. We note that for a linear case, the strain is proportional to the squared induction, where $N = 1$. For non-linear cases, due to the magnetic non-linearty and the saturation aspect, $N > 1$. In uniaxial magnetization, the magnetostriction macroscopic expression becomes:

$$[\varepsilon] = \sum_{n=0}^{N} \beta_n ||\mathbf{B}||^{2(n+1)} \begin{bmatrix} 1 & 0 & 0 \\ 0 & -\frac{1}{2} & 0 \\ 0 & 0 & -\frac{1}{2} \end{bmatrix} \tag{1.26}$$

1.5 Dynamic Magnetization

Previous models from the microscopic to the macroscopic scale explain the magnetization and magnetostriction phenomena. However, these models do not include the time rate dependent behavior. In fact, most of the times, magnetic materials are submitted to a relatively high frequenciy excitation (at least 50 Hz). In this case, the dynamic rate dependent process must be considered next to the static contribution. The resulting damped behavior generates dynamic losses and a time delay between the magnetization and the excitation field, and between the magnetization and the magnetostriction. In this section, this dynamic behavior will be discussed.

1.5.1 The Eddy Current

Based on the Faraday's law, a conductive material is subjected to an electro-motive force when an alternative magnetic field is applied. This generates eddy-current flow in the conductor. According to the Lenz's law, the eddy current opposes the variation of the magnetic flux, forcing it to merge to the skin of the material. This effect is known as the flux skin effect (**Fig. 1.9**), studied by Fallah [7]. At low frequencies, this effect is decreased by laminating the core. However, if the frequency of flux variation increases, the flux skin effect could not be neglected.

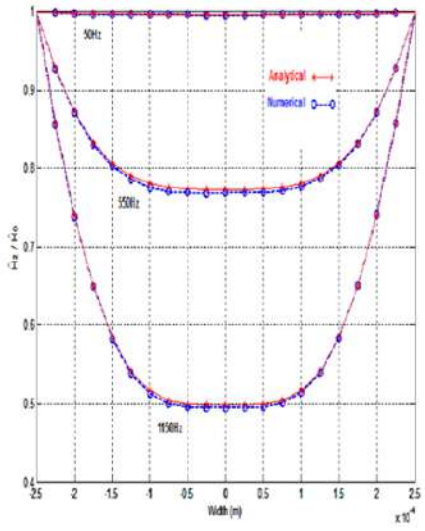

Fig. 1.9 Magnetic field variation in the thickness at different frequencies [7].

The eddy current come from the Maxwell's equations. In fact, at a local scale, the applied magnetic field vector **H** (in A.m^{-1}) variation in the medium generates an electrical current density **J** (in A.m^{-2}) with the following relation:

$$\nabla \times \mathbf{H} = \mathbf{J} \tag{1.27}$$

Furthermore, due to the material's conductivity σ, an electrical field vector $\mathbf{E}_{\text{field}}$ is generated:

$$\mathbf{J} = \sigma \mathbf{E}_{\text{field}} \tag{1.28}$$

The variation of the electrical field in the medium opposes the time variation of the magnetic flux density:

$$\nabla \times \mathbf{E}_{\text{field}} = -\frac{\partial \mathbf{B}}{\partial t} \tag{1.29}$$

From the Maxwell's equation, due to the presence of the time rate induction, a damping factor appears and generates the so-called eddy current losses. These losses are frequency dependent: for a static case, these losses are negligible. As for high frequencies, these losses are more effective and responsible for the skin effect that is due to both the time rate dependency and the dispersion effect in the volume.

1.5.2 Dynamic Damping Property

The constitutive law that connects the local magnetic field to the local flux density is generally used as a static relationship. For the linear case, these two variables are related based on the permeability μ with $B = \mu H$. In a general point of view, we use of the Jiles-Atherton model that includes the walls movement, domains rotation, interdomain coupling and irreversibilities ($B = f(H_s)$).
The static model considers that a magnetic field application induces instantaneously the magnetization and the flux density of the material. However, the magnetization occurs with a time rate due to the walls velocity that creates a delay between the magnetic field and the magnetization. Maloberti et al. [8, 9, 29] have identified a dynamic magnetic property Λ at the mesoscopic scale that explains the origin of the magnetic delay (**Fig. 1.10**). The homogenized damping property Λ depends on the walls density, mobility and surface. This aspect is explained in Chapter 2.

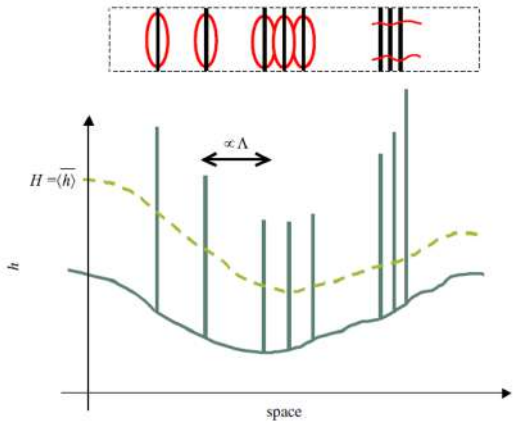

Fig. 1.10 Magnetic field smoothing and Averaging [8].

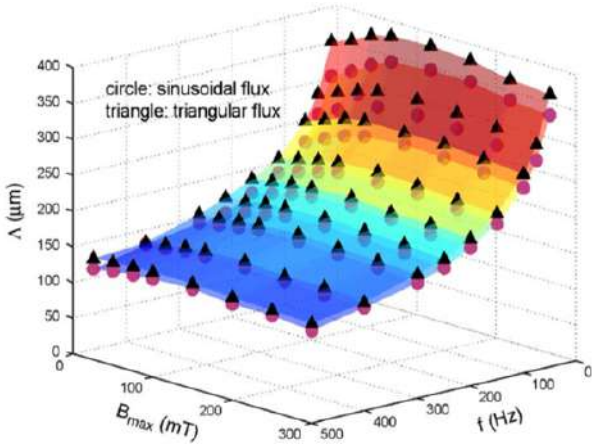

Fig. 1.11 Λ Identification [8].

Using the damping property Λ one gets the mesoscopic magnetic field **H** needed to obtain the induction **B**, with static and dynamic contributions:

$$\mathbf{H} = \mathbf{H}_s + \sigma \Lambda^2 \frac{\partial \mathbf{B}}{\partial t} \tag{1.30}$$

The constitutive law presented in **Eq. 1.30** contains on one hand the static magnetic field that includes the reversible contribution and the static irreversibility, and a dissipative dynamic field that corresponds to the dynamic irreversibility and is responsible of the delay between the field and the induction. This property depends on the flux density and its rate, furthermore, the magnitude and the frequency as shown in **Fig. 1.11**.
Fig. 1.12 shows respectively the variation of the module and the angle of the flux with the frequency, varying the dynamic property Λ. Results show the damping effect that Λ brings: a higher Λ means a bigger domain size and a more damped magnetization. This effect appears especially at high frequencies. The damping includes a higher time delay and a decrease of the amplitude.

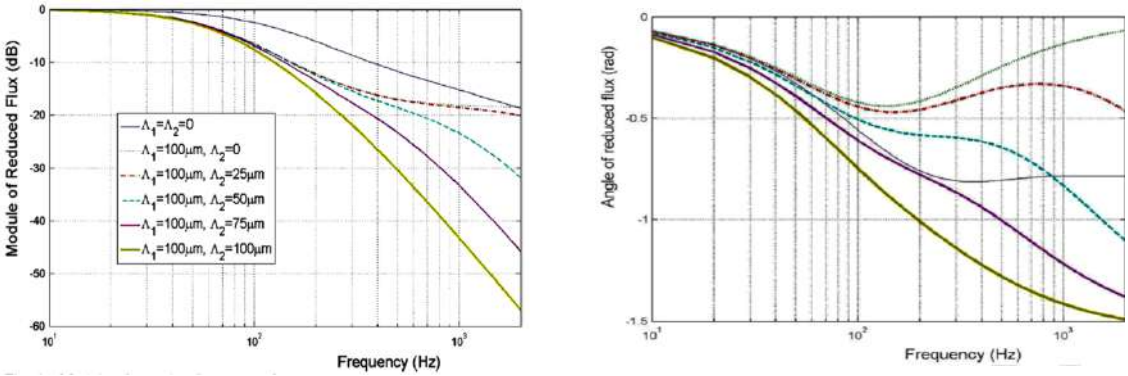

(a) Amplitude

(b) Phase angle.

Fig. 1.12 Complex flux vs frequency [9].

The damping property is responsible for the so-called excess losses P_{ex}. It validates the correlation between the measured hysteresis cycle and the modeled one (**Fig. 1.13**). The damping local effect has also been adopted in other studies but in a phenomenological way. Raulet et al. [10] have expressed the damping contribution with a parameter β:

$$\frac{\partial B}{\partial t} = \frac{1}{\beta}\left[H - H_s(B)\right] \tag{1.31}$$

The dynamic property, next to the Maxwell's dynamic equations have been used to identify some experimental results by fitting the dynamic hysteresis between the measurements and the model, showing a good agreement between the results (**Fig. 1.14**).

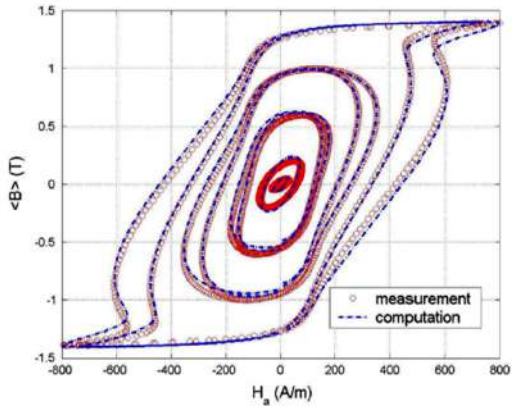

Fig. 1.13 Simulation of cycles with sinusoidal flux ($B = 0.05 - 1.4$ T, $f = 600$, 800 Hz) [9]

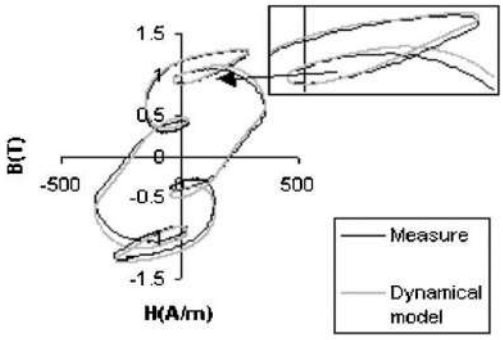

Fig. 1.14 Dynamic loops with 50 Hz sine wave excitation with harmonic 3 [10].

1.5.3 Bertotti Power Loss

In the dynamic mode, different losses contribute to the magnetization of the material: the static losses P_{hyst} due to static irreversibilities, the eddy current losses due to the electrical conductivity known by the classic losses P_{el} and the excess losses due to the moving walls dynamic P_{exc}. These losses were considered and identified by Bertotti [11, 30]. The total power loss in one cycle becomes:

$$P_T = P_{hyst} + P_{el} + P_{exc} \tag{1.32}$$

$P_{el} + P_{exc}$ are the dynamic contribution of the total losses. They are dominant at high frequencies. Bertotti has expressed the power as function of the exciting frequency f, the induction magnitude B_{max}, the conductivity σ and the thickness h. The hysteresis power losses, classic power losses and the excess power losses are respectively given by:

$$P_{hyst} = k_h f B_{max}^2 \tag{1.33}$$

$$P_{el} = k_c (B_{max} f)^2 \tag{1.34}$$

$$P_{exc} = k_e (B_{max} f)^{3/2} \tag{1.35}$$

k_h, k_c and k_e are the Bertotti parameters to be identified. The given loss expressions correspond to sinusoidal induction case. A generalized time dependent formulation can be obtained for a non-sinusoidal response by:

$$P_T(t) = P_{hyst} + \frac{\sigma h^2}{12}\left(\frac{dB}{dt}\right)^2 + C'\left(\frac{dB}{dt}\right)^{3/2} \tag{1.36}$$

Fig. 1.15 illustrates the loss per cycle for a Grain oriented 3% SiFe dependent on the frequency and the induction amplitude. It is shown that the loss increases with the induction and the frequency. Comparing with the static case near 0 Hz, an initial loss is also present, the static loss. It is negligible at high frequencies. The concept of energy and losses helps to understand the dynamic behavior by separating the different dynamic phenomena that occur simultaneously.

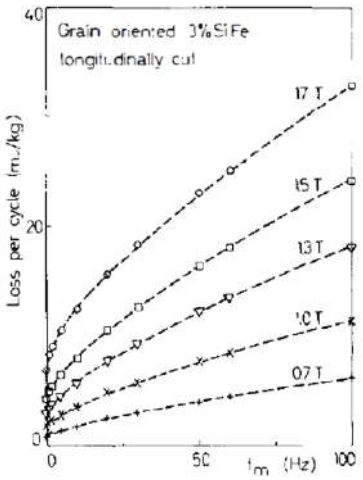

Fig. 1.15 Loss per cycle vs frequency for GO 3% FeSi [11].

1.6 Dynamic Deformation

1.6.1 Dynamic Hysteresis

The previous dynamic models show that the dynamic behavior takes into account the static contributions and some damping phenomena: the eddy current effect and the walls movement. In fact, the dynamic behavior may also have an impact on the magneto-mechanical behavior, by creating a time delay between the magnetization and the magnetostriction. This phenomenon can be illustrated by the so-called **butterfly loop**. By plotting the strain as function of the magnetization, a parabola shape with a delay is generated, similar to the magnetization hysteresis loop. Rasilo et al. [12] have studied next to the Jiles-Atheton-Sablik model, the dynamic response of the magnetostriction (**Fig. 1.16**). It was shown that the magnetostriction dynamic hysteresis increases with the frequency due to the skin effect provided by the eddy current. The dynamic magnetostriction has also been identified by Hilgert et al. [13] using the Neural Network technique that presents the frequency dependent magnetostriction and includes a dynamic hysteresis effect (**Fig. 1.17**).

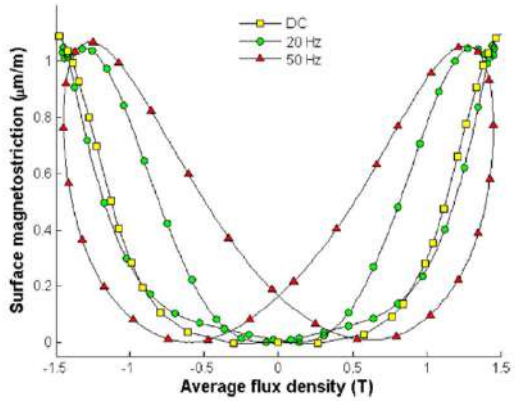

Fig. 1.16 Measured magnetostriction vs flux density [12]

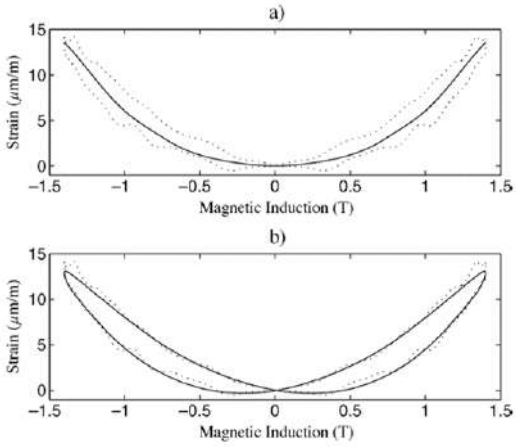

Fig. 1.17 Magnetostriction loops (a) Static identification; (b) Time-rate dependent [13].

1.6.2 Analogy with the Mechanical Elasticity

The magnetostrictive anisotropy of NO steels was studied by Moses and Somkun [17, 31]. The measurements were performed under rotating magnetic field in order to study the behavior in the rolling direction (RD) and the transverse direction (TD) using strain gauges. Assuming a square dependence, the magnetostriction in two directions x and y are given by:

$$\lambda_x = \lambda_s(M_x/M_s)^2 - \frac{1}{2}\lambda_s(M_y/M_s)^2 \tag{1.37}$$

$$\lambda_y = \lambda_s(M_y/M_s)^2 - \frac{1}{2}\lambda_s(M_x/M_s)^2 \tag{1.38}$$

M_x and M_y are the magnetization components in the RD and TD respectively. Magnetostriction under rotating magnetic field can be modeled as function of the induction based on an analogy with the mechanical elasticity by:

$$\tau \frac{d}{dt}\begin{bmatrix}\lambda_x\\ \lambda_y\\ \gamma_{xy}\end{bmatrix} + \begin{bmatrix}\lambda_x\\ \lambda_y\\ \gamma_{xy}\end{bmatrix} = \frac{1}{\mu_0}\begin{bmatrix}\frac{1}{P_x} & -\frac{\xi_x}{P_y} & 0\\ -\frac{\xi_y}{P_x} & \frac{1}{P_y} & 0\\ 0 & 0 & \frac{1}{G_{xy}}\end{bmatrix}\begin{bmatrix}B_x^2\\ B_y^2\\ B_xB_y\end{bmatrix} \tag{1.39}$$

where P_x, P_y the magnetic moduli (in GPa), ξ_x and ξ_y are the magnetic Poisson ratios and G_{xy} is the shear magnetic modulus between RD and TD. **Eq. 1.39** is a first order differential equation with a time delay τ adjusting the hysteresis between the magnetization and the magnetostriction. Identification results are shown in **Table 1.2**. The considered model is not applicable for high magnetization due to the non-linearity when the magnetization is close to saturation. In this case, the domain wall annihilation and nucleation processes modify the magnetic and magnetostrictive behavior.

Table 1.2 2-D Magnetostriction model parameters [17].

Material	P_x (GPa)	ξ_x	P_y (GPa)	ξ_y	G_{xy} (GPa)	τ (ms)
0.35 mm thick	141	0.9	128	0.9	40	0.10
0.50 mm thick	2145	1.0	81	1.0	42	0.17

The magneto-elastic/mechanical analogy was developed by Lundgren [32] where B^2/μ_0 is considered as a magnetic stress that is responsible for the strain vector generation. The matrix connecting the stress to the strain is a magnetic stiffness matrix analogy to the mechanical stiffness. As for the delay τ, it represents the magnetic viscosity that is responsible for the delay between the magnetic stress and the strain.

1.7 Modeling Novelty

A litterature review for different magnetic and magneto-mechanical models developed and identified by researchers at different scales was presented. The modeling is performed at the domains scale, the mesoscopic scale, then the macroscopic scales with a transition between the different scales. Some models are limited to the static state while others include the behavior in the dynamic state responsible of the generation of magnetic and magneto-mechanical damping and losses.
Based on the presented state of the art, chapters 2 and 3 present the models used in this work to characterize the magnetic and the magneto-mechanical behavior.
The magnetic and the magneto-mechanical modeling will be performed from the domain scale where a specific simple structure is studied and from which, behavioral properties are homogenized at the mesoscopic scale. These properties presented at the mesoscopic scale are next applied in macroscopic models. The latter are chosen in a way to adapt with measurements performed in deliverable 3.4.
The modeling is performed in the static and the dynamic mode. We mainly focus on the magnetic level using the Λ model and the Jiles-Atherton model while performing some modifications adapted to the magnetization mechanisms using the Maxwell-Boltzmann's statistical distribution. At the magneto-mechanical level, we focus on the magnetostriction model with the local maximum and the magneto-elastic analogy, taking into consideration the time delay between the induction and the strain.

1.8 Laser Treatment: A Review

1.8.1 Laser Treatment and the Magnetic Behavior

Laser have been extensively used for materials processing since their invention. One of its applications is the surface treatment, a technique used to improve the magnetic performances within magnetic circuits inside electrical machines. In fact, the surface laser treatment (irradiation, scribing or ablation) can generate stress and magnetic poles, which can induce various closure domains and domains refinement (**Fig. 1.18**).

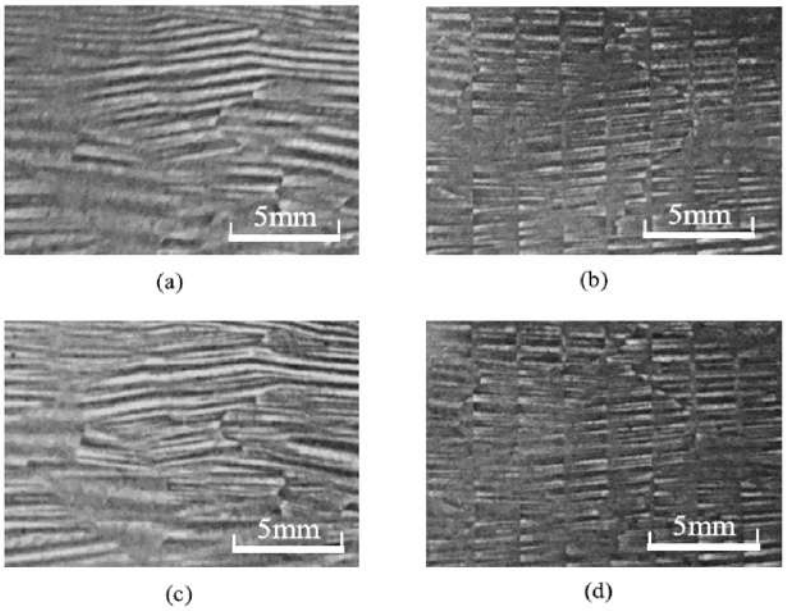

Fig. 1.18 Magnetic Domain (a) Without Laser (b) Laser Direction is TD (c) Laser Direction is RD (d) Laser Direction is TD+RD [14].

The factors that are affected the most are: size of grains, purity of the material, degree of refinement of the magnetic domains, surface tension and internal strains. Many studies have concentrated their researches on the effect of each of these factors, especially domain refinement and wall movement, on the core loss of the ferromagnetic material.
The enhancement of magnetic properties (hysteresis loss, total core loss, coercivity, remanence, permeability and saturation induction) of 3% silicon steel laminations using three different lasers for scribing has been investigated by Patri et al. [33]. The improvement of the material's softness by the laser treatment is explained by three mechanisms: relaxation of internal stress, domains refinement, walls' multiplication, walls' nucleation, walls' activation and walls mobility increase. In fact, the high concentration of laser energy deforms plastically the substrate forming a localized zone of compressive stress creating subdomains that tend to decrease the magnetoelastic energy and refine the magnetic domain. This mechanism leads to breakage of bonds, internal stress relaxation and domain wall movement during magnetizing and demagnetizing cycles, decreasing the total core loss. The domain refinement concept has been illustrated by Kajiwara and Enokizono [14] using a parametric study where iron loss decreases for transerve and rolling direction of laser scratches. But when both scratches are applied simultaneously, the iron loss decreases much more. Iron loss decrease is also improved by applying smaller pitches of laser scratches. Different results collected by Kajiwara

are displayed in **Fig. 1.19**.

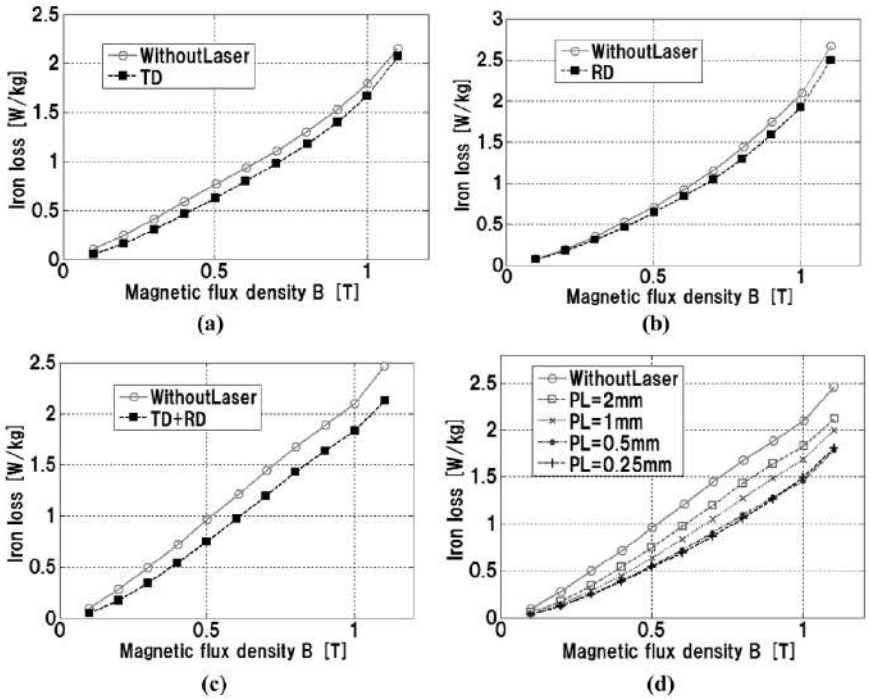

Fig. 1.19 Comparison between case without laser and with laser for iron losses with diferent configurations (a) TD (b) RD (c) TD + RD (d) irradiation pitch PL variation [14].

Johnson et al. [34] revealed the importance of laser surface scribing with optimum parameters (scribe speed, scribe spacing, power and pulse frequency) on core losses reduction in amorphous metallic ribbons based on domain refinement.
On the other hand, the influence of dotted lines produced by laser scribing on the domain structure and shape of the hysteresis loops has been described by Zeleňáková et al. [15]. It was shown that the hysteresis loop is steeper for samples with small density of dotted lines than for non-treated samples. This is due to the fact that magnetic polarization vector rotates much narrower and the number of movable domain walls is larger. For high density dots, a wavy hysteresis curve is generated; the domain wall displacement and the rotation of the spontaneous magnetic polarization vector happen simultaneously.
Zeleňáková et al. [15] also revealed the impact of laser treatment on the coercivity that increases with the increase of the dots density. Different results are plotted in **Fig. 1.20**.

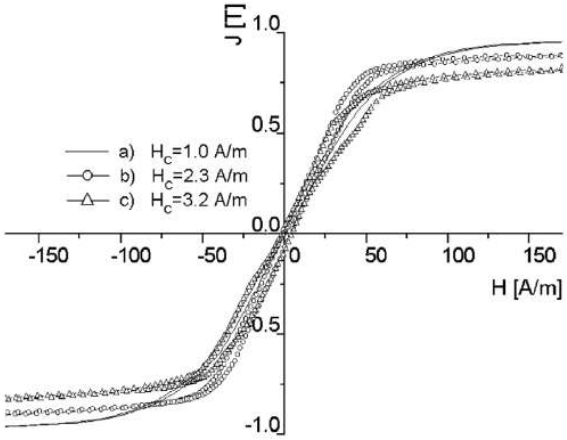

Fig. 1.20 Hysteresis loops of Finemet: a) Non-treated sample b) Laser treated sample with small density dotted lines c) Laser treated sample with high density dotted lines [15].

1.8.2 Laser Treatment and the Noise Reduction

Most studies mainly focus on the importance of laser treatment on magnetic losses and the improvement of softness in magnetic materials. Very few consider the effect of laser treatment on the vibration and the noise behavior that is generated from magnetic forces induced in the magnetic materials. This approach, next to losses analysis, have been considered by Lahn et al. [16] and have been studied on grain oriented electrical steel present in three-phase transformer cores. The main source of transformer noise to be taken into account is the magnetostriction; it gives a rough indication but it is not the final indicator of the behavior of the real cores. Optimized laser parameters are generated so that the noise behavior is improved by laser domain refinement as shown in **Fig. 1.21**. Otherwise, non-optimal characteristics will increase the magnetostriction and the generated noise.

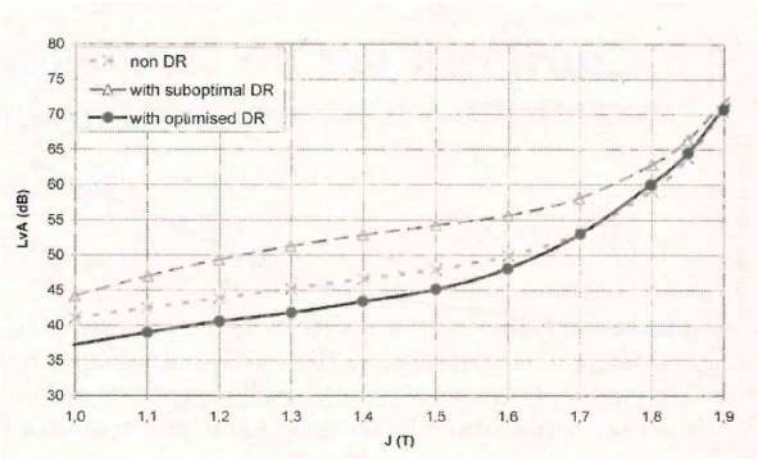

Fig. 1.21 Calculated noise on basis of magnetostriction by considering laser domain refinement (DR)[16].

1.8.3 Work Novelty

In this thesis, based on the different strategies (modeling, experimentation and characterization), the impact of the laser treatment on the magnetic and the magneto-mechanical behavior is investigated. Although the laser treatment effect on the iron losses has been widely studied, a detailed study on the magnetic properties such as the permeability and the dynamic property Λ has not been presented yet. On the other hand, a higher focus is applied on the magneto-mechanical behavior. Few studies are performed on the sensitivity of noise and vibration to laser treatment. Similarly to the magnetic interpretation, this thesis describes the effect on the magneto-mechanical properties and the mechanical response, responsible of the vibration and noise generation in magnetic components. Based on this sensitivity investigation on the magnetic and the magneto-mechanical study, one can evaluate the laser's effect on the iron losses and the magnetic performances on one hand, and the effect on the vibration and noise on the other hand. The obtained results constitute a powerful tool for upscaling and application of the laser technology in magnetic components.

1.9 Conclusion

This chapter presents a litterature review for different magnetic and magneto-mechanical models developed and identified by researchers at different scales. The modeling is performed at the domains scale, the mesoscopic scale, then the macroscopic scales with a transition between the different scales. Some models are limited to the static state while others include the behavior in the dynamic state responsible for the generation of magnetic and magneto-mechanical damping and losses.
Based on the presented state of the art, chapters 2 and 3 present the models used in the thesis to characterize the magnetic and the magneto-mechanical behavior.
The magnetic and the magneto-mechanical modeling will be performed from the domain scale where a specific simple structure is studied and from which, behavioral properties are homogenized at the mesoscopic scale. These properties are presented at the mesoscopic scale are next applied in macroscopic models. The latter are chosen in a way to adapt with measurements performed in deliverable 3.4.
The modeling is performed in the static and the dynamic mode. We mainly focus on the magnetic level on the Λ model, the Jiles-Atherton model while performing some modifications adapted to the magnetization mechanisms using the Maxwell-Boltzmann's statistical distribution. At the magneto-mechanical level, we focus on the magnetostriction model with the local maximum and the magneto-elastic analogy, taking into consideration the time delay between the induction and the strain.

Chapter 2

Magnetic Modeling

2.1 Introduction

In this chapter, the magnetic modeling strategy is presented. The target is to present the magnetic models that describe the static and dynamic behavior. The presented models are chosen in a way to describe the experimental bevahior. In this way, the models can be used to identify the magnetic properties based on the measured data.
The modeling technique includes the magnetic local behavior including static and dynamic properties:

- The static contribution is based on a statistical Maxwell-Boltzmann's distribution that quantifies the magnetization mechanisms at the microscopic scale (walls displacement and domains rotation) and on the Jiles-Atherton model that includes the static losses.
- The dynamic contribution considers the dynamic damping term Λ that represents the losses due to the microscopic eddy currents.

In addition, we present the space dispersion that shows the gradient of magnetic variables in the geometry. The modeling is based on the Maxwell's diffusion equations at the mesoscopic scale.

2.2 Static Behavior

2.2.1 Microscopic Study

Without considering the irreversibilities at the microscopic scale, the magnetization process presents two mechanisms: the walls displacement and the domains rotation. In fact, the magnetic structure is constituted of saturated domains with a M_s magnetization. The total magnetization of the structure is the vectorial sum of the different domain contributions. In general, a magnetic structure includes different domains orientations. For a Grain-Oriented material, most of domains are oriented in the rolling direction, with the presence of other dis-oriented domains.
The indices $\rightarrow$ and $\leftarrow$ are defined for the 180° domains in the x direction, $\uparrow$ and $\downarrow$ for the 90° domains in the y direction and $\bullet$ and $\otimes$ for the 90° domains in the z direction. The indices $\nearrow$, $\swarrow$, $\nwarrow$ and $\searrow$ are also defined for the domains oriented in other random directions.
In general, the domains cosine director is designated by α. Their corresponding fraction volumes when no magnetic field is applied, are equal to f_α^0. In a more general way, we consider the indice $\parallel$ for the 180° domains components with an orientation α (in the case: $\rightarrow$, $\leftarrow$, and

the parallel components of ↗, ↙, ↖ and ↘) and the indice ⊥ for the perpendicular components (in this case: ↑ and ↓ and the perpendicular components of ↗, ↙, ↖ and ↘). In order to simplify the modeling, we consider that the different initial energy contributions are responsible for the creation of the considered structure. During magnetization, the magnetostatic energy is responsible for the structure evolution with the magnetic field.
At rest, the initial total magnetization is given by:

$$< M^0 >= \sum_{\alpha} f_\alpha \mathbf{M}(\alpha) = (f^0_{\alpha\parallel} + f^0_{\alpha\perp}) M_s = 0 \tag{2.1}$$

When a magnetic field is applied, the domains volume fraction f_α varies with the magnetic field and the total magnetization is non zero. The average magnetization of a grain using a linear combination of all the magnetization vectors becomes:

$$< M > (\mathbf{H}) = \sum_{\alpha} f_\alpha \mathbf{M}(\alpha) \tag{2.2}$$

f_α is calculated using the volume fractions of Maxwell-Boltzmann's type f_α based on a probability density approach [28] as function of the applied magnetic field **H**. It is a statistical theory in a canonical type set without degeneration that considers the energy density of $E_T(\alpha)$.

$$f_\alpha(\mathbf{H}) = \frac{e^{-A_s.E_T(\alpha)}}{\sum_\beta e^{-A_s.E_T(\beta)}} \tag{2.3}$$

$$\sum_{\alpha} f_\alpha = 1 \tag{2.4}$$

A_s is a phenomenological parameter that takes into account the domain walls and the inhomogeneities. A_s was identified by Daniel et al. [35, 36] for single and polycrystals by neglecting the rotation phenomenon at very low magnetic field (near zero):

$$A_s = \frac{3\chi^0}{\mu_0 M_s^2} \tag{2.5}$$

Where χ^0 is the material's initial susceptibility, μ_0 is the vacuum permeability and M_s is the magnetization at saturation.

In order to calculate the volume fractions as function of the applied magnetic field, the sum of the different energy contributions is considered for zero magnetic field defined by E^0_T. The initial volumes fractions can be written as:

$$f^0_\alpha = \frac{e^{-A_s.E^0_T(\alpha)}}{\Sigma_\beta e^{-A_s.E^0_T(\beta)}} \tag{2.6}$$

When the magnetic field is applied, the fraction volume includes the magnetostatic energy. **Eq. 2.3** becomes:

$$f_\alpha(\mathbf{H}) = \frac{e^{-A_s.(E^0_T(\alpha) - \mu_0 A_s \boldsymbol{M_\alpha}.\boldsymbol{H})}}{\sum_\beta e^{-A_s.(E^0_T(\beta) - \mu_0 A_s \boldsymbol{M_\beta}.\boldsymbol{H})}} = \frac{\frac{e^{-A_s.E^0_T(\alpha)}}{\sum_\gamma e^{-A_s.E^0_T(\gamma)}} e^{\mu_0 A_s \boldsymbol{M_\alpha}.\boldsymbol{H}}}{\sum_\beta \frac{e^{-A_s.E^0_T(\beta)}}{\sum_\gamma e^{-A_s.E^0_T(\gamma)}} e^{\mu_0 A_s \boldsymbol{M_\beta}.\boldsymbol{H}}} \tag{2.7}$$

$$f_\alpha(\mathbf{H}) = \frac{f_\alpha^0 e^{\mu_0 A_s \boldsymbol{M_\alpha}.\boldsymbol{H}}}{\sum_\beta f_\beta^0 e^{\mu_0 A_s \boldsymbol{M_\beta}.\boldsymbol{H}}} \tag{2.8}$$

Hence, the average magnetization and the magnetostriction can be determined as function of the initial volume fractions and the applied magnetic field. The parallel and perpendicular fraction volumes for a domain with an α orientation can be derived from **Eq. 2.8**.

$$f_{\alpha\parallel}(\mathbf{H}) = \frac{f_{\alpha\parallel}^0 \cosh(\mu_0 A_s M_{s\alpha\parallel} H)}{\sum_\beta f_{\beta\parallel}^0 \cosh(\mu_0 A_s M_{s\alpha\parallel} H) + \sum_\beta f_{\beta\perp}^0 \cosh(\mu_0 A_s M_{s\alpha\perp} H)} \tag{2.9}$$

In this study, for simplification of the process, the structure given in **Fig. 2.1** is considered, containing domains oriented in the magnetic field's direction (180°) and domains oriented in the transverse directions, without the presence of inclined domains. When no magnetic field is applied, the total magnetization equals to zero. When a magnetic field applied in the 180° direction, the size of 180° domains increases and the transverse domains size decreases. Considering the initial volume fractions, the volume fractions corresponding to a magnetic field H in **Eq. 2.9** become:

$$\begin{aligned}
f_\rightarrow(H) &= \frac{f_\rightarrow^0 e^{A_s\mu_0 M_s H}}{f_\parallel^0 \cosh(A_s\mu_0 M_s H) + f_\perp^0}, f_\leftarrow(H) = \frac{f_\leftarrow^0 e^{-A_s\mu_0 M_s H}}{f_\parallel^0 \cosh(A_s\mu_0 M_s H) + f_\perp^0} \\
f_\uparrow(H) &= \frac{f_\uparrow^0}{f_\parallel^0 \cosh(A_s\mu_0 M_s H) + f_\perp^0}, f_\downarrow(H) = \frac{f_\downarrow^0}{f_\parallel^0 \cosh(A_s\mu_0 M_s H) + f_\perp^0} \\
f_\bullet(H) &= \frac{f_\bullet^0}{f_\parallel^0 \cosh(A_s\mu_0 M_s H) + f_\perp^0}, f_\otimes(H) = \frac{f_\otimes^0}{f_\parallel^0 \cosh(A_s\mu_0 M_s H) + f_\perp^0}
\end{aligned} \tag{2.10}$$

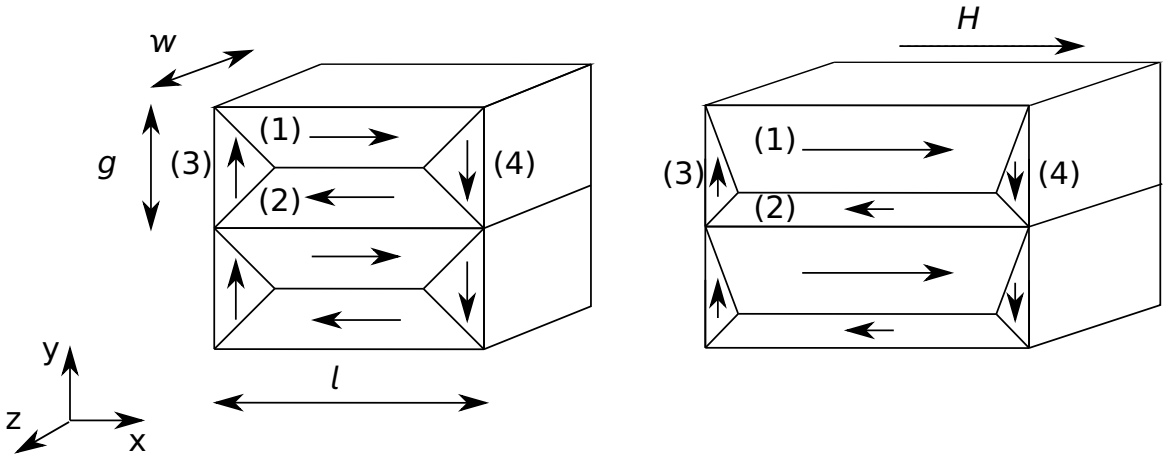

Fig. 2.1 Magnetization of a magnetic domain with 180° and 90°.

The magnetization in the 180° orientation as function of the magnetic field becomes:

$$M_\parallel(H) = \frac{f_\parallel^0 \sinh(A_s\mu_0 M_s H)}{f_\parallel^0 \cosh(A_s\mu_0 M_s H) + f_\perp^0} M_s \tag{2.11}$$

For low magnetization, **Eq. 2.11** is linear. This corresponds to the magnetization range where the walls displacement phenomenon occurs. The linearization of these equations using a first order Taylor development gives:

$$M_{\parallel}(H) \sim \left(1 - f_{\perp}^{0}\right) 3\chi_0 H \tag{2.12}$$

The relative permeability is then defined:

$$\mu_r = 3\chi_0 \left(1 - f_{\perp}^{0}\right) + 1 \tag{2.13}$$

Based on **Eq. 2.13**, the increase of the 90° domains fraction decreases the permeability in the x direction and increases the permeability in the other directions. A maximal permeability in the x direction is obtained for zero 90° domains.
If the applied magnetic field and the magnetization were not parallel (more realistic case), the domains rotation is triggered in order to align the magnetization of the domain with the applied magnetic field. In this case, the permeability depends also on the domains density: a higher density reduces the permeability because the anisotropy decreases and the demagnetizing energy becomes more important. However, for magnetization close to saturation and corresponding to a very high magnetic field (1,000 A/m), the disorientation and the domains density have no more effect on the permeability because the disorientation effect vanishes due to the total domains rotation at saturation.

2.2.2 Mesoscopic Approach: Anhysteretic Magnetization

In this section, an upscale of the microscopic analysis is presented at the mesoscopic scale. At this level, the reversible process represents the variation of the flux density B with an anhysteretic magnetic field H_{an} without taking into account the static losses. For a specific magnetization level, the magnetic mechanisms are present with different proportions quantified by the statistical function $W(M)$:

- The walls displacement with a fraction volume of $1 - W(M)$ for a specific induction
- The domains rotation with a fraction volum of $W(M)$

At low magnetization, the first phenomenon is only present ($W(M) = 0$) with a linear behavior characterized by the permeability μ (or the suseptibility χ).
However, when reaching a certain magnetization M_{sw}, the domains rotation mechanism starts to appear due to the maximal capacity of the corresponding walls to move. This is related to the fact that the demagnetizing energy becomes more important than the anisotropy. This transitional region, where the displacement and rotation phenomena coexist, is characterized by a property k_m. A higher k_m means a lower permeability at saturation. In fact, this property is related to the contribution of the anisotropy energy and the demagnetizing energy. When the domains rotation phenomenon occurs, the anisotropy energy begins to disappear and the demagnetizing energy increases. Therefore, the apparent permeability decreases and the saturation phenomenon occurs. The transition between the linear region and the saturation is described by the k_m parameter sensitive to the energy contributions in this region.
For a perfect case, when all the principal domains are parallel to the magnetic field, this transitional region does not exist. In the practical case, this region exists and $W(M)$ increases gradually from 0 to 1. At the final state, the saturation is obtained, leading to $W(M) = 1$. $W(M)$ is a statistical distribution defined by Szewczyk [5], using the Maxwell-Boltzmann statistical distribution with the following cumulative distribution function:

$$\begin{cases} W(M) = \operatorname{erf}\left(\dfrac{M - M_{sw}}{k_m\sqrt{2}}\right) - \dfrac{\sqrt{2}}{\pi}\dfrac{(M - M_{sw})e^{-(M-M_{sw})/(2k_m^2)}}{k_m} & \text{if } |M| > |M_{sw}| \\ W(M) = 0 & \text{elsewhere} \end{cases} \tag{2.14}$$

With erf(x) being the error function given by:

$$\text{erf}(x) = \frac{1}{\sqrt{\pi}} \int_{-x}^{x} e^{-t^2} dt \tag{2.15}$$

Szewczyk [5] has used the Maxwell-Boltzmann distribution to analyze the magnetostrictive behavior. In this study, we also include this concept in the magnetization. In fact, we consider the first mechanism, the walls displacement as a linear process where the application of a magnetic field increases proportionally the flux density B_{mov} with a relative permeability μ_r. This property is sensitive to the domains structure as described in section 2.2.1, it increases with the closure domains decrease.

$$\frac{dM_{mov}}{dH} = \mu_r - 1 \tag{2.16}$$

As for the second mechanism, the domains rotation, the magnetization reaches the saturation even with the application of an extra magnetic field:

$$\frac{dM_{rot}}{dH} = 0 \tag{2.17}$$

Therefore, using the combination with the statistical distribution $W(M)$, we get the total variation:

$$\frac{dM}{dH} = \frac{dM_{mov}}{dH}(1 - W(M)) + \frac{dM_{rot}}{dH} W(M) = \chi(1 - W(M)) \tag{2.18}$$

and

$$H = \int_0^M \frac{1}{\chi(1 - W(x))} dx = f(M, \chi, M_{sw}, k_m) \tag{2.19}$$

This equation gives the total magnetization anhysteretic curve. The originality of this equation appears in the static parameters involved. In fact, χ is generally shown in linear relations between H and M, but here we can see it even with the non-linearity. Furthermore, we can notice where the transition of phenomena begins using M_{sw} and what is the intensity of this process based on k_m. Therefore, this model describes what happens in the microscopic scale and expresses it in the mesoscopic scale in a clear way.
We introduce the magnetic flux density or induction given by:

$$B = \mu_0(H + M) \tag{2.20}$$

When $H <<< M$, $B = \mu_0 M$. The anhysteretic model can replace M by B, by replacing the M_{sw}, k_m and χ by B_{sw}, k_b and μ, where $B_{sw} = \mu_0 M_{sw}$, $k_b = \mu_0 k_m$ and $\mu = \chi + 1$ (the permeability).

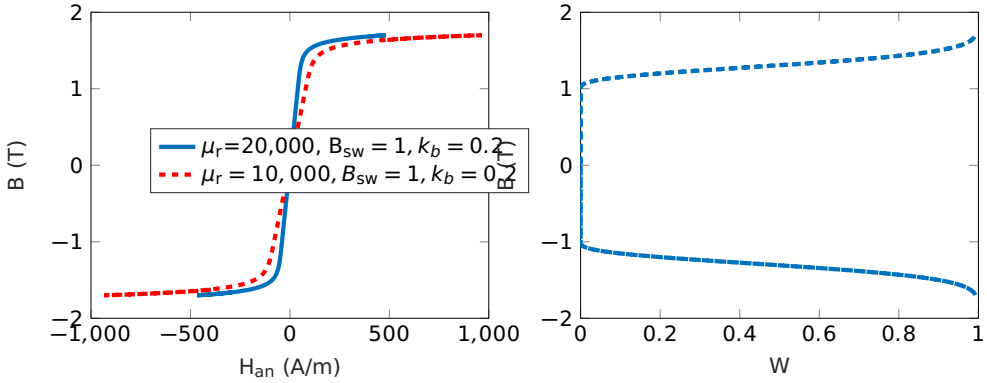

Fig. 2.2 Modeling the changes in the mechanism of magnetization with the permeability μ.

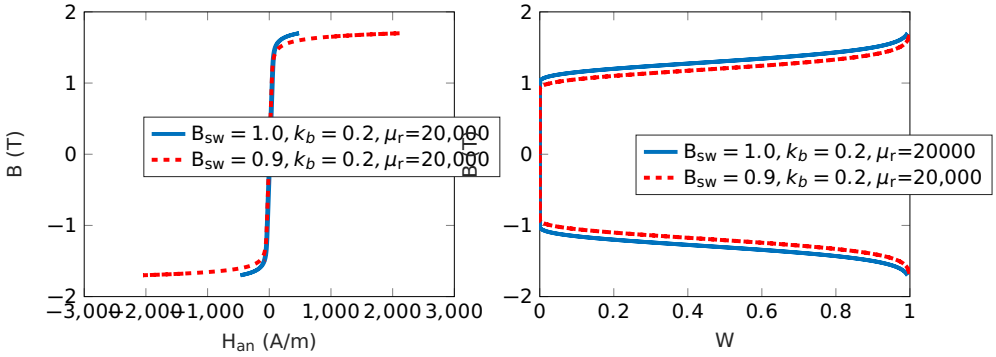

Fig. 2.3 Modeling the changes in the mechanism of magnetization with the switching induction B_{sw}.

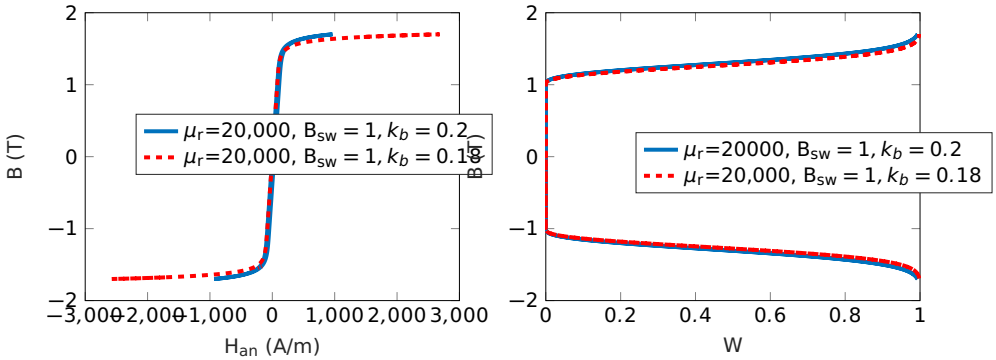

Fig. 2.4 Modeling the changes in the mechanism of magnetization with transition intensity k_b.

Fig. 2.2, **Fig. 2.3** and **Fig. 2.4** show the magnetization curve compared with the processes distribution by varying the model's parameters μ, B_{sw} and k_b. The increase of the permeability μ increases the slope of the linear region without changing the mechanisms distribution. As for the B_{sw} increase, the transition region begins at higher induction. Finally, the increase of k_b leads to a faster transition between the two magnetic mechanisms.

2.2.3 Irreversibilities Consideration

In this section, the non-linearity effect due to the static behavior and the static losses effect is presented. The static behavior at a specific induction magnitude can be identified using the Jiles-Atherton model. In fact, the static behavior is observed at very low exciting frequency (5 Hz), where the dynamic behavior is neglected. Considering a static magnetic field H_s and its corresponding magnetization M, the effective field $H_{\text{eff}} = H_s + \alpha M$. The anhysteretic magnetization M_{an} expressed initially by the Langevin function is replaced by **Eq. 2.19** for H_{eff} as function of M_{an}. The other Jiles-Atherton equations are the same as **Eq. 1.13** and **Eq. 1.15**: In the Jiles-Atherton's model, the irreversibility process is modeled by the irreversibility magnetization M_{irr}:

$$\frac{dM_{\text{irr}}}{dH_{\text{eff}}} = \frac{M_{\text{an}} - M_{\text{irr}}}{k\delta} \tag{2.21}$$

,

$$M = (1-c)M_{\text{irr}} + cM_{\text{an}} \tag{2.22}$$

and

$$B = \mu_0(H_s + M) \tag{2.23}$$

The presented model includes the anhysteretic behavior related to the anhysteretic magnetization processes (walls displacement and domains rotation), and considers the static losses responsible of the static hysteresis. The model is presented by a function of the induction:

$$H_s = J_A(B) \tag{2.24}$$

The static model is independent of the volume: we consider that the material magnetizes uniformly in the static mode and the Maxwell equations are not effective. In the next part, the high frequency excitation requires the inclusion of the dynamic losses and the effect of the volume dispersion (included in the Maxwell's equation) on the induction and magnetic field distribution.

2.3 Dynamic Behavior

At the mesoscopic scale, we propose to model the dynamic behavior using the Λ model developed by Maloberti [8, 9, 29]. In fact, microscopic eddy currents are generated around the walls. This creates microscopic losses given by:

$$p_{\mu w} = \iiint \sigma^{-1} j_{\mu w}^2(r) d^3r = \left(\frac{2\vartheta J_s S_w}{m_w}\right) v_w^2 \tag{2.25}$$

The lost power appears in the form of microscopic current density $j_{\mu w}$ around the moving walls. When the material is magnetized in the linear case, the walls displacement phenomenon occurs between the 180° domains within a distance Δx. The average magnetization of the domains set of **Fig. 2.1** can be written as:

$$< M >= \frac{2\Delta x}{g} M_s \tag{2.26}$$

By replacing the magnetizations M and M_s by their corresponding induction $\mathbf{B}$ and saturation induction J_s we obtain the velocity of one wall v_w:

$$v_w = \frac{g}{2J_s}\frac{\partial \mathbf{B}}{\partial t} \tag{2.27}$$

At the grains scale, g is proportional to the domains density n_w and the walls surface S_w based on the following:

$n_w \propto \frac{2}{gwl}$ and $S_w \propto wl$

This means that $g \propto \frac{2}{n_w S_w}$.

Upscaling to a set of domains, the domains wall velocity v_w becomes:

$$v_w = \frac{1}{n_w S_w J_s}\frac{\partial \mathbf{B}}{\partial t} \tag{2.28}$$

Replaceing it in **Eq. 2.25**, the dissipated power can be expressed as follows:

$$p_{\mu w} = (2\vartheta J_s S_w m_w n_w^2)^{-1}\left(\frac{\partial \mathbf{B}}{\partial t}\right)^2 = \iiint \mathbf{H}.\frac{\partial \mathbf{B}}{\partial t} d^3r \tag{2.29}$$

Where σ is the electrical conductivity, J_s is the saturation magnetic polarization, ϑ a real number between 0 and 1, v_w is the average walls velocity, S_w their mean surface, m_w their

average mobility and n_w their volume density. Accumulating microscopic energy on each wall, we get the total magnetic field $\mathbf{H}$ as the sum of a static contribution $\mathbf{H}_s$ and a time dependent term containing the induction rate $\frac{\partial \mathbf{B}}{\partial t}$.

$$\mathbf{H} = \mathbf{H}_s + \sum_w \sigma \Lambda^2 (\partial_t \mathbf{B}) n_w^{-1} S_w^{-1} \Gamma(\mathbf{r} - \mathbf{r}_w, \mathbf{r}_w \in S_w) \tag{2.30}$$

$$\iiint \Gamma(\mathbf{r} - \mathbf{r}_w, \mathbf{r}_w \in S_w) d^3 r = S_w \tag{2.31}$$

Homogenizing the damping behavior, one gets,

$$\Lambda = \sqrt{\frac{1}{2\sigma \vartheta J_S n_w m_w S_w}} \tag{2.32}$$

The total magnetic field is the sum of the static magnetic field and the dynamic magnetic field due to Λ. The time and space dependent magnetic field and flux density at time t and a position $\mathbf{r}$ are given by:

$$\begin{aligned} H(\mathbf{r}, t) &= H_s(\mathbf{r}, t) + H_{dyn}(\mathbf{r}, t) \\ H(\mathbf{r}, t) &= H_s(B(\mathbf{r}, t)) + \sigma \Lambda^2 \frac{\partial B}{\partial t}(\mathbf{r}, t) \end{aligned} \tag{2.33}$$

The locally induced flux density presents a delay with the local magnetic field due to the damping behavior resulting from the microscopic eddy current losses around each magnetic wall. This damping property is responsible of the so-called excess losses, increasing with the frequency.
A 3-D approach similar to the anhysteretic case can be adopted when studying the dynamic contribution. In fact, Λ has different responses from one direction to another when the anisotropy is relatively high. The damping coefficient can relatively increase or decrease based on the magnetic structure in each direction. The 3-D dynamic representation is given by the following tensor:

$$[\Lambda] = \begin{bmatrix} \Lambda_{xx} & \Lambda_{xy} & \Lambda_{xz} \\ \Lambda_{yx} & \Lambda_{yy} & \Lambda_{yz} \\ \Lambda_{zx} & \Lambda_{zy} & \Lambda_{zz} \end{bmatrix} \tag{2.34}$$

The considered behavioral law is used in this study to describe the connection at the mesoscopic scale between the local magnetic field to the flux density. It is an essential key for solving the dynamic Maxwell equation presented in the next section.

2.4 Energy Formulation

A representation of the magnetic behavior at the mesoscopic scale is presented based on an energy formulation. The derivation of time and space dependent differential Maxwell's equation for the mesoscopic magnetic field and flux density is performed. Solving these equations can be performed by including the considered behavior law with the static and dynamic contributions. The energy formulation consists in itemizing the applied energies (action) and the internal energies (reaction) based on the concept of energy conservation.

2.4.1 Electrical Work

The current density **J** representing the speed of the moving electrical charges is coupled with the electrical field $\mathbf{E}_{\text{field}}$ that provides the electromotive force which is the origin of the charges motion. The coupling of these variables gives the electrical work contained inside the material as follows:

$$E_{el} = \int \mathbf{E}_{\text{field}}.\mathbf{J}dt \tag{2.35}$$

2.4.2 Magnetic Work

The induction rate $\partial_t\mathbf{B}$ representing the magnetic charges velocity is coupled with the magnetic field **H** that provides magnetomotive force. The coupling generates the magnetic work given by:

$$E_{mag} = \int \mathbf{H}.\frac{\partial \mathbf{B}}{\partial t}dt \tag{2.36}$$

2.4.3 Lagrange Formulation

The total energy integrated in the volume Ω is the contribution of both the electrical and the magnetic energies. It gives the Lagrange energy:

$$\mathcal{L} = \int_t \int_\Omega (\mathbf{E}_{\text{field}}.\mathbf{J} + \mathbf{H}.\frac{\partial \mathbf{B}}{\partial t})d\Omega dt \tag{2.37}$$

The electromagnetic behavior at the local space is modeled using the Maxwell's equations (**Eq. 2.38**) that include both space and time dependency.

$$\begin{aligned} \nabla \times \mathbf{H} &= \mathbf{J} \\ \nabla \times \mathbf{E}_{\text{field}} &= -\frac{\partial \mathbf{B}}{\partial t} \\ \nabla.\mathbf{B} &= 0 \end{aligned} \tag{2.38}$$

Combining the set of equations **Eq. 2.38**, and considering a linear electrical behavior $\mathbf{J} = \sigma\mathbf{E}_{\text{field}}$, the following diffusion differential equation is obtained,

$$\frac{1}{\sigma}\nabla \times (\nabla \times \mathbf{H}) + \frac{\partial \mathbf{B}}{\partial t} = 0 \tag{2.39}$$

Using the Maxwell equations (**Eq. 2.38**) in the energy equation (**Eq. 2.37**),

$$\mathcal{L} = \int_t \int_\Omega \left[\frac{1}{\sigma}(\nabla \times \mathbf{H}).(\nabla \times \mathbf{H}) + \mathbf{H}.\frac{\partial \mathbf{B}}{\partial t}\right] d\Omega dt \tag{2.40}$$

Applying the integration by parts to **Eq. 2.40**,

$$\mathcal{L} = \int_t \int_\Omega \left\{\frac{1}{\sigma}[\nabla.(\mathbf{H} \times (\nabla \times \mathbf{H})) + \mathbf{H}.\nabla \times (\nabla \times \mathbf{H})] + \mathbf{H}.\frac{\partial \mathbf{B}}{\partial t}\right\} d\Omega dt \tag{2.41}$$

$$\mathcal{L} = \int_t \int_{\mathbf{S}} \frac{1}{\sigma}\mathbf{H} \times (\nabla \times \mathbf{H})d\mathbf{S}dt + \int_t \int_\Omega \mathbf{H}.\left[\frac{1}{\sigma}\nabla \times (\nabla \times \mathbf{H}) + \frac{\partial \mathbf{B}}{\partial t}\right] d\Omega dt \tag{2.42}$$

Applying Eq. 2.39 in Eq. 2.42 and Eq.2.40,

$$\int_t \int_\Omega \frac{1}{\sigma}(\nabla \times \mathbf{H}).(\nabla \times \mathbf{H})d\Omega dt + \int_t \int_\Omega \mathbf{H}.\frac{\partial \mathbf{B}}{\partial t}d\Omega dt = \int_t \int_{\mathbf{S}} \frac{1}{\sigma}\mathbf{H} \times (\nabla \times \mathbf{H})d\mathbf{S}dt \tag{2.43}$$

The left terms of **Eq. 2.43** are respectively the electrical and the magnetic energies representing the internal materials reaction due to the application of the external energy E_{app} (right term of **Eq. 2.43**) that is supplied by an external magnetic field and that takes effect on the material's surface. This leads to the following energy conservation: the applied external energy on the surface of the body generates magnetic and electrical volume energies.

$$E_{el} + E_{mag} = E_{app} \tag{2.44}$$

2.5 Unidirectional Diffusion

2.5.1 1D Case: Problem

The 1D case is a simple application of the magnetic problem described in Section 2.4, describing the magnetic sheet's behavior insite the Single Sheet Tester. A unidirectional magnetic field $H(\pm\frac{h}{2}, t) = H_a(t)$ is applied on the surface of the sheet as shown in **Fig. 2.5**. In this case, the complexity of the problem is reduced to a 1D analysis thanks to the following contributions:

1. The geometry is symmetric with respect to the xy plane in the SST.
2. The in-plane dimensions are more significant than the thickness.
3. The applied magnetic field in the x direction is symmetric with respect to the xy-plane and uniform on the surface.
4. Measurements are only collected in the x direction.

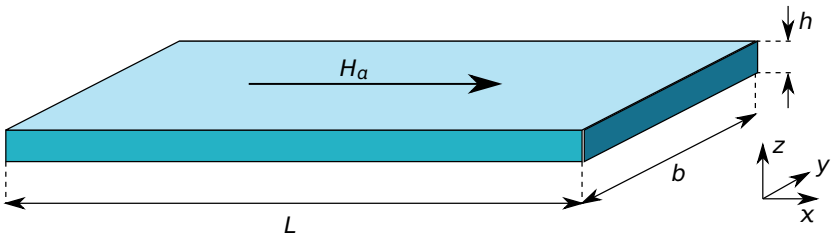

Fig. 2.5 1D Case.

When the surface magnetic field is applied in the x direction, the magnetization occurs in all directions due to the anisotropy energy. However, we only consider the magnetization in the lamination direction (x direction) because measurements are only provided in the longitudinal direction. The horizontal variables vary with the sheet's cross-section (z direction). The 3D Maxwell's equation (**Eq. 2.43**) is reduced to a 1D diffusion equation (**Eq. 2.45**). 1D power equations with two local variables $B(z,t)$ and $H(z,t)$ are obtained:

- Maxwell's Equation

$$\frac{1}{\sigma}\frac{\partial^2 H}{\partial z^2} = \frac{\partial B}{\partial t} \tag{2.45}$$

- Boundary Conditions

$$H(\pm\frac{h}{2}, t) = H_a(t) \tag{2.46}$$

- Electrical Power:

$$P_{el} = bL\int_{-\frac{h}{2}}^{\frac{h}{2}} \frac{1}{\sigma}\frac{\partial H}{\partial z}.\frac{\partial H}{\partial z}dz \tag{2.47}$$

- Magnetic Power:

$$P_{mag} = bL \int_{-\frac{h}{2}}^{\frac{h}{2}} H.\frac{\partial B}{\partial t} dz \tag{2.48}$$

- Applied Power:

$$P_{app} = bL \left[\frac{1}{\sigma} H.\frac{\partial H}{\partial z} \right]_{-\frac{h}{2}}^{\frac{h}{2}} \tag{2.49}$$

Due to the symmetry, $H(\frac{h}{2}, t) = H(-\frac{h}{2}, t) = H_a(t)$ and $\frac{\partial H}{\partial z}(\frac{h}{2}, t) = -\frac{\partial H}{\partial z}(-\frac{h}{2}, t)$, the applied energy becomes:

$$P_{app} = \frac{bL}{\sigma}.H_a(t).\left[\frac{\partial H}{\partial z} \right]_{-\frac{h}{2}}^{\frac{h}{2}} = \frac{bL}{\sigma}.H_a(t).\int_{-\frac{h}{2}}^{\frac{h}{2}} \frac{\partial^2 H}{\partial z^2} dz \tag{2.50}$$

Using the 1-D Maxwell's equation (**Eq. 2.45**) and the average relation $B_{av}(t) = \frac{1}{h}\int_{-\frac{h}{2}}^{\frac{h}{2}} B(z,t)dz$, the applied power becomes:

$$P_{app} = bL.H_a(t).\int_{-\frac{h}{2}}^{\frac{h}{2}} \frac{\partial B}{\partial t} dz = bLh.H_a(t).\frac{\partial B_{av}}{\partial t} \tag{2.51}$$

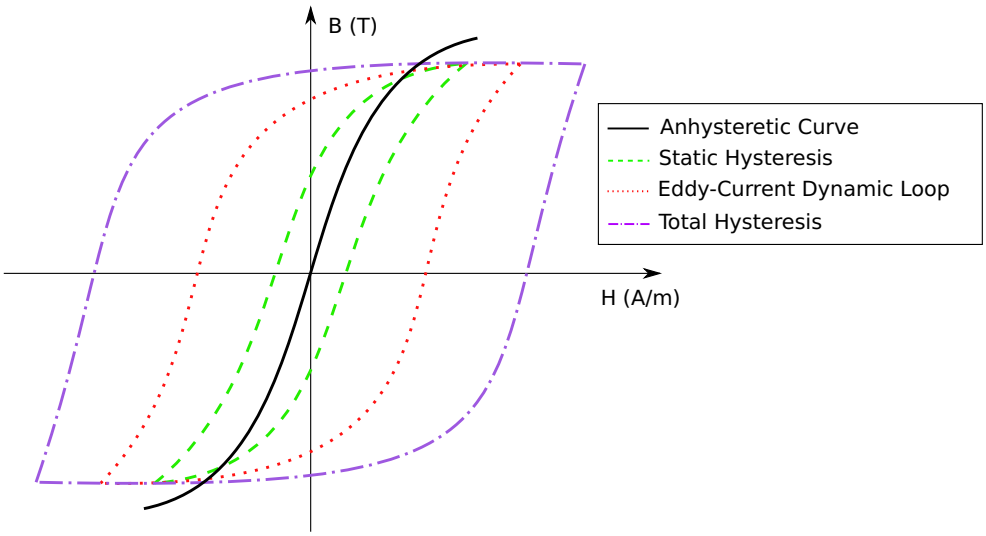

Fig. 2.6 Schematic hysteresis loops with static and dynamic magnetizations.

2.5.2 Power Sorting

Solving the Maxwell integral equation that contains two variables $B(z,t)$ and $H(z,t)$ requires the knowledge of a behavior law that connects the local induction to the local magnetic field.

$$H(z,t) = H_s(B(z,t)) + \sigma\Lambda^2\left(B, \frac{\partial B}{\partial t}\right)\frac{\partial B}{\partial t}(z,t) \tag{2.52}$$

Replacing the behavior law (**Eq. 2.52**) in the energy equation, we get:

$$bL\int_{-\frac{h}{2}}^{\frac{h}{2}} \frac{1}{\sigma}\left(\frac{\partial H}{\partial z}\right)^2 dz + bL\int_{-\frac{h}{2}}^{\frac{h}{2}} H_s(t)\frac{\partial B}{\partial t}dz + bL\int_{-\frac{h}{2}}^{\frac{h}{2}} \sigma\Lambda^2\left(\frac{\partial B}{\partial t}\right)^2 dz = bLhH_a(t)\frac{\partial B_{av}}{\partial t} \tag{2.53}$$

$$P_{el} + P_{stat} + P_{exc} = P_{app} \tag{2.54}$$

The total supplied power is equal to the sum of the electrical power (eddy current power) P_{el} (**Fig. 2.6**), the area between the green and red loops), the static power due to the static irreversibilities P_{stat} (**Fig. 2.6**), green loop's area) and the excess losses due to the local damping contribution P_{exc} (**Fig. 2.6**), area between the red and purple loops). The applied power P_{app} is the hysteresis loop between the applied field and the average induction, macroscopic variables that can be determined experimentally.

2.5.3 1-D Case: Analytical Solution

We present the analytical linear solution of the diffusion equation with a sinusoidal input/output system. Assuming that the static and the dynamic properties are independent of the magnetic variables and neglecting the static losses, the diffusion differential equation is analytically solved thanks to the linearity of the model and the behavior law. A transformation of the transient equations of **Eq. 2.45** and **Eq. 2.46** to the frequency domains is considered and a dispersion relation is obtained using the Fourier time and space transform [9]. The permeability μ is the static linear property ($B = \mu H_s$). The behavior law is then given by,

$$H = \mu^{-1}B + \sigma\Lambda^2\partial_t B \tag{2.55}$$

The time and space (x, t) dependent equation is converted to a (k, ω) space using the Fourier Transform, we get the following dispersal equation:

$$k^2(1 + j\omega\sigma\mu\Lambda^2) + j\omega\sigma\mu = 0 \tag{2.56}$$

k is the wave vector and ω the angular velocity related to the exciting frequency by $\omega = 2\pi f$. The solution of the dispersal equation gives the following: k is a complex number in the form $k = k_- - jk_+$ where,

$$k_\pm(\mu,\Lambda,\sigma,\omega) = \sqrt{\frac{1}{2}\left(\frac{\mu\sigma\omega}{1+(\sigma\Lambda^2\mu\omega)^2}\right)\left(\pm\sigma\Lambda^2\mu\omega + \sqrt{1+(\sigma\Lambda^2\mu\omega)^2}\right)} \tag{2.57}$$

The complex magnitude of the local magnetic flux density $\tilde{B}(z,\omega)$, solution of **Eq. 2.45** with the boundary conditions (**Eq. 2.46**) can be expressed by:

$$\tilde{B}(z) = \frac{\mu\tilde{H_a}}{1+j\sigma\Lambda^2\mu\omega}\frac{\cosh[(k_+ + jk_-)z]}{\cosh[(k_+ + jk_-)h/2]} = |\tilde{B}(z)|e^{j\varphi} \tag{2.58}$$

Therefore, the average flux density is eventually obtained.

$$\tilde{B}_{av} = \frac{1}{h}\int_{-\frac{h}{2}}^{-\frac{h}{2}} \tilde{B}(z)dz = \frac{2\mu\tilde{H_a}}{h(k_+ + jk_-)(1+j\sigma\Lambda^2\mu\omega)}\tanh((k_+ + jk_-)\frac{h}{2}) \tag{2.59}$$

2.5.4 Adaptation of the Dispersion Equation with the SST

Measurements performed in the Single Sheet Tester (SST) consist in measuring the applied magnetic field for a specific average induction signal specified by the user with a specific amplitude and exciting frequency. The problem considers the inversion of **Eq. 2.59**.

$$\tilde{H}_a = \frac{h(k_+ + jk_-)(1 + j\sigma\Lambda^2\mu\omega)}{2\mu\tanh((k_+ + jk_-)h/2)}\tilde{B}_{av} \tag{2.60}$$

The determination of the surface magnetic field (**Eq. 2.60**) allows the calculation of the local flux density's complex magnitude using **Eq. 2.58**, and derives a time response of this variable:

$$B(z,t) = |\tilde{B}(z)|\cos(\omega t + \varphi) \tag{2.61}$$

The proposed analytical solution calculates the local dynamic behavior based on the knowledge of the magnetic properties and a given average magnetic field. It is also the key for determining the effect of the magnetic properties on the dynamic local response (section 2.5.6).

2.5.5 1-D Case: Sensitivity of the Measured Signals

In this section, we present the effect that produces the static property μ and the dynamic property Λ on the magnetic field signal $H_a(t)$ when applying the same induction signal $B_{av}(t)$. The purpose of the study is to understand modification of the dynamic response when changing the magnetic properties. The effect of the permeability μ on the hysteresis loop is shown in **Fig. 2.7a**, and its effect on the magnetic field response is illustrated in **Fig. 2.8a**. An increase of the permeability increases the hysteresis cycle's slope and a decrease in the magnetic field's magnitude. On the other hand, the dynamic property Λ effect is studied in **Fig. 2.7b** and **Fig. 2.8b**. The hysteresis loops have the same slope but the hysteresis width increases with Λ, creating a higher excessive loss. Furthermore, the time response of the magnetic field shows a time delay increase with Λ. In fact, the dynamic property represents the magnetic damping property of the material that describes the microscopic dynamic behavior: a damping means a lower walls velocity, fewer domains and a lower mobility. At $\Lambda = 0$ μm, a small hysteresis persists, it is due to the eddy-current losses.

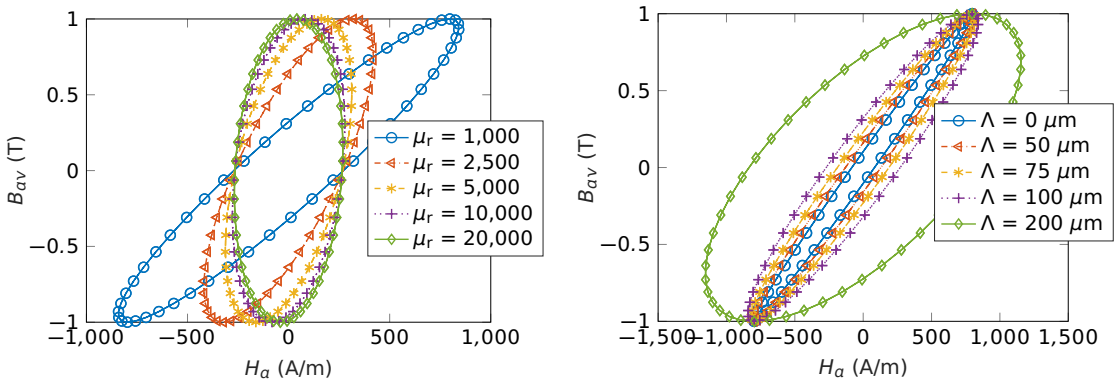

(a) Influence of the permeability.

(b) Influence of Λ.

Fig. 2.7 Hysteresis loop modification with the magnetic properties. (Model)

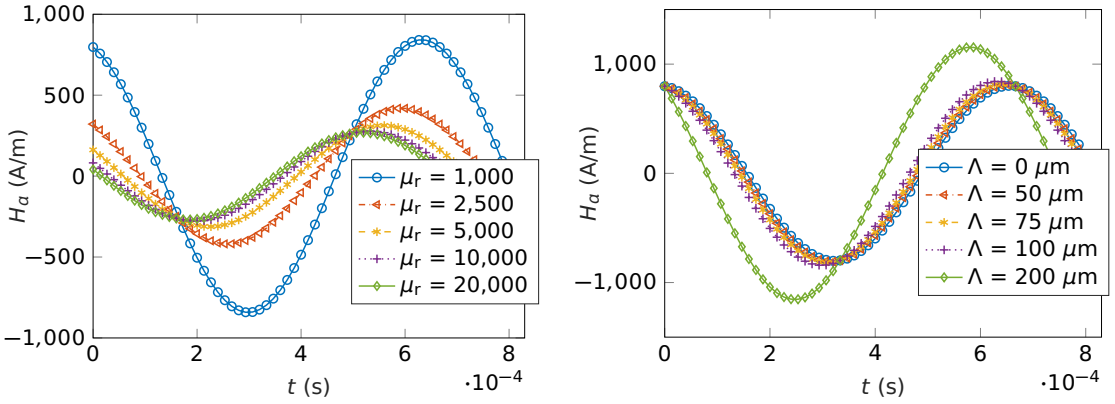

(a) Influence of the permeability. **(b)** Influence of Λ.

Fig. 2.8 Transient response of the applied magnetic field for the same induction. (Model)

2.5.6 Sensitivity of the Dynamic Response

The transient response of the flux density is calculated for different static μ and dynamic Λ properties using the linear analytical approach developed in section 2.5.3. This parametric study helps to understand the effect of magnetic properties and eventually the effect of the laser treatment sensitive to the magnetic properties. The reference parameters are: the thickness $h = 0.23\ mm$, the average induction magnitude $|\tilde{B}_{av}| = 1\ T$, the induction angle 0 rad, the exciting frequency $f = \omega/2\pi = 1{,}000$ Hz and the electrical conductivity $\sigma = 2.10^6\ (\Omega.m)^{-1}$. The variable parameters are the relative permeability $\mu_r = \mu/\mu_0$ and the dynamic property Λ. The effect of the static property μ_r and the dymanic property Λ in terms of magnitude and delay is observed by comparing the local induction with the average induction with respect to the magnetic field on one hand (**Fig. 2.9** and **Fig. 2.10**), and with respect to the average induction on the other hand (**Fig. 2.11** and **Fig. 2.12**).

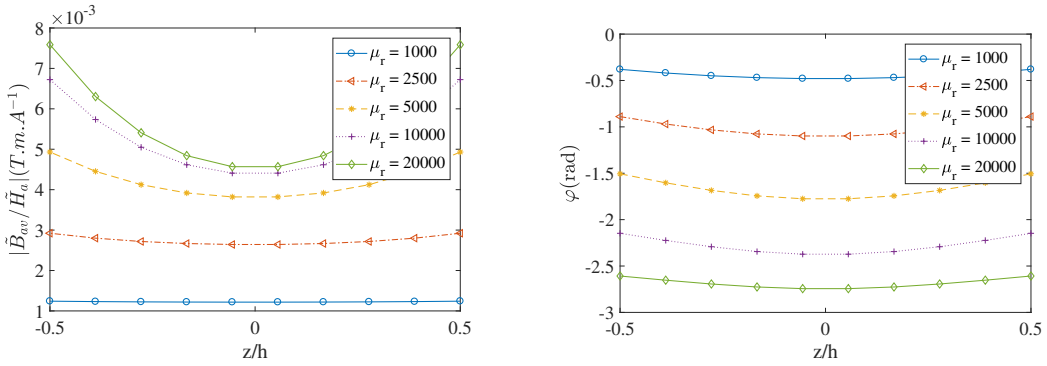

(a) Magnitude distribution **(b)** Delay distribution

Fig. 2.9 Effect of μ_r on the calculated flux density distribution with respect to the applied magnetic field.

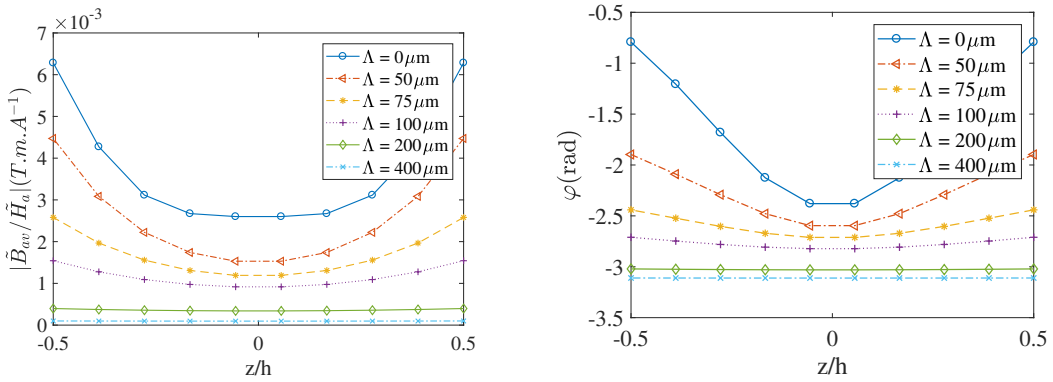

(a) Magnitude distribution **(b)** Delay distribution

Fig. 2.10 Effect of Λ on the calculated flux density distribution with respect the applied magnetic field.

The increase of the permeability induces an increase in the dispersion of the flux density profile (skin effect) as shown in Fig. 2.9. The magnitude and the delay of the induction with respect to the magnetic field increase. On the other hand, the decrease of the dynamic property (domains refinement) leads to an increase in the profile's dispersion with respect to the magnetic field as shown in Fig. 2.10. The magnitude increases and the induction's delay with respect to the magnetic field decreases when decreasing Λ.
Fig. 2.11 and Fig. 2.12 plot the distribution of the magnitude and the angle of the flux density in the cross section for different values of μ_r and Λ and with respect to the average induction. The increase of the permeability induces an increase in the dispersion of the flux density magnitude profile (Fig. 2.11a) and an increase in the dispersion of the flux density phase profile for a limit of $\mu_r = 5,000$ then a decrease of the profile dispersion (Fig. 2.11b). On the other hand, the decrease of the dynamic property leads to an increase in the magnitude dispersion with an optimum at Λ=100μm followed by a decrease (Fig. 2.12a). As for the angle between the local and the average induction, its profile is more dispersed when Λ decreases (Fig. 2.12b).

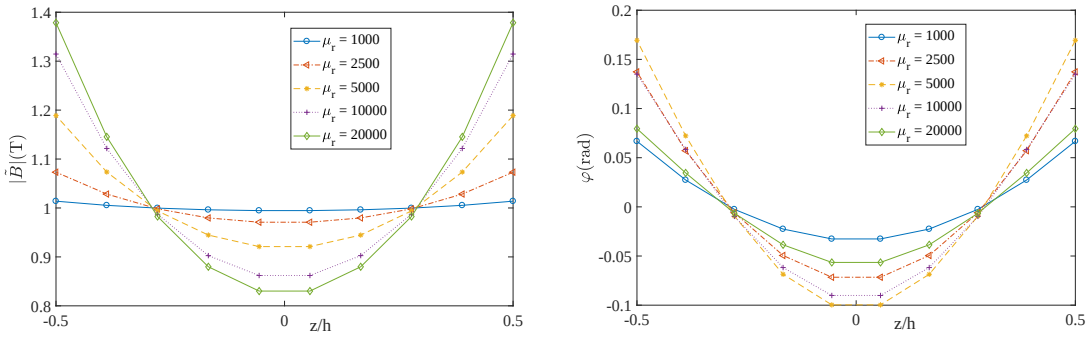

(a) Magnitude distribution (around 1 T) **(b)** Delay distribution (around 0 rad)

Fig. 2.11 Effect of μ_r on the calculated flux density distribution in the cross section.

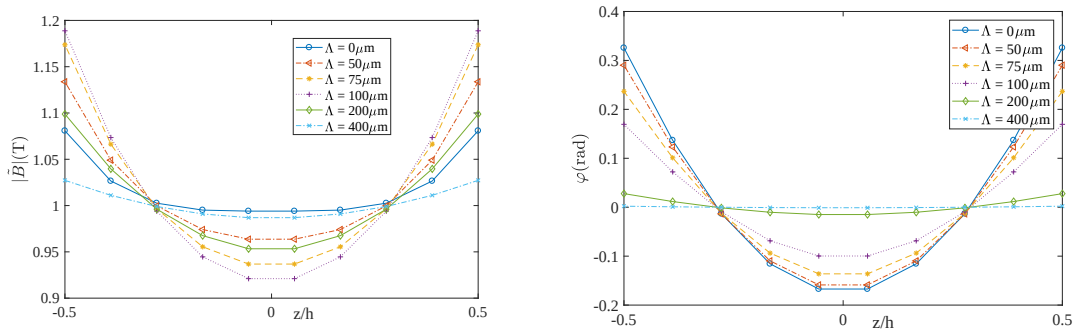

(a) Magnitude distribution (around 1 T) **(b)** Delay distribution (around 0 rad)

Fig. 2.12 Effect of Λ on the calculated flux density distribution in the cross section.

2.6 Conclusion

In this chapter, the static and dynamic modeling techniques adopted for the magnetic behavior are presented. The model methodology coupled with experimental measurements is described in deliverable 3.4 in order to identify the magnetic properties that describe the behavior of a measured sample, using a simple 1D model. In the next chapter, we present the models that describes the magneto-mechanical aspect of magnetic materials.

Chapter 3

Magneto-Mechanical Modeling

3.1 Introduction

The different magnetic factors responsible of the mechanical excitation and vibration in electrical steels are presented and described in this chapter. The contribution of each magnetic source can vary from one application to another. The potential sources are the following:

- **Lorentz force:** this force is due to the interaction between the magnetization and the electrical excitation represented by the charges of moving particles. The determination of these forces can be directly calculated from the magnetic model, once the induction and the current density distributions are known. The Lorentz force is expressed by,

$$\mathbf{f}_L = \mathbf{J} \times \mathbf{B} \tag{3.1}$$

  In a thin plate, this force is more important in the surface's normal direction where the transverse vibration is more significant than the longitudinal deformation.

- **Maxwell force:** this type of force is mainly found at the material's interface, and its effect is amplified in the airgap between two magnetic materials in rotating machines and inductors for example. This surface force corresponds to a pressure applied at the interface between two materials with different permeabilities (e.g. electrical steel vs air). Similarly, this force can be directly determined when the induction's gradient is known.

- **Magnetostriction:** it is the deformation of the magnetic material when subjected to a magnetic field. Magnetostriction is a property of the material defining the magneto-elastic coupling characteristic. It induces a behavior similar to that of the thermal expansion. The determination of the magnetostriction is not so obvious because it is an intrinsic characteristic and it depends on the magnetic domain structure. Therefore, this property is identified by measurements. We can define a model that represents the magnetostrictive behavior as function of the induction.

3.2 Contribution of the Acting Forces on Vibration in Electrical Machines

Different studies on transfomers, inductors and electrical machines have been carried out in order to determine the forces' effects on the vibration of the structure. The contribution of the Maxwell forces and magnetostriction has been mainly considered. In fact, Maxwell forces inside the material are neglected, but they are significant on the interface between air and the material due to the high variation of magnetization between air and the magnetic material [37]. Maxwell forces are especially effective with the presence of airgaps in electrical machines. For transformers, where closed circuit is considered, the effect of Maxwell forces compared with magnetostriction is neglected because no airgap is considered. Rossi and Le Besnerais [38] have analyzed in the case of a inductor with airgap the cancellation effects of the overall magnetic forces due to magnetostriction and Maxwell forces and have developed a model to better understand how to compensate Maxwell and magnetostrictive forces and reduce vibrations. They also showed that there is no general rule regarding the contribution of magnetostriction and Maxwell forces. In the case of rotating machines, the Maxwell forces are mainly dominant in the iron-air interface where rigid body displacements and elastic deformations of the structure occur at the same time, as for magnetostriction, only deformation of the structure's material occurs. Pellerey [39] and Hallal [40] neglected the effect of magnetostriction on the vibration of rotating machines in front of the Maxwell forces that were treated carefully.

3.3 The Maxwell's Forces

The Maxwell's forces are due to the variation in magnetization through a specific volume. In electrical steels, the Maxwell's forces appear in two ways: the volume forces $\mathbf{f}_{\text{mag}}$ due to the induction gradient, and the surface forces $\mathbf{F}_{\text{mag}}$ due to the sudden permeability change between the material and the air. The total Maxwell's forces, known as the electromagnetic forces, are given by,

$$\mathbf{f}_{\text{em}} = \iiint_{\Omega} \mathbf{f}_{\text{mag}} d\Omega + \iint_{S} \mathbf{F}_{\text{mag}} dS \tag{3.2}$$

The volume force $\mathbf{f}_{\text{mag}}$ integration can be expressed as an equivalent surface force using the gradient theorem (**Fig. 3.1**).

3.3.1 Application on a Plate without Airgap

In this study, we consider the Maxwell's forces in the case of a simple plate subjected to a uniform surface magnetic field. The considered plate is subjected to a magnetic field in a specific region of space (**Fig. 3.2**). In fact, the chosen configuration represents the 1D field diffusion studied in section 2.5 of chapter 2.

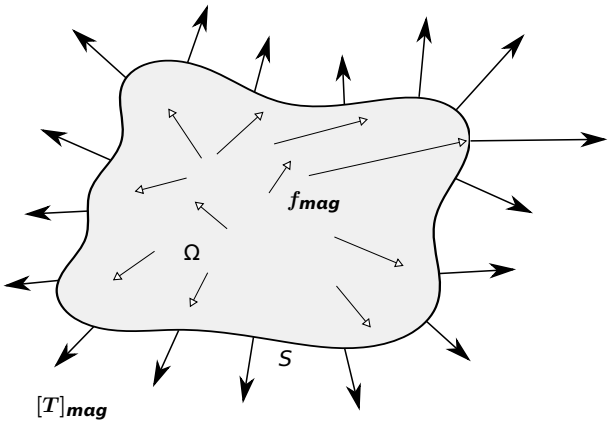

Fig. 3.1 The volume forces $\mathbf{f}_{\text{mag}}$ and the equivalent surface forces $[\mathbf{T}]_{\text{mag}}$.

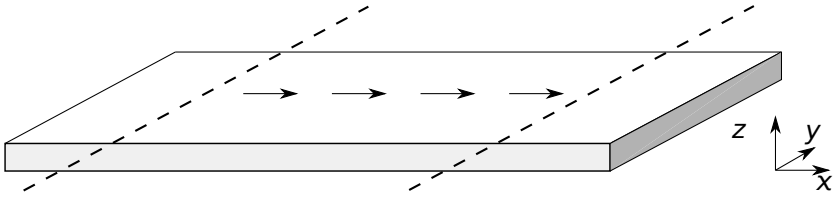

Fig. 3.2 Magnetic plate subjected to an in-plane magnetic field.

Body force

The volume force due to the magnetization variation is given by the following gradient relation[41, 42, 43, 44, 45, 46]:

$$\mathbf{f}_{\text{mag}} = \nabla \mathbf{B}.\mathbf{M} = \frac{1}{2\mu_0}\nabla \mathbf{B}^2 \tag{3.3}$$

Using the Gradient theorem on the volume Ω and the surface S:

$$\iiint_{\Omega} \frac{1}{2\mu_0}\nabla \mathbf{B}^2 d\Omega = \iint_{S} \frac{1}{2\mu_0}\mathbf{B}^2 d\mathbf{S} \tag{3.4}$$

Therefore, the equivalent surface forces on the upper and the lower plate's surfaces are:

$$\mathbf{T}_{\uparrow} = \frac{1}{2\mu_0}\mathbf{B}^2(\frac{h}{2})\mathbf{n}_{\uparrow} = \frac{\mathbf{B}.\mathbf{M}}{2}\mathbf{n}_{\uparrow} \tag{3.5}$$

$$\mathbf{T}_{\downarrow} = \frac{1}{2\mu_0}\mathbf{B}^2(-\frac{h}{2})\mathbf{n}_{\downarrow} = -\mathbf{T}_{\uparrow} = \frac{\mathbf{B}.\mathbf{M}}{2}\mathbf{n}_{\downarrow} \tag{3.6}$$

$\mathbf{n}_\uparrow$ and $\mathbf{n}_\downarrow$ are the normal vectors of the upper and the lower surfaces respectively. When the magnetic field is the same, both surface forces are equal in magnitude but opposite in orientation. The corresponding stress tensor at any surface becomes:

$$[\mathbf{T}]_{\text{mag}} = \begin{bmatrix} \frac{\mathbf{B}.\mathbf{M}}{2} & 0 \\ 0 & \frac{\mathbf{B}.\mathbf{M}}{2} \end{bmatrix} \tag{3.7}$$

On the other hand, the horizontal body force is equal to zero. In fact, considering a uniform horizontal magnetization, the gradient of the induction $\nabla\mathbf{B}$ is equal to zero. The equivalent surface forces oriented to the right $\mathbf{T}_\rightarrow$ and to the left $\mathbf{T}_\leftarrow$ in the longitudinal direction are:

$$\mathbf{T}_\rightarrow = \mathbf{T}_\leftarrow = \mathbf{0} \tag{3.8}$$

In reality the horizontal body force exists due to the variation of the induction. But this variation is local at the transition position between the magnetized and the non-magnetized zone. This variation induces negligible force.

Surface Force

Another force is applied on the surface force between the material and air and is due to the discontinuity between both media and is considered as a pressure force perfomed on the surface. The surface force $\mathbf{F}_\uparrow$ and $\mathbf{F}_\downarrow$ on the upper and the lower surfaces is given by [47]:

$$\mathbf{F}_\uparrow = \left(\frac{\left(B_n^+\right)^2}{2\mu_0} - \frac{\left(B_\tau^+\right)^2}{2\mu_0} \right) \mathbf{n}_\uparrow - \left(\frac{\left(B_n^-\right)^2}{2\mu_0} - \frac{\left(B_\tau^-\right)^2}{2\mu_0} \right) \mathbf{n}_\uparrow \tag{3.9}$$

$$\mathbf{F}_\downarrow = \left(\frac{\left(B_n^+\right)^2}{2\mu_0} - \frac{\left(B_\tau^+\right)^2}{2\mu_0} \right) \mathbf{n}_\downarrow - \left(\frac{\left(B_n^-\right)^2}{2\mu_0} - \frac{\left(B_\tau^-\right)^2}{2\mu_0} \right) \mathbf{n}_\downarrow = -\mathbf{F}_\uparrow \tag{3.10}$$

n and τ correspond to the normal and the tangentiel components. The sign + and − correspond respectively to the magnetized material and air. The magnetic continuity conditions are:

$$\begin{aligned} B_n^+ &= B_n^- \\ H_\tau^+ &= H_\tau^- \end{aligned} \tag{3.11}$$

Using **Eq. 3.11**, **Eq. 3.9** and **Eq. 3.10** become:

$$\mathbf{F}_\uparrow = \left[-\frac{\left(B_\tau^+\right)^2}{2\mu_0} + \frac{\mu_0}{2}\left(H_\tau^+\right)^2 \right] \mathbf{n}_\uparrow \tag{3.12}$$

$$\mathbf{F}_\downarrow = \left[-\frac{\left(B_\tau^+\right)^2}{2\mu_0} + \frac{\mu_0}{2}\left(H_\tau^+\right)^2 \right] \mathbf{n}_\downarrow \tag{3.13}$$

Now working in the xz plane, the total magnetic tension force (**Fig. 3.3**) applied on the upper and the lower surfaces is given by:

$$q_z(x, \frac{h}{2}) = \int_0^{\frac{h}{2}} \left[f_{z-mag}(x,z)dz + F_{z-mag}(x, \frac{h}{2}) \right] dz \tag{3.14}$$

$$q_z(x,-\frac{h}{2}) = \int_{-\frac{h}{2}}^{0} \left[f_{z-mag}(x,z)dz + F_{z-mag}(x,-\frac{h}{2}) \right] dz \tag{3.15}$$

f_{z-mag} and F_{z-mag} are the z components of the volume and surface forces $\mathbf{f}_{mag}$ and $\mathbf{F}_{mag}$ respectively. Using **Eq. 3.5**, **Eq. 3.6**, **Eq. 3.12** and **Eq. 3.13**, **Eq. 3.14** and **Eq. 3.15** become,

$$q_z(x,\frac{h}{2}) = \frac{1}{2}B_z(x,\frac{h}{2})M_z(x,\frac{h}{2}) - \frac{1}{2}H_x(x,\frac{h}{2})M_x(x,\frac{h}{2}) \tag{3.16}$$

$$q_z(x,-\frac{h}{2}) = \frac{1}{2}B_z(x,-\frac{h}{2})M_z(x,-\frac{h}{2}) - \frac{1}{2}H_x(x,-\frac{h}{2})M_x(x,-\frac{h}{2}) \tag{3.17}$$

In general, when the surface magnetic field is horizontal, the transverse components B_z, M_z and H_z is neglected. Furthermore, for a uniform magnetiz ation in the x direction, the transverse forces become:

$$q_z(\frac{h}{2}) = -\frac{1}{2}H_x(\frac{h}{2})M_x(\frac{h}{2}) \tag{3.18}$$

$$q_z(-\frac{h}{2}) = -\frac{1}{2}H_x(-\frac{h}{2})M_x(-\frac{h}{2}) \tag{3.19}$$

We also define the axial load N_x applied on the plate due to the Maxwell's stresses:

$$N_x(x) = -\int_x^L \int_{-\frac{h}{2}}^{\frac{h}{2}} f_{x-mag}(x,z)dzdx \approx 0 \tag{3.20}$$

f_{x-mag} and F_{x-mag} are the x components of the volume and surface forces $\mathbf{f}_{\text{mag}}$ and $\mathbf{F}_{\text{mag}}$ respectively.
The total Maxwell force contribution shown in **Eq. 3.18** and **Eq. 3.19** is negligible in front of the magnetostriction for the considered configuration. For a magnetic structure without any airgap, the magnetostriction is the only magnetic source of vibration.

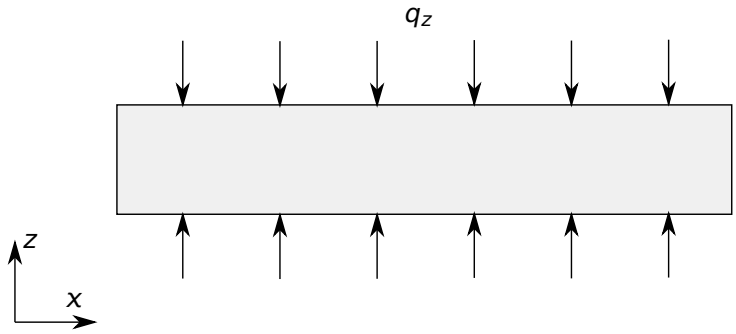

Fig. 3.3 Balance of magnetic loads.

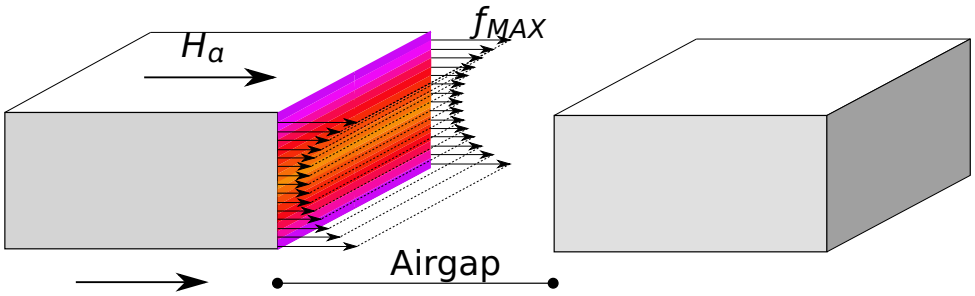

Fig. 3.4 Maxwell surface force in the airgap between two magnetic materials.

3.3.2 Application on a Structure with Airgap

Now considering a structure with an airgap, an in-plane magnetic field is applied on the structure's surface. A significant Maxwell force is generated in the interface between the material and the air as shown in **Fig. 3.4**.
In this case, due to the surface magnetic field and the diffusion behavior described in chapter 2, an induction gradient is obtained (colored cross-section in **Fig. 3.4**) and it is responsible for the generation of a Maxwell force's gradient (arrows in **Fig. 3.4**). The Maxwell force per surface unit f_{em} is equal to $\frac{B^2}{2\mu_0}$. The global surface force for a plate with a thickness h and a width b is given by:

$$f_{\text{em}}(t) = b\int_{-\frac{h}{2}}^{\frac{h}{2}} \frac{B^2}{2\mu_0}(z,t)dz = bh\frac{< B^2 >}{2\mu_0}(t) \tag{3.21}$$

For a specific space position, the Maxwell force is proportional to the square of the induction; a parabola is obtained. However, at the macroscopic scale (**Eq. 3.21**), the parabola includes a phase shift called the magneto-mechanical hysteresis. It is due to the diffusion effect generated in the cross section. In fact, the induction distribution in the thickness is non-uniform as mentioned in chapter 2 due to the presence of the eddy currents and the dynamic property Λ, and as shown **Fig. 3.4**. Using the diffusion equation analysis, the time dependent $B^2(z,t)$ can be obtained from $B(z,t)$. Then, $B^2(z,t)$ is averaged and plotted as function of the average of $B(z,t)$. The calculation strategy is the same as the one performed in section 2.5.3 of chapter 2. The calculated local induction $B(z,t)$ is given by:

$$B(z,t) = |\tilde{B}(z)|\cos(\omega t + \varphi) \tag{3.22}$$

And the time dependent average of the squared induction becomes:

$$< B^2 > (t) = \frac{1}{h}\int_{-\frac{h}{2}}^{\frac{h}{2}} B^2(z,t)dz \tag{3.23}$$

The difference between the squared average induction and the average of the squared induction, showing the effect in the mesoscopic and the macroscopic scales is illustrated in **Fig. 3.5**. It is shown that the square of the average is different than the average of the square:

$$< B^2 > \neq < B >^2 \tag{3.24}$$

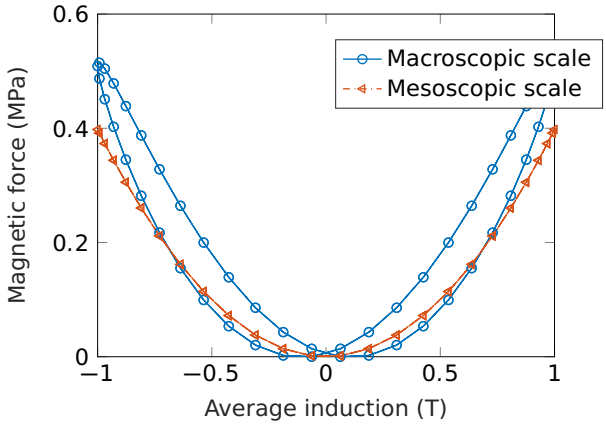

Fig. 3.5 Calculation of the magnetic force behavior at the mesoscopic (red) and the macroscopic (blue) scale for 1 T, 1500 Hz and $\Lambda = 60$ μm.

A change in the force amplitude is noticed with a factor β and the generation of a time delay τ_d between the strain and the induction. The relationship between the Maxwell force f_{em} and the average induction is given in the following macroscopic first order differential equation for a specific induction amplitude and frequency:

$$f_{em} + \tau_d \frac{df_{em}}{dt} = \beta \frac{< B >^2}{2\mu_0} \tag{3.25}$$

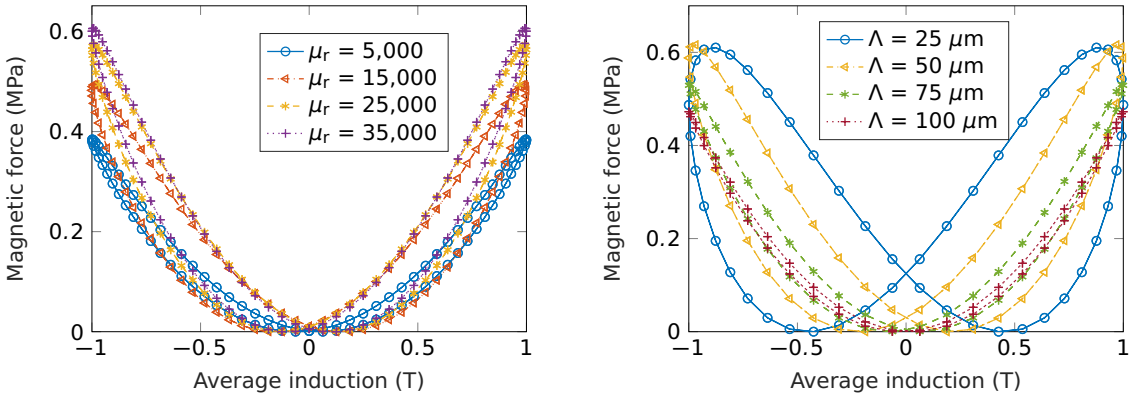

(a) On the permeability μ at 1 T, 1,500 Hz and Λ =50 μm.

(b) On the Damping property Λ at 1 T, 1,500 Hz and $\mu_r = 16,000$.

Fig. 3.6 Calculation of the magnetic force dependence on the magnetic properties.

Theoretical calculation of the amplification factor β

Based on the linear study performed on the diffusion in section 2.5.3. In this part, the average squared induction is expressed as function of the squared average induction. Combining **Eq. 2.58** and **Eq. 2.59**, one gets:

$$\frac{\tilde{B}(z)}{\tilde{B}_{av}} = \frac{h}{2} \frac{\cosh\left[(k_+ + jk_-)\, z\right]}{\sinh\left[(k_+ + jk_-)\, \frac{h}{2}\right]} \tag{3.26}$$

The squared modulus and the angle are:

$$Mod(z) = \frac{h^2}{4}\left(k_+^2 + k_-^2\right)\frac{\cosh^2(k_+ z) - \sin^2(k_- z)}{\cosh^2\left(k_+\frac{h}{2}\right) - \cos^2\left(k_-\frac{h}{2}\right)} \tag{3.27}$$

and

$$\phi(z) = \tan^{-1}\frac{k_+}{k_-} - \tan^{-1}\frac{\tanh\left(k_+\frac{h}{2}\right)}{\tan\left(k_-\frac{h}{2}\right)} + \tan^{-1}\left(\tanh(k_+ z)\tan(k_- z)\right) = \phi_1 + \phi_2(z) \tag{3.28}$$

The time response of the squared induction at a position z is:

$$\begin{aligned}\frac{B^2(z)}{B_{av}^2} &= Mod(z)\left(\frac{1+\cos(4\pi f t + 2\phi_1 + \phi_2(z)}{2}\right)\\ = \frac{h^2}{8}\left(k_+^2 + k_-^2\right))\frac{\cosh^2(k_+ z) - \sin^2(k_- z)}{\cosh^2\left(k_+\frac{h}{2}\right) - \cos^2\left(k_-\frac{h}{2}\right)}&\left(1 + \cos(4\pi f t + 2\phi_1)\frac{1-\tanh^2(k_+ z)\tan^2(k_- z)}{1+\tanh^2(k_+ z)\tan^2(k_- z)}\right)\\ &- \sin(4\pi f t + 2\phi_1)\frac{2\tanh(k_+ z)\tan(k_- z)}{1+\tanh^2(k_+ z)\tan^2(k_- z)}\end{aligned} \tag{3.29}$$

Average the squared induction:

$$\begin{aligned}\frac{< B^2 >}{B_{av}^2} = \frac{h^2}{8}&\frac{k_+^2 + k_-^2}{\cosh^2\left(k_+\frac{h}{2}\right) - \cos^2\left(k_-\frac{h}{2}\right)}\left[\frac{\sinh(k_+ h)}{2k_+} + \frac{\sin(k_- h)}{2k_-}\right.\\ &+ \left(h/2 + \frac{k_+\cos(k_- h)\sinh(k_+ h) + k_-\cosh(k_+ h)\sin(k_- h)}{2(k_+^2 + k_-^2)}\right)\cos(4\pi f t + 2\phi_1)\\ &\left.- \left(\frac{k_+\sin(k_- h)\cosh(k_+ h) - k_-\sinh(k_+ h)\cos(k_- h)}{2(k_+^2 + k_-^2)}\right)\sin(4\pi f t + 2\phi_1)\right]\end{aligned} \tag{3.30}$$

$$\frac{< B^2 >}{B_{av}} = \alpha\left(a_0 + a_1\cos(4\pi f t + 2\phi_1) + a_2\sin(4\pi f t + 2\phi_1)\right) \tag{3.31}$$

The amplification factor β is given

$$\beta = \alpha\sqrt{a_1^2 + a_2^2} = \frac{h}{4}\frac{\sqrt{k_+^2 + k_-^2}\sqrt{\left[k_+ h + \cos(k_- h)\sinh(k_+ h)\right]^2 + \left[k_- h + \sin(k_- h)\cosh(k_+ h)\right]^2}}{\cosh k_+ h - \cos k_- h} \tag{3.32}$$

Impact of the Diffusion at the Macroscopic Scale

The effect of the magnetic parameters (the relative permeability $\mu_r = \mu/\mu_0$ and the dynamic property Λ) on the B-squared response in the linear case is investigated in this section. We consider the following reference parameters: the thickness h =0.27 mm, the average induction magnitude $|\tilde{B}_{av}|$ =1 T, the induction angle 0 rad and the electrical conductivity σ =2.10^6 $(\Omega.m)^{-1}$. **Fig. 3.6a** and **Fig. 3.6b** show the butterfly loops of the averaged squared induction as function of the average induction.

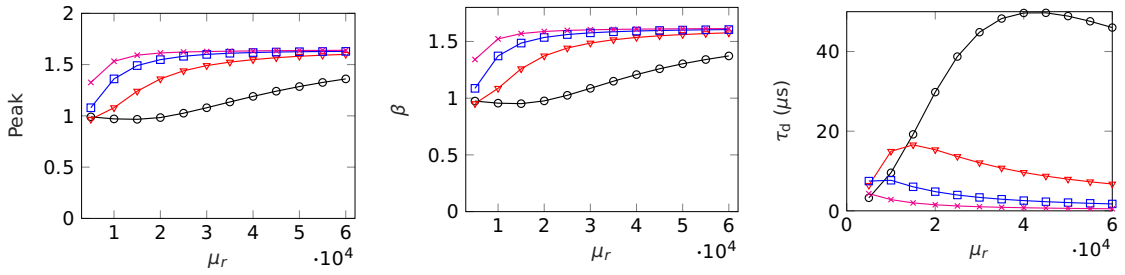

(a) Peak-To-Peak. **(b)** Amplification factor. **(c)** Time Delay.

Fig. 3.7 Dependence on the permeability at 1 T and $\Lambda = 50$ μm. [$f = 500$ Hz $f = 1,500$ Hz $f = 3,000$ Hz $f = 5,500$ Hz]

Fig. 3.7 plots the permeability effect on the force peak value, the amplification factor β and the time delay for different frequencies. Fig. 3.8 plots the Λ effect on these properties. The magnetic properties modify the loop's width and maximal amplitude. The increase of the permeability increases the loop's amplitude in all cases. In parallel, the amplification factor β increases with the permeability. As for the loop's hysteresis (time delay), it first increases till reaching its maximum and it then decreases for the 500 Hz and the 1,500 Hz frequencies. For higher frequencies, the delay decreases. We notice that the increase of the frequency shifts the maximum of the delay to the lower values of μ_r.

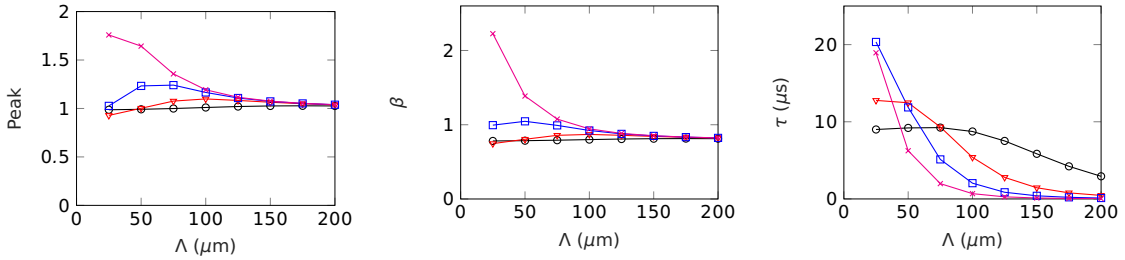

(a) Peak-To-Peak. **(b)** Amplification factor. **(c)** Time Delay.

Fig. 3.8 Dependence on Λ at 1 T and $\mu_r = 5,000$. [$f = 500$ Hz $f = 1,500$ Hz $f = 3,000$ Hz $f = 5,500$ Hz]

On the other hand, the amplitude increases to a maximum than decreases for frequencies 500 Hz and 1,500 Hz. It decreases for higher frequencies. We also notice a shift to the left of the maximum with respect to Λ. As for the amplification factor β, it increases with Λ for low frequency 500 Hz and it decreases with Λ for higher frequencies. In addition, the increase of Λ reduces the loop's width in all cases till reaching zero.
At low Λ values (< 150 μm), the peak increases with the frequency, the amplification factor and the time delay decrease. At high values of Λ (> 150 μm), the peak, amplification factor and time delay become the same and the diffusion effect disappears for the different frequencies.
This study is important when dealing with laser treatment that modifies the magnetic properties μ_r and Λ, responsible for the improvement or the deterioration of the Maxwell force in airgaps.
All these results show the importance of the diffusion on the Maxwell force response in the airgap and reveal the critical difference between the square of the average induction and the average of the squared induction. The diffusion also takes effect on the magnetostriction as

described in the next section.

3.4 Magnetostriction: Microscopic Approach

3.4.1 Static Behavior

Magnetostriction is a strain induced by the magnetization phenomenon. It is caused by the deformation of the magnetic domains. As explained in section 1.3 of chapter 1, magnetostriction is a coupling property to the generation of a magneto-elastic energy when an elastic medium is magnetized. At equilibrium, the magnetostriction tensor dependent on the domain's cosine director vector $[\alpha_1, \alpha_2, \alpha_3]$ and characterized by the magneto-elastic properties λ_{100} and λ_{111} is given by:

$$[\varepsilon] = \frac{3}{2}\begin{bmatrix} \lambda_{100}\left(\alpha_1^2 - \frac{1}{3}\right) & \lambda_{111}\alpha_1\alpha_2 & \lambda_{111}\alpha_1\alpha_3 \\ \lambda_{111}\alpha_2\alpha_1 & \lambda_{100}\left(\alpha_2^2 - \frac{1}{3}\right) & \lambda_{111}\alpha_2\alpha_3 \\ \lambda_{111}\alpha_3\alpha_1 & \lambda_{111}\alpha_3\alpha_2 & \lambda_{100}\left(\alpha_3^2 - \frac{1}{3}\right) \end{bmatrix} \tag{3.33}$$

Considering the particular case were only parallel and perpendicular domains are present, the deformation observed in the longitudinal direction $\alpha_1 = 1$, $\alpha_2 = 0$ and $\alpha_3 = 0$ gives the following tensor:

$$[\varepsilon]^0 = \begin{bmatrix} \lambda_{100} & 0 & 0 \\ 0 & -\lambda_{100}/2 & 0 \\ 0 & 0 & -\lambda_{100}/2 \end{bmatrix} \tag{3.34}$$

Here the property λ_{111} disappears due to the orthogonality between domains. But in reality, inclined domains are present and the λ_{111} contributes to the magnetostriction expression. In order to understand the magnetostrictive behavior when a magnetic field is applied, the same domain structure is considered as illustrated in **Fig. 3.9**.

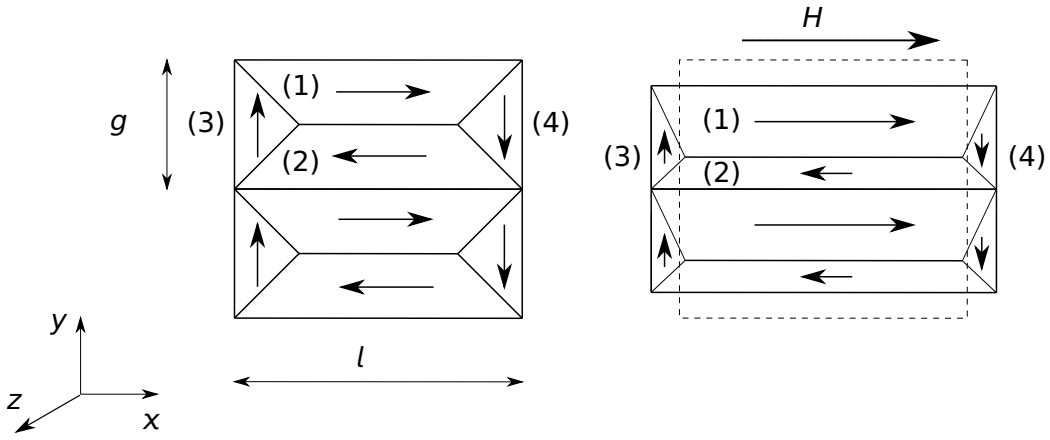

Fig. 3.9 Magnetization and Magnetostriction of a magnetic domain with 180° and 90°.

Considering the strain tensor at equilibrium (**Eq. 3.34**), the initial global deformation tensor can be obtained using the combination with volume fractions without magnetic field application:

$$< \varepsilon_{\parallel}^0 >= \sum_{\alpha} f_\alpha \varepsilon_\alpha = (f_{\parallel}^0 - f_{\perp}^0/2)\lambda_{100} = (1 - \frac{3}{2} f_{\perp}^0)\lambda_{100} \tag{3.35}$$

When a magnetic field is applied, the same approach applied for the magnetization is presented here for the magnetostriction based on the volume fraction variation with the energy. Using the initial fraction volumes in **Eq. 2.10**, the total magnetostriction becomes:

$$< \varepsilon_{\parallel}^{0} > (H) = \frac{f_{\parallel}^{0} \cosh(A_s \mu_0 M_s H) - f_{\perp}^{0}/2}{f_{\parallel}^{0} \cosh(A_s \mu_0 M_s H) + f_{\perp}^{0}} \lambda_{100} \tag{3.36}$$

The magnetization is an odd function because the same direction volume fractions are substracted; a line is obtained in the linear region. However, the magnetostriction is an even function because the same direction volume fractions are added up; a parabola is obtained in the linear case. Its linearization using a second order Taylor development gives the following parabola equation:

$$\varepsilon_{\parallel} - \varepsilon_{\parallel}^{0} \sim \frac{27 \chi_0^2}{2 M_s^2} f_{\perp}^{0} (1 - f_{\perp}^{0}) \lambda_{100} H^2 \tag{3.37}$$

Using the magnetization linear equation (**Eq. 2.12**), the previous equation can be written as function of the magnetization as:

$$\varepsilon_{\parallel} - \varepsilon_{\parallel}^{0} = \frac{3}{2} \frac{f_{\perp}^{0}}{1 - f_{\perp}^{0}} \left(\frac{M_{\parallel}}{M_s} \right)^2 \lambda_{100} \tag{3.38}$$

Eq. 3.38 sets a microscopic relationship between the magnetostriction and the magnetization for an oriented structure in the linear case where the walls displacement is considered. The magnetostriction is an even function of the magnetization in the linear case. Furthermore, an initial magnetostriction exists at rest before magnetization as shown in **Eq. 3.35** and a magnetization dependent magnetostriction appears as shown in **Eq. 3.38**. Now considering $B = \mu_0 M$ and $J_s = \mu_0 M_s$ for magnetization in the linear case **Eq. 3.38** can be written as function of $B^2/2\mu_0$, by analogy to the Maxwell's force:

$$\varepsilon_{\parallel} - \varepsilon_{\parallel}^{0} = \frac{f_{\perp}^{0}}{1 - f_{\perp}^{0}} \frac{3 \mu_0 \lambda_{100}}{J_s^2} \frac{B_{\parallel}^2}{2 \mu_0} \tag{3.39}$$

The following parameter is introduced:

$$P_{\parallel} = \frac{1 - f_{\perp}^{0}}{f_{\perp}^{0}} \frac{J_s^2}{3 \mu_0 \lambda_{100}} \tag{3.40}$$

$P_{\parallel}$ is defined as the magnetic modulus that links the strain to the magnetic stress. A static magneto-elastic relation is obtained between the induction and the induction strain:

$$\varepsilon_{\parallel} - \varepsilon_{\parallel}^{0} = \frac{B_{\parallel}^2}{2 \mu_0 P_{\parallel}} \tag{3.41}$$

The increasing fraction of the 90° domains, increases the magnetostriction level and decreases the modulus. Based on **Eq. 3.41**, the magnetic modulus $P_{\parallel}$ varies in the same way as the relative permeability in the linear case. Therefore, the reduction of the closure domains fraction improves the permeability and reduces the magnetostriction. Now considering the case of domains rotation and assuming that the walls displacement phenomenon is achieved, one single domain is considered as shown in **Fig. 3.10**.

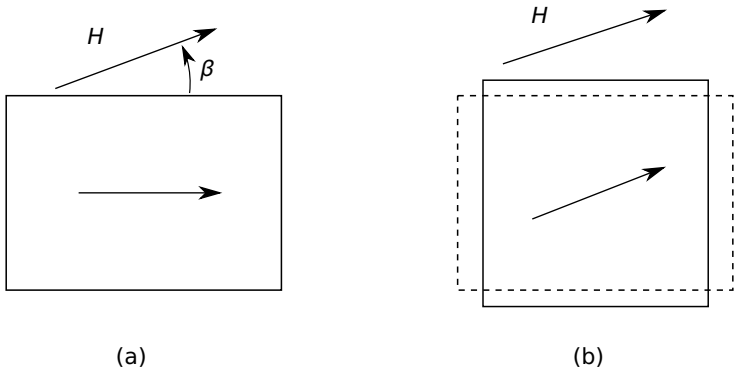

Fig. 3.10 Domains rotation phenomenon (a) After walls displacement (b) Total rotation (Final state). (- - - - Shape before rotation)

An angle of cosine equal to β is formed between the fix applied magnetic field and the domain's orientation. In the magnetic field direction, the magnetization was initially equal to $< M_1 >= \beta M_s$. But after the domains rotation, it becomes $< M_2 >= M_s$. As for the deformation, when the domain rotates, it shrinks from a distance l to a distance βl [37, 5]. The deformation before (1) and after (2) domains rotation is given in the magnetic field direction by:

$$< \varepsilon^1 >= \lambda_{100} \tag{3.42}$$

$$< \varepsilon^2 >= \beta \lambda_{100} \tag{3.43}$$

Therefore, in the domains rotation case, the variation of the deformation with the magnetization is linear and negative:

$$\frac{d\varepsilon_{\parallel}}{dM_{\parallel}} = -\frac{\lambda_{100}}{M_s} \tag{3.44}$$

$$\frac{d\varepsilon_{\parallel}}{dB_{\parallel}} = -\frac{\lambda_{100}}{J_s} \tag{3.45}$$

In this case, the material shrinks with the domain's rotation in a linear way. The saturation is obtained when the magnetization is aligned with the magnetic field.

3.4.2 Dynamic Behavior: Inclusion of the Microscopic Damping

Similar to the dynamic microscopic analysis for the magnetic behavior, a mechanical damping is present in the linear region due to the magnetization process. In fact, the coupling between the motion in a direction x and the induction in the perpendicular directions generates a conducting current density dependent on the velocity of the structure and producing a velocity dependent Lorentz force [48]. In this case, we are interested in the motion in the x direction with a velocity $v_{\parallel}$. The generated current density is obtained due to the magnetization in the transverse directions due to the 90° domains ($B_{\perp}$). The generated current density j_v in the z direction is given by (for a velocity in the parallel direction $v_{\parallel}$):

$$j_v = \sigma(\mathbf{v} \times \mathbf{B})_z = \sigma(v_{\parallel} B_{\perp}) \tag{3.46}$$

A velocity dependent Lorentz force is also obtained in the x direction (for a velocity in the parallel direction $v_{\parallel}$):

$$f^L = \sigma[(\mathbf{v} \times \mathbf{B}) \times \mathbf{B}]_x = \sigma v_{\parallel} B_{\perp}^2 \tag{3.47}$$

The corresponding dissipation energy is given by:

$$E^L = f^L.v_{\parallel} = \sigma B_{\perp}^2 v_{\parallel}^2 = \sigma J_s^2 f_{\perp}^2 v_{\parallel}^2 \tag{3.48}$$

The strain and the velocity at this level can be connected using the domain's length l_w:

$$v_{\parallel} = l_w.\frac{d\varepsilon_{\parallel}}{dt} + \frac{dl_w}{dt}.\varepsilon_{\parallel} \tag{3.49}$$

Based on the fact that the domains length rate is not considered in this study, the previous equation becomes:

$$v_{\parallel} = l_w.\frac{d\varepsilon_{\parallel}}{dt} \tag{3.50}$$

The transverse fraction volume is given by:

$$f_{\perp} = \frac{f_{\perp}^0}{f_{\parallel}^0 \cosh(A_s \mu_0 M_s H) + f_{\perp}^0} \tag{3.51}$$

A linearization of **Eq. 3.51** using the second order Taylor development gives:

$$f_{\perp} \sim f_{\perp}^0 - \frac{9\chi_0^2}{M_s^2} f_{\perp}^0 (1 - f_{\perp}^0) H^2 = f_{\perp}^0 - \frac{f_{\perp}^0}{1 - f_{\perp}^0} \left(\frac{M_{\parallel}}{M_s}\right)^2 \tag{3.52}$$

Using **Eq. 3.52** and **Eq. 3.50**, **Eq. 3.48** becomes:

$$E^L = \sigma J_s^2 (f_{\perp}^0)^2 \left[1 - \frac{1}{1 - f_{\perp}^0} \left(\frac{M_{\parallel}}{M_s}\right)^2\right]^2 l_w^2 \left(\frac{d\varepsilon_{\parallel}}{dt}\right)^2 \tag{3.53}$$

3.4.3 Energy Contributions and Behavior Law

Based on the previous analysis, the different energy contributions are presented. In fact, considering a local analysis that does not take into account the inertia, the magneto-elastic energy E_{me} supplied due to the magnetization is partially converted into an elastic energy E_{el} and the second part is dissipated E^L due to the Lorentz force.

$$E_{me} = E_{el} + E^L \tag{3.54}$$

In the studied case, the energy contributions per unit volume in the longitudinal direction are given by:

$$E_{me} = \frac{2\mu_0 b_1}{J_s^2} \frac{f_{\perp}^0}{1 - f_{\perp}^0} \frac{B_{\parallel}^2}{2\mu_0} \varepsilon_{\parallel} \tag{3.55}$$

$$E_{el} = \frac{1}{2} E \varepsilon_{\parallel}^2 \tag{3.56}$$

E being the Young modulus and b_1 the magneto-elastic coupling modulus presented in Appendix **??**.

$$E^L = \sigma J_s^2 (f_{\perp}^0)^2 \left[1 - \frac{1}{1 - f_{\perp}^0} \left(\frac{B_{\parallel}}{J_s}\right)^2\right]^2 l_w^2 \left(\frac{d\varepsilon_{\parallel}}{dt}\right)^2 \tag{3.57}$$

The second order equation that describes the magneto-mechanical dynamic behavior is obtained using the Hamilton's principle:

$$\frac{2\mu_0 b_1}{J_s^2}\frac{f_\perp^0}{1-f_\perp^0}\frac{B_\parallel^2}{2\mu_0} = E\varepsilon_\parallel + \sigma J_s^2 (f_\perp^0)^2\left[1-\frac{1}{1-f_\perp^0}\left(\frac{B_\parallel}{J_s}\right)^2\right]^2 l_w^2\frac{d\varepsilon_\parallel}{dt} \tag{3.58}$$

Dividing **Eq. 3.58** by the coefficient $\frac{2\mu_0 b_1}{J_s^2}\frac{f_\perp^0}{1-f_\perp^0}$ one gets:

$$\frac{B_\parallel^2}{2\mu_0} = \frac{1-f_\perp^0}{f_\perp^0}\frac{EJ_s^2}{2\mu_0 b_1}\varepsilon_\parallel + \frac{\sigma J_s^4 l_w^2}{2\mu_0 b_1} f_\perp^0(1-f_\perp^0)\left[1-\frac{1}{1-f_\perp^0}\left(\frac{B_\parallel}{J_s}\right)^2\right]^2\frac{d\varepsilon_\parallel}{dt} \tag{3.59}$$

The magnetic modulus $P_\parallel$ from **Eq. 3.40** is obtained in **Eq. 3.59**:

$$P_\parallel = \frac{1-f_\perp^0}{f_\perp^0}\frac{EJ_s^2}{2\mu_0 b_1} = \frac{1-f_\perp^0}{f_\perp^0}\frac{J_s^2}{3\mu_0\lambda_{100}} \tag{3.60}$$

where $\lambda_{100} = \frac{2b_1}{3E}$. We also define a damping factor $\eta_\parallel$ given by:

$$\eta_\parallel = \frac{\sigma J_s^4 l_w^2}{2\mu_0 b_1} f_\perp^0(1-f_\perp^0)\left[1-\frac{1}{1-f_\perp^0}\left(\frac{B_\parallel}{J_s}\right)^2\right]^2 \tag{3.61}$$

The domains length l_w can be written in a more concrete way using the domains density n_w the projected surface of the transverse domains $S_{w\perp}$.

$$l_w = \frac{1}{n_w S_{w\perp}} \tag{3.62}$$

The Lorentz delay is given by:

$$\tau_\Lambda = \frac{\eta_\parallel}{P_\parallel} = \frac{\sigma J_s^2}{E n_w^2 S_{w\perp}^2}\left(f_\perp^0\right)^2\left[1-\frac{1}{1-f_\perp^0}\left(\frac{B_\parallel}{J_s}\right)^2\right]^2 \tag{3.63}$$

The delay τ_Λ increases with the transverse domains volume fractions. Furthermore, the magneto-mechanical delay depends on the induction and the domains length. An increasing induction decreases slightly the product $\left[1-\frac{1}{1-f_\perp^0}\left(\frac{B_\parallel}{J_s}\right)^2\right]^2$ but increases much more the square of the domain's length l_w and eventually decreases the domains density n_w. Therefore, the Lorentz delay increases with the induction. τ_Λ also increases with the electrical conductivity, and decreases with the Young modulus. On the other hand, **Eq. 3.59** becomes:

$$\frac{B_\parallel^2}{2\mu_0 P_\parallel} = \varepsilon_\parallel + \tau_\Lambda\frac{d\varepsilon_\parallel}{dt} \tag{3.64}$$

A first order magneto-mechanical behavior law is obtained between the strain and the squared induction. This is a Kelvin-Voigt rheological model that includes a magnetic conservative elasticity and a damping factor.

3.5 Magneto-Elasticity: 1-D study

3.5.1 Mesoscopic Scale

Considering the 1-D magnetic problem developed in Chapter 2, a plate is subjected to a uniform magnetic field. Taking into consideration the magnetization in the longitudinal direction, a symmetry is obtained with respect to the xz plane and the y-dimension is removed. We define the magneto-elastic linear relation in the static mode given by:

$$\lambda_x(z) = \frac{1}{2\mu_0 P} B^2(z) \tag{3.65}$$

λ_x is the local magnetic induced strain in the x direction due to the presence of the magnetic field. In the linear case, the relation between the equivalent strain and the induction is quadratic. When taking into account the damping delay τ_Λ due to the microscopic Lorentz force, and based on the homogenization study in **Eq. 3.64**, the behavior follows a first order dynamic law given by:

$$\lambda_x(z,t) + \tau_\Lambda \frac{d\lambda_x}{dt}(z,t) = \frac{1}{2\mu_0 P} B^2(z,t) \tag{3.66}$$

3.5.2 Semi-Mesoscopic Scale

When studying plates, its is impossible to measure or analyze the strain variation in the cross-section because of the thin characteritic of the thickness in comparison with the width and the length. Therefore, the strain measurements and the identification cannot be performed at the local mesoscopic scale described in 3.5.1. The strain is integrated through the thickness using **Eq. 3.67** that represents the magneto-elastic behavior in a 1-D case for a magnetic plate.

$$\varepsilon_{ms}(t) + \tau_\Lambda \frac{d\varepsilon_{ms}}{dt}(t) = \frac{1}{2\mu_0 h P} \int_{-\frac{h}{2}}^{\frac{h}{2}} B^2(z,t) dz = \frac{1}{2\mu_0 P} < B^2 > (t) \tag{3.67}$$

ε_{ms} is the average induced axial strain in the x direction.

3.5.3 Macroscopic Scale

As shown in **Eq. 3.67**, the magnetic induced strain depends on the average of the squared induction. However, as described in details in section 3.3.2. The average of the square induction generates an amplitude amplification β and a time delay τ_d, in addition to the microscopic delay due to the eddy current in the magnetostriction case. Therefore, in order to develop a macroscopic magneto-mechanical law, the diffusion effect is included and the relation between the observed strain ε_{ms} and the observed average induction $< B >$ given by:

$$\tau \frac{d\varepsilon_{ms}}{dt} + \varepsilon_{ms} = \frac{1}{2\mu_0 Q} < B >^2 \tag{3.68}$$

The macroscopic model includes the following variables:

- The amplitude factor Q that replaces P. This factor includes next to the magnetic modulus P, the amplification due to the diffusion effect. We define the amplification factor as $\beta = P/Q$. We call Q the apparent magnetic Young modulus.
- The time delay τ that shows the phase shift between the induction and the strain, and is responsible of the magnetostriction hysteresis and it is due to both the diffusion induced delay τ_d and the microscopic Lorentz force delay τ_Λ.

Fig. 3.11 illustrates the modeled butterfly loops as function of the macroscopic magneto-mechanical parameter Q and τ and as function of the frequency. The increase of the magnetic modulus decreases the strain amplitude, the increase of the delay τ and the frequency decreases the amplitude and increases the butterfly loop's width.

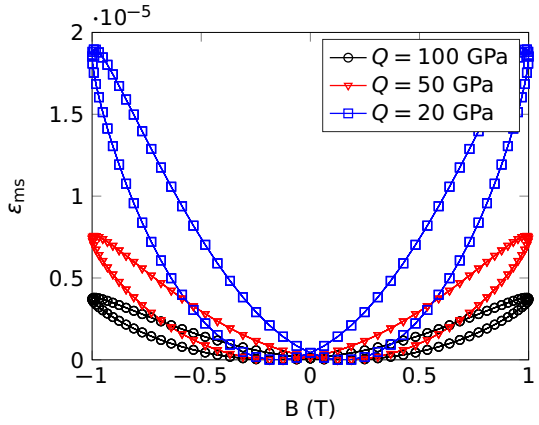

(a) Variation with the apparent magnetic modulus Q.

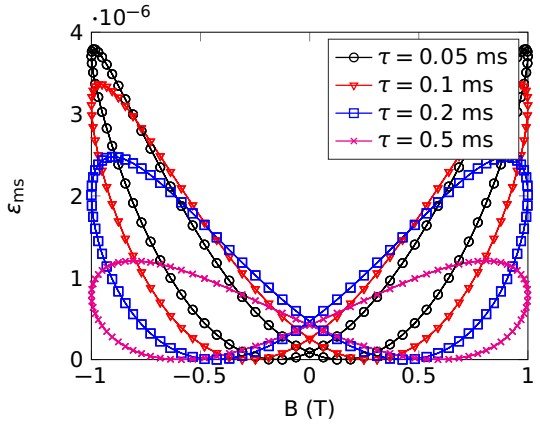

(b) Variation with the magneto-mechanical delay τ.

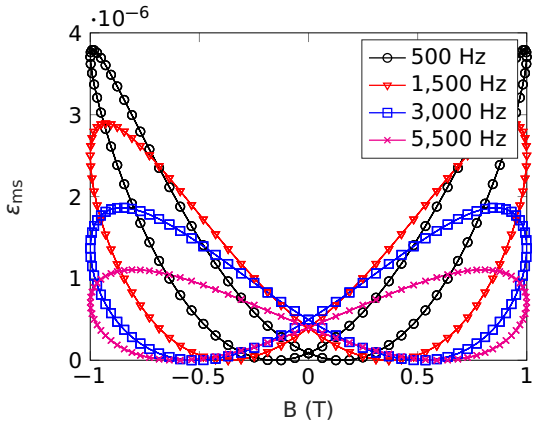

(c) Variation with the frequency.

Fig. 3.11 Modeling of the magneto-elastic dynamic behavior (Reference values: $Q = 100$ GPa, $\tau = 0.05$ ms and 500 Hz).

3.6 Magneto-Elasticity: Generalization

3.6.1 Analogy with the Elasticity

Based on the 1D modeling, one can generalize the magneto-elastic behavior by performing an analogy with the elasticity in mechanics and the plates theory. This is performed by expressing the relationship between the magnetic induced strain and its equivalent stress. In fact, when the material is constraint free, the magnetization induces a magnetic strain. However, when the material is constrainted (for example clamped) , a stress equivalent to the induced strain is generated. In order to make a similarity with the Maxwell's stress, we consider the following

3-D stress vector with Voigt notations in the xy plane:

$$\sigma_{mag} = \begin{bmatrix} \sigma_{xx} & \sigma_{yy} & \sigma_{zz} & \tau_{xy} & \tau_{xz} & \tau_{yz} \end{bmatrix}^T = \frac{1}{2\mu_0} \begin{bmatrix} B_x^2 & B_y^2 & B_z^2 & B_x B_y & B_x B_z & B_y B_z \end{bmatrix}^T \quad (3.69)$$

Where σ_{xx}, σ_{yy} and σ_{zz} are the axial stresses along x, y and z axis respectively and τ_{xy}, τ_{xz} and τ_{yz} are the shear stresses in xy, xz and yz planes respectively.
The corresponding strain vector is given by:

$$\lambda = \begin{bmatrix} \varepsilon_{xx} & \varepsilon_{yy} & \varepsilon_{zz} & \gamma_{xy} & \gamma_{xz} & \gamma_{yz} \end{bmatrix}^T \quad (3.70)$$

Where ε_{xx}, ε_{yy} and ε_{zz} are respectively the axial strain components along x, y and z axis, and γ_{xy}, γ_{xz} and γ_{yz} are respectively the shear strains along xy, xz and yz planes.

3.6.2 Anisotropic Behavior

The magnetic induced strain called magnetostriction can be considered as if it was generated by an equivalent magnetic stress vector; we define a stiffness matrix **P** equivalent to the elastic matrix in mechanics, linking the stress to the strain:

$$\sigma_{mag} = \mathbf{P}\lambda = \begin{bmatrix} P_{xxxx} & P_{xxyy} & P_{xxzz} & P_{xxxy} & P_{xxxz} & P_{xxyz} \\ & P_{yyyy} & P_{yyzz} & P_{yyxy} & P_{yyxz} & P_{yyyz} \\ & & P_{zzzz} & P_{zzxy} & P_{zzxz} & P_{zzyz} \\ & & & P_{xyxy} & P_{xyxz} & P_{xyyz} \\ & sym. & & & P_{xzxz} & P_{xzyz} \\ & & & & & P_{yzyz} \end{bmatrix} \begin{bmatrix} \varepsilon_{xx} \\ \varepsilon_{yy} \\ \varepsilon_{zz} \\ \gamma_{xy} \\ \gamma_{xz} \\ \gamma_{yz} \end{bmatrix} \quad (3.71)$$

P_{ijkl} presents the magneto-elastic coupling property that connects the equivalent magnetic stress in the kl plane to the magnetostriction in the ij plane. **Eq. 3.71** presents the static magneto-elastic behavior [32]. It includes the anisotropic behavior. Similarly to the magnetization, the magnetostriction behaves in a different way in each direction due to the grain orientation and the easy axis magnetization. The magneto-elastic anisotropy is less important in the case of non-grain oriented materials where the magnetization can easily occur in any direction. In this case, an isotropic aspect of **Eq. 3.71** becomes:

$$\sigma_{mag} = \mathbf{P}\lambda = \begin{bmatrix} P_{11} & P_{12} & P_{12} & 0 & 0 & 0 \\ & P_{11} & P_{12} & 0 & 0 & 0 \\ & & P_{11} & 0 & 0 & 0 \\ & & & \frac{P_{11}-P_{12}}{2} & 0 & 0 \\ & sym. & & & \frac{P_{11}-P_{12}}{2} & 0 \\ & & & & & \frac{P_{11}-P_{12}}{2} \end{bmatrix} \begin{bmatrix} \varepsilon_{xx} \\ \varepsilon_{yy} \\ \varepsilon_{zz} \\ \gamma_{xy} \\ \gamma_{xz} \\ \gamma_{yz} \end{bmatrix} \quad (3.72)$$

Where $P_{11} = \frac{P}{1-\xi^2}$ and $P_{12} = \frac{\xi P}{1-\xi^2}$. P is the isotropic magnetic Young modulus, and ξ is the isotropic magnetic Poisson ratio.

3.6.3 Application to the theory of Plates

A plate is a mechanical structure that has a small thickness compared with the planar dimensions (length and width). The thickness to width ratio of a plate must be less than 0.1. The considered stress and strain components are in-plane terms in the xy plane. The stresses components generate the so-called in-plane load resultants defined by:

$$\begin{bmatrix} N_x \\ N_y \\ N_{xy} \end{bmatrix} = \int_{-\frac{h}{2}}^{\frac{h}{2}} \begin{bmatrix} \sigma_{xx} \\ \sigma_{yy} \\ \tau_{xy} \end{bmatrix} dz = \frac{1}{2\mu_0} \int_{-\frac{h}{2}}^{\frac{h}{2}} \begin{bmatrix} B_x^2 \\ B_y^2 \\ B_x B_y \end{bmatrix} dz \tag{3.73}$$

In a more general case, a transverse response occurs due to the presence of resultant moments:

$$\begin{bmatrix} M_x \\ M_y \\ M_{xy} \end{bmatrix} = \int_{-\frac{h}{2}}^{\frac{h}{2}} \begin{bmatrix} z\sigma_{xx} \\ z\sigma_{yy} \\ z\tau_{xy} \end{bmatrix} dz = \frac{1}{2\mu_0} \int_{-\frac{h}{2}}^{\frac{h}{2}} \begin{bmatrix} zB_x^2 \\ zB_y^2 \\ zB_x B_y \end{bmatrix} dz \tag{3.74}$$

In the case of easy-direction magnetization, the global magneto-mechanical behavior is similar to an orthotropic plate:

$$\begin{bmatrix} N_x \\ N_y \\ N_{xy} \\ M_x \\ M_y \\ M_{xy} \end{bmatrix} = \int_{-\frac{h}{2}}^{\frac{h}{2}} \begin{bmatrix} \frac{B_x^2}{2\mu_0} \\ \frac{B_y^2}{2\mu_0} \\ \frac{B_x B_y}{2\mu_0} \\ \frac{zB_x^2}{2\mu_0} \\ \frac{zB_y^2}{2\mu_0} \\ \frac{zB_x B_y}{2\mu_0} \end{bmatrix} dz = \begin{bmatrix} \frac{hP_x}{1-\xi_x\xi_y} & \frac{h\xi_x P_x}{1-\xi_x\xi_y} & 0 & 0 & 0 & 0 \\ \frac{h\xi_y P_y}{1-\xi_x\xi_y} & \frac{hP_y}{1-\xi_x\xi_y} & 0 & 0 & 0 & 0 \\ 0 & 0 & hG_{xy} & 0 & 0 & 0 \\ 0 & 0 & 0 & \frac{h^3 P_x}{12(1-\xi_x\xi_y)} & \frac{h^3\xi_x P_x}{12(1-\xi_x\xi_y)} & 0 \\ 0 & 0 & 0 & \frac{h^3\xi_y P_y}{12(1-\xi_x\xi_y)} & \frac{h^3 P_y}{12(1-\xi_x\xi_y)} & 0 \\ 0 & 0 & 0 & 0 & 0 & \frac{h^3 G_{xy}}{12} \end{bmatrix} \begin{bmatrix} \varepsilon_x^0 \\ \varepsilon_y^0 \\ \gamma_{xy}^0 \\ \kappa_x \\ \kappa_y \\ \kappa_{xy} \end{bmatrix} \tag{3.75}$$

Where κ_x, κ_y and κ_{xy} are the twisting strain components along x and y axis, and γ_{xz} and γ_{yz} are the shear strain components along the planes xz and yz respectively. This relation includes magneto-elastic properties:

- P_x and P_y are the magnetic Young moduli, analogous to the elastic Young moduli E_x and E_y.
- ξ_x and ξ_y are the magnetic Poisson ratios equivalent to the elastic Poisson ratios ν_x and ν_y.
- G_{xy} is the magnetic shear modulus.

Inversing **Eq. 3.75**, we get,

$$\begin{bmatrix} \varepsilon_x^0 \\ \varepsilon_y^0 \\ \gamma_{xy}^0 \\ \kappa_x \\ \kappa_y \\ \kappa_{xy} \end{bmatrix} = \begin{bmatrix} \frac{1}{hP_x} & \frac{-\xi_x}{hP_y} & 0 & 0 & 0 & 0 \\ \frac{-\xi_y}{hP_x} & \frac{1}{hP_y} & 0 & 0 & 0 & 0 \\ 0 & 0 & \frac{1}{hG_{xy}} & 0 & 0 & 0 \\ 0 & 0 & 0 & \frac{12}{h^3P_x} & -\frac{12\xi_x}{h^3P_y} & 0 \\ 0 & 0 & 0 & -\frac{12\xi_y}{h^3P_x} & \frac{12}{h^3P_y} & 0 \\ 0 & 0 & 0 & 0 & 0 & \frac{12}{h^3G_{xy}} \end{bmatrix} \frac{1}{2\mu_0} \int_{-\frac{h}{2}}^{\frac{h}{2}} \begin{bmatrix} B_x^2 \\ B_y^2 \\ B_xB_y \\ zB_x^2 \\ zB_y^2 \\ zB_xB_y \end{bmatrix} dz \tag{3.76}$$

As for the isotropic case, **Eq. 3.75** becomes:

$$\begin{bmatrix} N_x \\ N_y \\ N_{xy} \\ M_x \\ M_y \\ M_{xy} \end{bmatrix} = \int_{-\frac{h}{2}}^{\frac{h}{2}} \begin{bmatrix} \frac{B_x^2}{2\mu_0} \\ \frac{B_y^2}{2\mu_0} \\ \frac{B_xB_y}{2\mu_0} \\ \frac{zB_x^2}{2\mu_0} \\ \frac{zB_y^2}{2\mu_0} \\ \frac{zB_xB_y}{2\mu_0} \end{bmatrix} dz = \begin{bmatrix} \frac{hP}{1-\xi^2} & \frac{h\xi P}{1-\xi^2} & 0 & 0 & 0 & 0 \\ \frac{h\xi P}{1-\xi^2} & \frac{hP}{1-\xi^2} & 0 & 0 & 0 & 0 \\ 0 & 0 & \frac{hP}{2(1+\xi)} & 0 & 0 & 0 \\ 0 & 0 & 0 & \frac{h^3P}{12(1-\xi^2)} & \frac{h^3\xi P}{12(1-\xi^2)} & 0 \\ 0 & 0 & 0 & \frac{h^3\xi P}{12(1-\xi^2)} & \frac{h^3P}{12(1-\xi^2)} & 0 \\ 0 & 0 & 0 & 0 & 0 & \frac{h^3P}{24(1+\nu)} \end{bmatrix} \begin{bmatrix} \varepsilon_x^0 \\ \varepsilon_y^0 \\ \gamma_{xy}^0 \\ \kappa_x \\ \kappa_y \\ \kappa_{xy} \end{bmatrix} \tag{3.77}$$

and,

$$\begin{bmatrix} \varepsilon_x^0 \\ \varepsilon_y^0 \\ \gamma_{xy}^0 \\ \kappa_x \\ \kappa_y \\ \kappa_{xy} \end{bmatrix} = \begin{bmatrix} \frac{1}{hP} & -\frac{\xi}{hP} & 0 & 0 & 0 & 0 \\ -\frac{\xi}{hP} & \frac{1}{hP} & 0 & 0 & 0 & 0 \\ 0 & 0 & \frac{2(1+\xi)}{hP} & 0 & 0 & 0 \\ 0 & 0 & 0 & \frac{12}{h^3P} & -\frac{12\xi}{h^3P} & 0 \\ 0 & 0 & 0 & -\frac{12\xi}{h^3P} & \frac{12}{h^3P} & 0 \\ 0 & 0 & 0 & 0 & 0 & \frac{24(1+\nu)}{h^3P} \end{bmatrix} \frac{1}{2\mu_0} \int_{-\frac{h}{2}}^{\frac{h}{2}} \begin{bmatrix} B_x^2 \\ B_y^2 \\ B_xB_y \\ zB_x^2 \\ zB_y^2 \\ zB_xB_y \end{bmatrix} dz \tag{3.78}$$

The magneto-elastic behavioral law for a plate can be written as:

$$\lambda = \mathbf{P}_e^{-1}.\mathbf{N}_B \tag{3.79}$$

λ is the magnetostriction vector, $\mathbf{P}_e$ is the magnetic stiffness matrix of the plate and $\mathbf{N}_B$ is the magnetic resultant load vector. $\mathbf{P}_e$ and $\mathbf{N}_B$ correspond to the compliance matrix and the squared induction vector in **Eq. 3.78**.

3.7 Mechanical Modeling

Considering the magnetic induced deformation presented in this chapter, we introduce the reaction of the plate to the magnetic excitation. In fact, the mechanical modeling is based on different energy contributions:

- **Excitation (Input)**: When a load is applied, an input mechanical stress is generated. The corresponding energy is called the mechanical energy and it is responsible of the mechanical excitation.
- **Elasticity (Output)**: The response to the mechanical excitation appears in the local deformation due to the elastic property of the material that follows the Hooke's law.
- **Kinetics (Output)**: In the dynamic mode, the effect of the mass and the inertia of the structure, combined with the velocity generates a kinetic energy.
- **Damping (Output)**: Also in the dynamic mode, one part of the provided input energy is dissipated due to a damping property present in the material.

In this study, the considered structure for modeling the mechanical behavior is the plate, a geometric configuration where the thickness is way smaller than the other dimension. The strain, displacement stress and force vectors are adapted to this structure using the plates theory in order to generate the energy formulation. Due to the 1D aspect of the magnetic problem, the mechanical modeling is performed in the longitudinal direction. The target of this study is to present in the simplest way a mechanical configuration that can be applied experimentally and used for identification of the magneto-mecchanical properties presented previously in this chapter.

3.7.1 Dynamic Equation

We consider the case where a plate with Young modulus E, a Poisson ratio ν, a density ρ, and a length L is fixed at one end and free at the other (**Fig. 3.12**). A surface magnetic field is applied uniformily on both surface sides between a position L_1 and L_2. The plate's magnetization induces Maxwell's and magnetostrictive forces, leading a mechanical dynamic excitation.

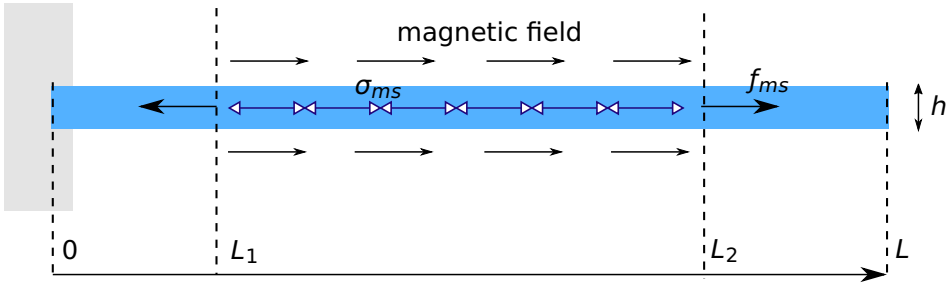

Fig. 3.12 Mechanical configuration.

As mentioned in section 3.3, the magnetostrictive effect dominates on the Maxwell's forces. Studying the axial case, a 1-D dynamic equation is derived using the Lagrange equation by only considering the longitudinal displacement $u(x,t)$ in the $x-$ direction and including the boundary conditions of the fixed-free plate [49],

$$-E\frac{\partial^2 u}{\partial x^2}+c\frac{\partial u}{\partial t}+\rho\frac{\partial^2 u}{\partial t^2}=f_{ms}+f_{em} \tag{3.80}$$

$$u(0,t)=0 \tag{3.81}$$

$$\frac{\partial u}{\partial x}(L,t)=0 \tag{3.82}$$

c is the damping factor, f_{ms} is the magnetostrictive equivalent force due to magnetostrictive strain and f_{em} is the Maxwell's force. As mentioned earlier, the Maxwell's force contribution is negligible in front of the magnetostriction force in this studied case. Therefore, using **Eq. 3.80**, the magnetostriction effect can be directly studied in the longitudinal direction. Using the stress-force relation, with the magnetostrictive stress σ_{ms} and the strain ε_{ms}, we obtain,

$$f_{ms}=-\frac{d\sigma_{ms}}{dx}=-E\frac{d\varepsilon_{ms}}{dx} \tag{3.83}$$

3.7.2 Mechanical Behavioral Analysis

Eq. 3.80 includes the elastic, damping and inertial components (the left terms) resulting from the excitation components (the right terms). We define ε_a the apparent strain directly resulting from the displacement $u(t)$ solution of **Eq. 3.80**.

$$\varepsilon_a(t)=\frac{\partial u}{\partial x}(t) \tag{3.84}$$

The apparent strain contains information concerning the magnetostriction, but also includes the inertia and damping effect. It represents the apparent strain that is locally measured when using a strain gauge. In the case where the inertia effect is negligible compared to the stiffness, the apparent strain is equal to ε_{ms}. Furthermore, ε_a describes the observed behavior related to vibrations and noise due to the combination of the geometric conditions and the magneto-mechanical properties. Both ε_a and ε_{ms} are averaged through the cross section (z independent) but they are potentially x-dependent. However, the SST gives a uniform strain in the magnetized area through the x direction which makes the identification of local magneto-mechanical properties easier.
The sample is discretized using the 1D Finite Element Method (FEM) by only considering the component $\hat{u}$:

$$\hat{\mathbf{M}}_u\ddot{\hat{\mathbf{u}}}+\hat{\mathbf{C}}_u\dot{\hat{\mathbf{u}}}+\hat{\mathbf{K}}_u\hat{\mathbf{u}}=\varepsilon_{ms}\hat{\mathbf{f}}_u \tag{3.85}$$

From a static point of view, using **Eq. 3.85**, one gets the static displacement vector $\mathbf{u}_s$ from the static excitation vector $\mathbf{f}_s$ ($\mathbf{u}_s=\varepsilon_{ms}\hat{\mathbf{K}}_u^{-1}.\mathbf{f}_s$). The shape of the deformed sample and its deformation are illustrated in **Fig. 3.13**. Three regions are distinguished: between the fixed position and the position L_1 no deformation or displacement are shown, between L_1 and L_2 the displacement linearly increases and the deformation is uniform, and in the free region a constant displacement is observed with no deformation. However, for the dynamic behavior, the shape function is modified, specially when the study is near the resonance.

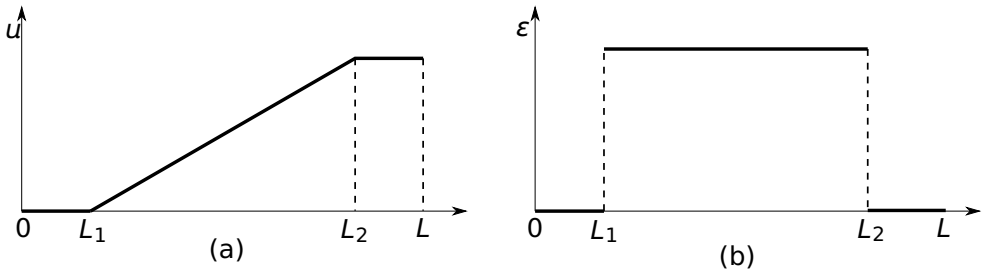

Fig. 3.13 Displacement and strain versus sheet's length under static conditions.

Then the apparent strain can be expressed as a function of the displacement $u_{meas}(t)$ at the end of the sample by,

$$\varepsilon_a(t) = \frac{\partial u}{\partial x}(t) = \frac{u_{meas}(t)}{L_2 - L_1} \tag{3.86}$$

3.7.3 Natural, Magnetic and Mechanical Frequencies

The considered magnetic sheet is clamped at one end and free at the other. Therefore, the i^{th} theoretical natural frequency of the structure for this mechanical configuration is given by [50]:

$$f_i = \frac{(2i+1)}{4L}\sqrt{\frac{E}{\rho}} \tag{3.87}$$

Furthermore, the natural frequencies vector can also be calculated using the derived mass and stiffness matrices.

$$\omega^2 = eig(\hat{\mathbf{M}}_u^{-1}.\hat{\mathbf{K}}_u) \tag{3.88}$$

$$f_i = \frac{\omega_i}{2\pi} \tag{3.89}$$

The calculated natural frequencies analysis is fundamental. In fact, if the mechanical excitation frequency is close to one natural frequency, resonance with occur and the displacement will strongly increase in an uncontrollable way. Therefore, the study must be performed far from the resonance frequency in order to identify the magnetostrictive behavior. In addition, when the excitation frequency is much lower than the fundamental natural frequency, the stiffness effect is mainly dominant. In this case, the magnetostriction ε_{ms} is equal to the apparent measured strain ε_a, the magnetostriction can be simply identified using **Eq. 3.86**.

3.8 Conclusion

This chapter deals with magneto-mechanical modeling of electrical steels applied for plates with the following originalities:

- Modeling of the Maxwell's force in the presence and the absence of airgaps.
- Studying the effect of the magnetic diffusion on the Maxwell's forces.
- Sensitivity of the Maxwell's forces to the magnetic properties.
- Domain scale study of a specific structure showing the local relationship between the induced strain and the magnetization.
- Study of the effect of the mechanical dissipation due to the microscopic Lorentz force.
- Homogenization of the static behavior at the mesoscopic scale, introducing the property P.
- Homogenization of the dynamic damping behavior at the mesoscopic scale, introducing the property τ.
- Analogy with the mechanical elasticity applied to plates.
- Study of the magnetic diffusion effect on the magneto-mechanical coupling, introducing the property Q.
- Mechanical response and longitudinal vibration due to the magnetic excitation.

This modeling strategy is a must when dealing with material's characterization. It is useful for identification with measurements that will be performed in deliverable 3.4. It is also a link between the magnetic modeling introduced in chapter 2 and the mechanical modeling. Finally, this modeling study is a must for understanding the laser treatment effect on the magneto-mechanical behavior, due to the modification of the domains structure.

Chapter 4

The Laser Treatment Technology

This chapter presents the theoretical physical study of the laser treatment effect on the magnetic structure. The adopted techniques are the ablation, scribing and irradiation.

4.1 Energy Minimization

As mentioned in chapter 1, magnetization does not occur homogeneously, it requires an energy minimization by creating a magnetic structure constituted of magnetized domains and walls between the domains. The main energy contributions are the magnetoelastic energy, the magnetocrystalline anisotropy energy, the magnetic exchange energy, and the magnetostatic demagnetizing energy. For a non closure domains configuration, the demagnetizing energy increases with the size of domains and for a closure domains configuration, the anisotropy energy increases with the size of domains. The sum of the anisotropy and exchange energy increases with the walls number or walls density inversely proportional to the size of domains. As a result, the material chooses a compromise by creating domains and walls with size and density that minimize the global energy. The aim of the first surface magnetic model presented below is to describe this compromise and to analyze the impact of a surface laser treatment on any improvement of this energy balance that should lead to performances enhancement.
We assume that the laser can affect very locally the magnetic polarization and permeability of the material such that it disturbs the domains and walls by doing the two following assumptions:

- Laser "scribes" modify very locally the magnetic properties such that the polarization is greatly reduced inside the affected zone (induced stress, ablation, damage, ...)
- Laser patterns create located closure domains or magnetic poles that will define one dimension of surface magnetic domains due to an energy minimization principle.

Fig. 4.1 illustrates two magnetic images perfomed in our laboratory using a fast and practical technique: the **Magneto Optical Indicator Film (MOIF)**. The images show the magnetic structure before (**Fig. 4.1a**) and after treatment (**Fig. 4.1b**). In this case, the treatment technology is the ablation with a 500 fs pulse width. Images show the laser lines (in yellow) and the effect domain refinement. In effect, the laser lines cut the magnetic structure in perpendicular to the 180° domains. Furthermore, the domains thickness is also reduced.

4.2 Magnetic Poles and Equivalent Charges

A magnetic pole appears at an interface between two different materials when the angle between the magnetic polarization and the unit vector normal to the interface is different from zero. When the anisotropy is very strong, the material won't create closure domains that cost a huge amount of energy and it prefers to keep domains oriented in accordance with its easy axis. As a consequence, magnetic poles appear at the vicinity of the area affected by the laser (**Fig. 4.2**). Considering one magnetic domain that goes from one line to another, positive magnetic poles will appear at one extremity against one line and negative magnetic poles will appear at the other extremity against the other line. In case of irradiated, scribed or ablated lines, we have got a succession of positive and negative magnetic poles all along each line.

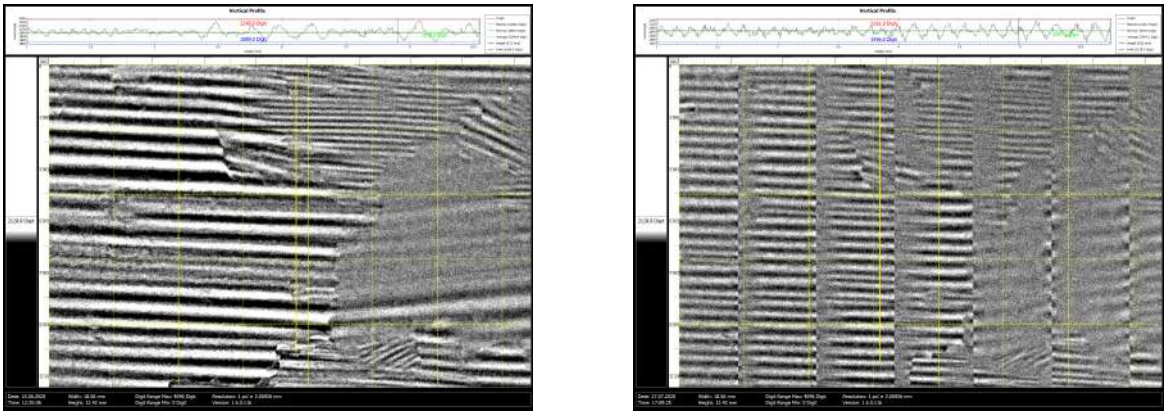

(a) Reference sample. **(b)** After ablation.

Fig. 4.1 Magnetic structure observation using the Magneto Optical Indicator Film technique.

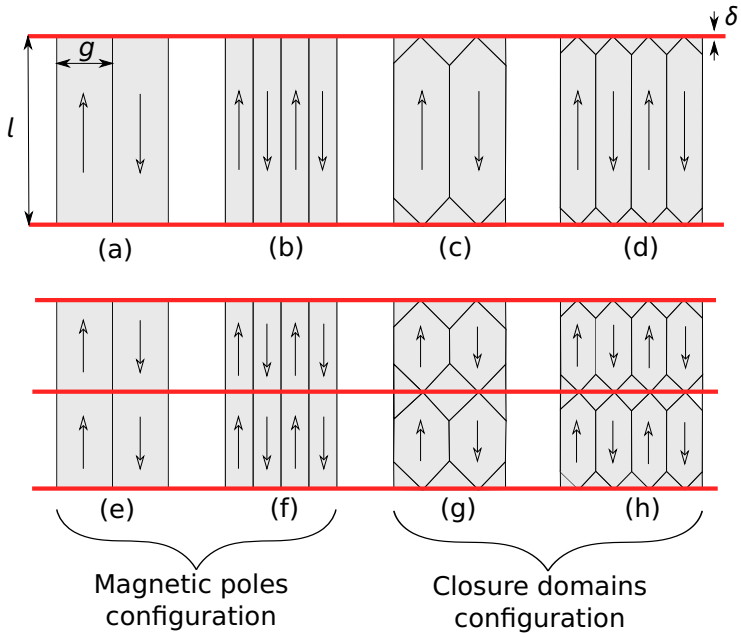

Fig. 4.2 Impact of laser lines (in red) on the magnetic structure.

4.3 Closure Domains

Magnetic poles contribute to a certain amount of energy called the magnetostatic demagnetizing energy. The latter come from the interaction at long distance between magnetic poles. When the anisotropy of the material is not so high, and the magnetic poles are close to each other, closure domains cost less energy than the demagnetizing energy and then the material prefers to create closure domains at the vicinity of the area affected by the laser (**Fig. 4.2**). Considering one magnetic domain that goes from one line to another, opposite closure domains will appear at the two extremities against the lines. In case of scribing lines, a succession of opposite closure domains all along each line are obtained.

4.4 Walls Pinning, Nucleation and Multiplication

Adding some scribed patterns on the surface of a materials may create some defects which will probably affect the static motion of magnetic walls. Defects usually act as pinning sites that prevent the walls to move at low speed and so increase what we call the static hysteresis losses and the static coercive force. At low frequencies, the walls will jump from one defect to another and induce additional loss. At the same time, the walls will require a highest field to detach from one defect and contribute to the magnetization reversal mechanism. On the contrary, some defects can become nucleation or activation sites, i.e. the location where walls can be either created by the presence of magnetic poles or activated by the presence of small walls around closure domains. It is then necessary to specify the optimal laser patterns type and geometry (first lines type, width, depth and spacing) to maximize the dynamic loss reduction due to walls motion and by minimizing the static hysteresis loss increase due to pinning effects but still favoring the walls activation and nucleation.

4.5 Laser Effect on the Magnetization and the Magnetostriction

In this section, we present the theoretical effect of the domains refinement by laser treatment on the magnetization and the magnetostriction. Considering the domain structures shown in **Fig. 4.2**, the magnetization and magnetostriction are calculated in the linear case (low induction) using the microscopic analysis performed in chapters 2 and 3. Results are plotted in **Fig. 4.3** and **Fig. 4.4**, showing the effect of the 90° closure domains fraction volume on the magnetization and the magnetostriction. A bigger fraction of 90° domains increases the magnetostriction and decreases the permeability. The best configuration corresponds to a fraction equal to zero, where the permeability is at its maximum in the linear region. On the other hand, the laser treatment enables a domains refinement which creates a disoriented domains. Although the 90° domains fraction decreases, the domains density increases. Therefore, at higher induction, the anisotropy energy of the closing and disoriented domains being lower, for some domains it is even negligible (Lancet domains, spike-like domains ...) , the threshold for triggering the rotation of the domains will be reached for a lower level of induction for which the demagnetizing energy and the Zeeman energy are more important than the other energies. In this case, the permeability and magnetostriction decrease at higher inductions.

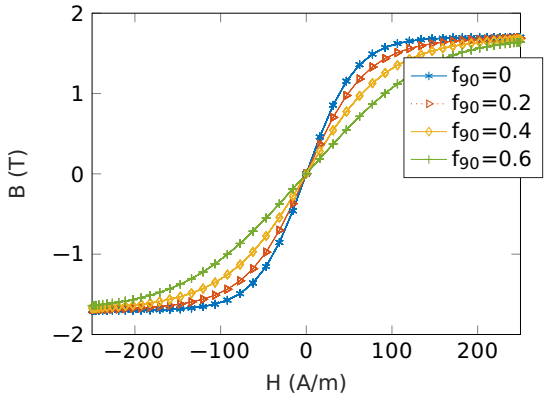

Fig. 4.3 Anhysteretic microscopic magnetization for different domain structures.

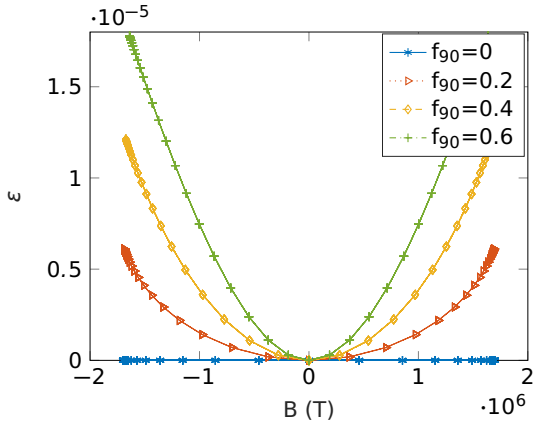

Fig. 4.4 Anhysteretic microscopic magnetostriction for different domain structures.

4.6 Conclusion

This chapter deals with the description of the laser treatment technology used for the improvement of the magnetic and the magneto-mechanical behavior. The laser possible effects on the magnetic structure are presented. Experimental plannings and results are revealed in deliverable 3.4.

Bibliography

[1] F. Alves and R. Barrué. Magnétisme microscopique à l'échelle des domaines magnétiques dans les matériaux ferromagnétiques doux. *J3eA*, (3(6)), 2004. 6, 11, 12

[2] A. Moses, P. Anderson, and S. Somkun. Modeling 2-d magnetostriction in nonoriented electrical steels using a simple magnetic domain model. *IEEE Transactions on Magnetics*, 51(5):6000407, 2015. 6, 13

[3] L. Daniel, O. Hubert, N. Buiron, and R. Billardon. Reversible magneto-elastic behavior: A multiscale approach. *Journal of the mechanics and physics of solids*, 56(3):1018–1042, 2008. 6, 8, 14, 15, 16

[4] D. G. Rethwisch W. D. Callister. *Materials Science and Engineering, An Introduction*. Wiley, 2009. 6, 17

[5] R. Szewczyk, A. Bienkowski, and J. Salach. Extended jiles-atherton model for modelling the magnetic characteristics of isotropic materials. *Journal of Magnetism and Magnetic Materials*, 320(20):e1049–e1052, April 2008. 6, 18, 19, 34, 35, 58

[6] U. Aydin, P. Rasilo, F. Martin, D. Singh, L. Daniel, A. Belahcen, M. Rekik, O. Hubert, R. Kouhia, and A. Arkkio. Magneto-mechanical modeling of electical steel sheets. *Journal of Magnetism and Magnetic Materials*, (439):82–90, 2017. 6, 19, 20

[7] E. Fallah and V. Badeli. A New Approach for Modeling of Hysteresis in 2-D Time-Transient Analysis of Eddy Current Using FEM. *IEEE Transactions on Magnetics*, (53(7)):7402714, 2017. 6, 21

[8] O. Maloberti, A. Kedous Lebouc, G. Meunier, and V. Mazauric. Field diffusion-like representation and experimental identification of a dynamic magnetization property. *Journal of Magnetism and Materials*, (304):507–509, 2006. 6, 22, 37

[9] O. Maloberti, G. Meunier, and A. Kedous Lebouc. On Hysteresis of Soft Materials Inside Formulations: Delayed Diffusion Equations, Fields Coupling, and Nonlinear Properties. *IEEE Transactions on Magnetics*, (44(6)):914–917, 2008. 6, 22, 23, 37, 42

[10] M. A. Raulet, B. Ducharne, J. P. Masson, and G. Bayada. The Magnetic Field Diffusion Equation Including Dynamic Hysteresis: A Linear Formulation of the Problem. *IEEE Transactions on Magnetics*, (40(2)):872–875, 2004. 6, 23

[11] G. Bertotti. General properties of power losses in soft ferromagnetic materials. *IEEE Transactions on Magnetics*, 24(1):621–630, 1988. 6, 24

[12] P. Rasilo, D. Singh, A. Belahcen, and A. Arkkio. Iron losses, magnetoelasticity and magnetostriction in ferromagnetic steel laminations. *IEEE Transactions on Magnetics*, 49(5):2041–2044, 2013. 6, 25

[13] T. Hilgert, L. Vandevelde, and J. Melkebeek. Comparison of Magnetostriction Models for Use in Calculations of Vibrations in Magnetic Cores. *IEEE Transactions on Magnetics*, (44(6)):874–877, 2008. 6, 25

[14] T. Kajiwara and M. Enokizono. Effect of Laser Stress on Vector Magnetic Properties of Electrical Steel Sheets. *IEEE Transactions on Magnetics*, (50(4)):2002404, 2014. 6, 27, 28

[15] A. Zeleňáková, P. Kollár, M. Kuźmiński, M. Kollárová, Z. Vértesy, and W. Riehemann. Magnetic properties and domain structure investigation of laser treated finemet. *Journal of Magnetism and Magnetic Materials - J MAGN MAGN MATER*, 254:152–154, 01 2003. 6, 28, 29

[16] L. Lahn, C. Wang, A. Allwardt, T. Belgrand, and J. Blaszkowski. Impoved Transformer Noise Behavior by Optimized Laser Domain Refinement at ThyssenKrupp Electrical Steel. *IEEE Transactions on Magnetics*, (48(4)):1453–1456, 2012. 6, 29

[17] S. Somkun, A. J. Moses, and P. I. Anderson. Measurement and Modeling of 2-D Magnetostriction of Nonoriented Electrical Steel. *IEEE Transactions on Magnetics*, (48(2)):711–714, 2012. 8, 25, 26

[18] P. Brissonneau. Les domaines magnétiques. *Revue de physique appliquée*, (9(5)):783–792, 1974. 10, 11

[19] F. Delince, A. Genon, J. M. Gillard, H. Hedia, W. Legros, and A. Nicolet. Numerical computation of the magnetostriction effect in ferromagnetic materials. *Journal of Applied Physics*, (69(8)):5794–5796, 1991. 14

[20] C. Mudivarthi, S. Datta, J. Atulasimha, A. B. Flatau, P. G. Evans, and M. J. Dapino. Equivalence of magnetoelastic, elastic, and mechanical work energies with stress-induced anisotropy. *Behavior and Mechanics of Multifunctional and Composite Materials*, 6929:69291X–69291X–9, 2008.

[21] Buiron. *Modélisation multiéchelle du comportement magnétoélastique couplé des ferromagnétiques doux.* PhD thesis, Ecole normale supérieure de Cachan, 2000. 15

[22] D. C. Jiles and D. L. Atherton. Theory of ferromagnetic hysteresis. *Journal of Magnetism and Magnetic Materials*, 61(1):48–60, 1986. 17

[23] J. Szczyglowski. Influence of eddy currents on magnetic hysteresis loops in soft magnetic materials. *Journal of Magnetism and Magnetic materials*, 320(1):97–102, January 2001. 17

[24] U. Aydin, P. Rasilo, D. Singh, A. Lehikoinen, A. Belahcen, and A. Arkkio. Coupled Magneto-Mechanical Analysis of Iron Sheets Under Biaxial Stress. *IEEE Transactions on Magnetics*, (52(3)), 2015. 19

[25] A. Belahcen, K. Fonteyn, A. Hannukainen, and R. Kouhia. On numerical modeling of coupled magnetoelastic problem. pages 203–206, 2008. 19

[26] K. Fonteyn, A. Belahcen, R. Kouhi, P. Rasilo, and A. Arkkio. FEM for Directly Coupled Magneto-Mechanical Phenomena in Electrical Machines. *IEEE Transactions on magnetics*, (46(8)):2923–2926, 2010. 19

[27] K. A. Fonteyn. *Energy-based magneto-mechanical model for electrical steel sheets*. PhD thesis, Aalto University, School of Electronics, Communications and Automation, 2010. 19

[28] S. S. Mbengue. *Etude des déformations induites par l'aimantation des dispositifs électrotechniques : développement d'un modèle magnéto-élastique macroscopique*. PhD thesis, Université de Technologie de Compiègne, 2016. 20, 32

[29] O. Maloberti, V. Mazauric, G. Meunier, A. Kedous-Lebouc, P. Wendling, and B. Colin. A Magnetic Vector Potential Formulation to Deal With Dynamic Induced Losses Within 2-D Models. *IEEE Transactions on Magnetics*, (43(4)):1205–1208, 2007. 22, 37

[30] G. Bertotti. Connection between microstructure and magnetic properties of soft magnetic materials. *Journal of Magnetism and Magnetic Materials*, 320(20):2436–2442, April 2008. 24

[31] S. Somkun, A. Moses, P. Anderson, and P. Klimczyk. Magnetostriction anisotropy and rotational magnetostriction of nonoriented electrical steel. *IEEE Transactions on Magnetics*, 46(2):302–305, 2010. 25

[32] A. Lundgren. *On measurement and modelling of 2D magnetization and magnetostriction of SiFe sheets*. PhD thesis, Royal Institute of Technology Electric Power Engineering Stockholm, 1999. 26, 63

[33] S. Patri, R. Gurusamy, P.A. Molian, and M. Govindaraju. Magnetic domain refinement of silicon-steel laminations by laser scribing. *Journal of materials science*, (31(7)):1693–1702, 1996. 27

[34] M. J. Johnson, R. Chen, and D. C. Jiles. Reducing Core Losses in Amorphous $Fe_{80}B_{12}Si_8$ Ribbons by Laser-Induced Domain Refinement. *IEEE Transactions on Magnetics*, (35(5)):3865–3867, 1999. 28

[35] S. S. Mbengue. *Modélisation multi-échelle du comportement magnéto-mécanique des matériaux ferromagnétiques texturés*. PhD thesis, Ecole Normale Supérieure de Cachan, 2003. 32

[36] D. Vanoost, S. Steentjes, J. Peuteman, G. Gielen, H. De Gersem, D. Pissoort, and K. Hameyer. Magnetic hysteresis at the domain scale of a multi-scale material model for magneto-elastic behavior. *Journal of Magnetism and Magnetic Materials*, 414:168–179, 2016. 32

[37] A. Belahcen. *Magnetoelasticity, magnetic forces and magnetostriction in electrical machines*. PhD thesis, University of technology Helsinki, 2004. 48, 58

[38] M. Rossi and J. Le Besnerais. Vibration Reduction of Inductors Under Magnetostrictive and Maxwell Forces Excitation. *IEEE Transactions on Magnetics*, (51(12)), 2015. 48

[39] P. Pellerey. *Etude et Optimisation du Comportement Vibro-Acoustique des Machines Electriques, Application Au Domaine Automobile.* PhD thesis, Laboratoire d'Electromécanique de Compiègne, UTC, 2012. 48

[40] J. Hallal. *Etudes des vibrations d'origine électromagnétique d'une machine électrique : conception optimisée et variabilité du comportement vibratoire*. PhD thesis, Laboratoire d'Electromécanique de Compiègne, UTC, 2014. 48

[41] H.M. Zhou, Y.H. Zhou, X.J. Zheng, and J. Wei. A General Magnetoelastic Coupling Theory of Deformable Magnetized Medium Including Magnetic Forces and Magnetostriction Effects. *Tech Science Press*, (12(3)):237–249, 2009. 49

[42] Y.H. Zhou and X. Zheng. A generalized variational principle and theoretical model for magnetoelastic interaction of ferromagnetic bodies. *Science in China*, (42(6)), 1999. 49

[43] Y.H. Zhou and X. Zheng. A general expression of magnetic force for soft ferromagnetic plates in complex magnetic fields. *International Journal of Engineering Science*, (35(15)):1405–1417, 1997. 49

[44] Y.H. Zhouand K. Miya. A theoretical prediction of increase of natural frequency to ferromagnetic plates under in-plane magnetic fields. *Journal of Sound and Vibration*, (222(1)):49–64, 1999. 49

[45] S.A. Mohajerani, A. Mohammadzadeh, and M. Nikkhah Bahrami. An Exact Solution for Vibration Analysis of Soft Ferromagnetic Rectangular Plates Under the Influence of Magnetic Field with Levy Type Boundary Conditions. *Journal of Solid Mechanics*, (9(1)):186–197, 2017. 49

[46] L. Wei, S. A. Kah, and H. Ruilong. Vibration analysis of a ferromagnetic plate subjected to an inclined magnetic field. *International Journal of Mechanical Sciences*, (49):440–446, 2007. 49

[47] Y. Kou, L. Wang, and X. Zheng. Theoretical and experimental investigations on the resonance frequency shift characteristic of a ferromagnetic plate. *European Journal of Mechanics - A/Solids*, 50, 11 2014. 50

[48] C.B. Lin J.L. Lee. The Magnetic Viscous Damping Effect on the Natural Frequency of a Beam Plate Subject to an In-Plane Magnetic Field. *ASME Journal of Applied Mechanics*, 77(1):011014, 2010. 58

[49] S. S. Rao. *Mechanical Vibrations*. Prentice Hall, 2004. 66

[50] T. P. P. Phway, A. J. Moses, and D. C. Jiles. Frequency dependence of magnetostriction for magnetic actuators. *Journal of electrical engineering*, 55:7–10, 2004. 68

ESSIAL

Deliverable D 3.3
Magneto-mechanical dynamic modeling

WP3: Physical studies

Date of Delivery: 31/07/2019 (2nd update)

Lead Beneficiary: UPJV - Amiens

Type: Report

Dissemination Level: Public

Version: 3.5

ESSIAL has received funding from the European Union's Horizon 2020 research and innovation program under grant agreement No 766437.

Table of contents (2nd update)

List of Figures

Chapter 1

Modeling and identification of static and dynamic magnetic properties

1.1 Introduction

The purpose of this chapter is to identify the dynamic and static magnetic properties of magnetic sheets using a simple experimental apparatus, the Single Sheet Tester (SST). The identification is obtained using Maxwell's equations and a special dynamic law that defines the local behavior of the soft magnetic material. Next, the impact of the identified properties on the dynamic response is determined. This modeling study is the key to understand the effect of laser treatment on both the magnetic properties and the dynamic response in the magnetic structures. The magnetic study is eventually considered to define the relation between the magnetic behavior and the magnetostrictive efforts, main source of noise and vibration in electrical machines.

1.2 Electromagnetic modeling

1.2.1 Problem

A 150x150 mm^2 GO FeSi electrical steel sheet is considered with the following properties: thickness h, density ρ and electrical conductivity σ. The experiments are performed in the Single Sheet Tester, an apparatus dedicated for the measurement of the magnetic losses and the hysteresis. The sheet is magnetized inside the bench due to the presence of a uniform, in-plane and cycling magnetic field in the surrounding of the sheet (Fig. 1.1). This field is induced by the electrical currents generated in the primary coils. The problem consists in measuring the magnetic field $H_a(t)$ needed to magnetizes the sheet with a specific average induction $B_{av}(t)$ imposed by the user with a specific magnitude (induction level), frequency and signal shape. The latter is determined by the secondary coils of the bench. Fig. 1.2 shows the measured signals (applied magnetic field and average induction); a time delay is noticed between the two signals, representing the magnetic losses and hysteresis. The collected data are not able to give local information concerning the magnetic variables; then an identification of the measurements with a specific diffusion model is performed for this purpose, deriving at the meanwhile the static and dynamic properties to fit the model with the experiments.

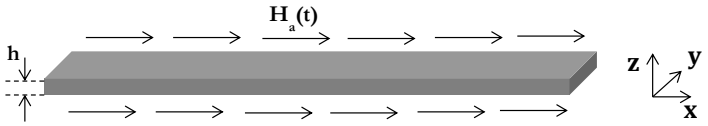

Fig. 1.1 Magnetization process in the SST

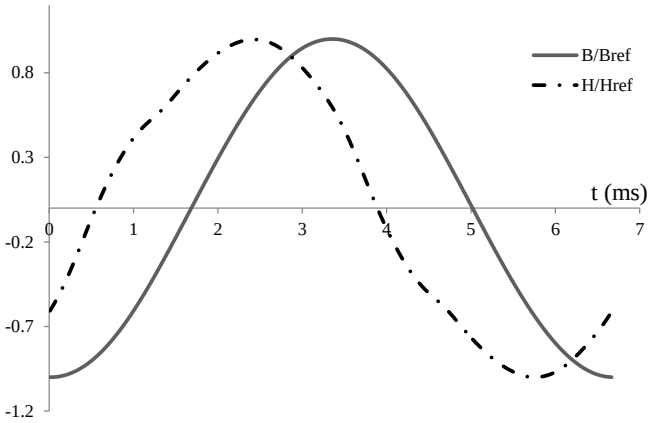

Fig. 1.2 Transient signals collected from the SST measurement.

1.2.2 Magnetic modeling: the Diffusion Equation

The electromagnetic behavior at the local space of the sample is modeled using the Maxwell's equations (Eqs. 1.1) that include space and time dependency.

$$\mathbf{rot}(\mathbf{H}) = \mathbf{J} \qquad \mathbf{rot}(\mathbf{E}) = -\frac{\partial \mathbf{B}}{\partial t} \tag{1.1}$$

J, **E**, **B** and **H** are the local vectors that correspond to the current density, the electrical field, the magnetic flux density and the magnetic field respectively. The problem presented in 1.2.1 reduces the complexity of the model to a 1-D analysis thanks to different contributions and assumptions:

1. The geometric symmetry with respect to the *xy* plane in the SST.
2. The in-plane dimensions are more significant than the thickness.
3. The symmetric applied magnetic field with respect to the *x*-axis.
4. The uniform magnetic field in the *x* direction.
5. The magnetic field is applied in the direction of lamination; the induced flux density is parallel to the magnetic field.

As a result, the magnetization occurs in the *x* direction and varies in the cross-section of the sheet (*z* direction). Considering a linear electrical behavior ($\mathbf{J} = \sigma\mathbf{E}$), the complex Maxwell's equations are reduced to a one-dimensional diffusion equation (Eq. 1.2), including the eddy current losses generated by the electromagnetic energy interchange. The equation correlates

two local variables: the local magnetic field $H(z,t)$ and the local flux density $B(z,t)$. The solution requires a magnetic behavioral law that correlates locally the two variables.

$$\frac{\partial^2 H(z,t)}{\partial z^2} = \sigma \frac{\partial B(z,t)}{\partial t} \qquad H(\pm\frac{h}{2},t) = H_a(t) \tag{1.2}$$

1.2.3 Dynamic behavioral law

The dynamic law behavior considered by Maloberti et al. [1] is adopted in this study. It includes the static behavior represented by the permeability of the material μ and a dynamic behavior modeled with a macroscopic dynamic property Λ that homogenizes and includes microscopic processes related to domains and walls.

$$\begin{aligned} H(z,t) &= H_{stat}(z,t) + H_{dyn}(z,t) \\ H(z,t) &= \mu(B)^{-1} B(z,t) + \sigma \Lambda^2(B, \frac{\partial B}{\partial t}) \frac{\partial B(z,t)}{\partial t} \end{aligned} \tag{1.3}$$

The law can be separated into static H_{stat} and dynamic terms H_{dyn}. The static contribution is conservative and represents the anhysteretic behavior independent of the exciting frequency; it follows a generally static non-linear law $\mu(H_{stat}) = B(H_{stat})/H_{stat}$. Meanwhile, the dynamic term represents the dissipation generated by the walls mobility and the domains size; the application of a local magnetic field does not contribute to an instantaneous magnetization of the material; a time delay is observed between the field and induction due to the domain structure leading to dynamic excessive magnetic losses in addition to the eddy current losses.

1.2.4 Analytical solution

The analytical solution of the diffusion equation (Eq. 1.2) with constant linear magnetic behavior (Eq. 1.3) is proposed. Assuming that the static and dynamic properties described in Eq. 1.3 are independent of the magnetic variables, the diffusion differential equation (Eq. 1.2) can be analytically solved due to the linearity of both the model and the law. A transformation of the transient equations to the frequency domains is considered and a dispersion relation is obtained [1] using the Fourier time and space transform.

$$k^2(1 + j\sigma\Lambda^2\mu\omega) + j\sigma\mu\omega = 0 \tag{1.4}$$

k is a complex number in the form $k = k_- - jk_+$,

$$k_\pm(\mu,\Lambda,\sigma,\omega) = \sqrt{\frac{1}{2}\left(\frac{\mu\sigma\omega}{1+(\sigma\Lambda^2\mu\omega)^2}\right)\left(\pm\sigma\Lambda^2\mu\omega + \sqrt{1+(\sigma\Lambda^2\mu\omega)^2}\right)} \tag{1.5}$$

The complex magnitude of the local magnetic flux density ($\tilde{B}(z,\omega)$), solution of Eq. 2.19 can be expressed.

$$\tilde{B}(z) = \frac{\mu\tilde{H}_a}{1+\sigma\Lambda^2\mu\omega}\frac{\cosh((k_+ + jk_-)z)}{\cosh((k_+ + jk_-)h/2)} = |\tilde{B}(z)|e^{j\varphi} \tag{1.6}$$

Therefore, the average flux density can be eventually derived.

$$\tilde{B}_{av} = \frac{1}{h}\int_{-\frac{h}{2}}^{-\frac{h}{2}} \tilde{B}(z)dz = \frac{2\mu\tilde{H}_a}{h(k_+ + jk_-)(1+j\sigma\Lambda^2\mu\omega)}\tanh((k_+ + jk_-)h/2) \tag{1.7}$$

The posed problem considers the determination of the applied magnetic field for a given average induction, Eq. 1.7 is inversed.

$$\tilde{H}_a = \frac{h(k_+ + jk_-)(1 + j\sigma\Lambda^2\mu\omega)}{2\mu\,\tanh((k_+ + jk_-)h/2)}\tilde{B}_{av} \tag{1.8}$$

The determination of the surface magnetic field (Eq. 1.8) allows the calculation of the local flux density's complex magnitude using Eq. 1.6, and derive a time response of this property (Eq. 1.9).

$$B(z,t) = |\tilde{B}(z)|\cos(\omega t + \varphi) \tag{1.9}$$

The proposed analytical solution calculates the local dynamic behavior based on the knowledge of the magnetic properties and a given average magnetic field. It is also the key to determine the effect of the magnetic properties on the dynamic local response.

1.3 Magnetic properties identification

The signals $H_a(t)$ and $B_{av}(t)$ measured in the SST are identified with a numerical model in order and allow the determination of the magnetic law that describes the material's dynamic behavior and allows the knowledge of the local variables that vary with the sheet's cross section. In this case, the non-linearity due to the static property specially for high inductions do not allow the use of the analytical solution. Therefore, a numerical discretization model is proposed.

1.3.1 Numerical Strategy

The dynamic problem (Eq. 1.2) includes a dependency with the z-direction. This constraint is solved using the finite element discretization technique that transforms the problem to a matrix formulation using 1-D quadratic shape functions with a 3-nodes element (Fig. 1.3). The quadratic methodolody gives accurate result for a limited number of elements. Combining Eq. 1.2 and Eq. 1.3, the discretization is presented by the matrix system:

$$\mathbf{U}\mu^{-1}(B)\mathbf{B}(t) + \sigma\mathbf{U}\Lambda^2\mathbf{B}(t) + \sigma\mathbf{V}\frac{\partial\mathbf{B}}{\partial t}(t) = H_a(t)\mathbf{f} \tag{1.10}$$

U and **V** are nodal matrices and **f** is a nodal vector; they include the quadratic shape functions and the geometric constraints, μ is the static property matrix and **Λ** is the dynamic property matrix. **B** and **H** are discretized vectors representing respectively local flux density and field, and H_a is the applied magnetic field. Eq. 1.10 is dynamically solved using a simple time discretization ($f(t) = \frac{\partial f}{\partial t}(t-1)dt + f(t-1)$) with a constant time step dt equal to the experimental sampling period. The starting point considers a uniform discretized vector B equal to the initial average induction $B_{av}(0)$.

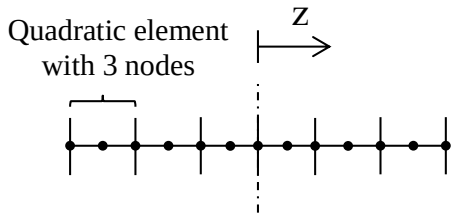

Fig. 1.3 Quadratic elements discretization

1.3.2 Static property

The identification of the static property at a specific induction magnitude corresponds to the mid-anhysteretic curve obtained for any measured cycle. This curve is obtained by removing the hysteresis between the signals of fig. 1.2 or by studying the magnetic behavior at very low frequency (3 or 5 Hz). Neglecting the static losses, a mid-anhysteretic curve is obtained as shown in fig. 1.4 independent of the dynamic behavior (frequency), but dependent on the induction level. The static property $\mu(H_{stat})$ is a non-linear parameter that directly correlates the induction to the magnetic field in the static state $\mu = B/H_{stat}$. Based on the Jiles-Atherton model [2], the non-linear static property can be modeled using a fitting with the Langevin function [3].

$$B = B_s \left[\coth\left(\frac{H_{stat}}{a}\right) - \frac{a}{H_{stat}} \right] \tag{1.11}$$

B_s and a are the model parameters. B_s is the saturation induction and $a = k_B T/\mu_0 m$ where k_B is the Boltzmann constant, T is the temperature, $\mu_0 = 4\pi.10^{-7} H/m$ is the permeability of vacuum and m is the mean effective domain size [4]. Fig. 1.5 compares the measured anhysteretic curve with the fitted Jiles-Atherton model and shows a very good agreement with the measurements. However, the use of the discretized equation (Eq. 1.10) to identify the dynamic property or to calculate the flux density vector **B** requires a reciprocal form of the proposed static law (Eq. 1.11): $H_{stat} = f(B)$. Since the use of inverse numerical optimization techniques for modeling this law requires high computational time. An easy-to-use approximation inverse Langevin function proposed by Jedynak [3] is a fast and accurate solving method (Eq. 1.12).

$$H_M(B) = \frac{B/B_s}{a} \frac{2.999 - 2.573B/B_s + 0.655(B/B_s)^2}{1 - 0.895B/B_s - 0.105(B/B_s)^2} \tag{1.12}$$

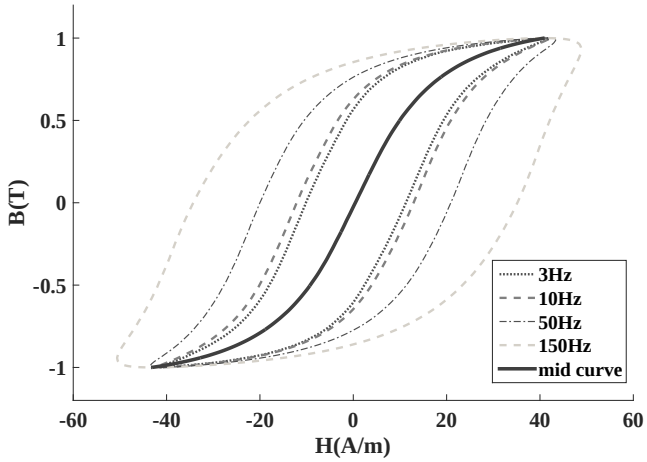

Fig. 1.4 Mid-anhysteretic curve at 1T induction level for a reference sample with different frequencies

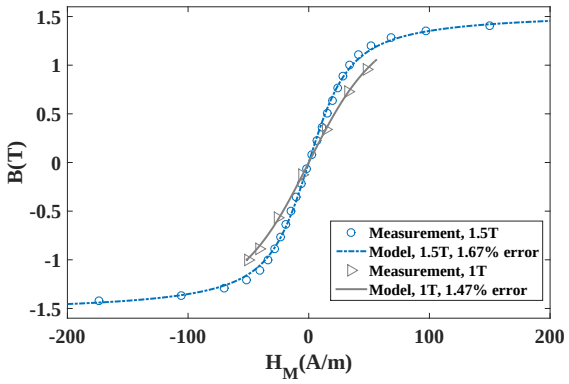

Fig. 1.5 Mid-anhysteretic curve fitting using Eq. 1.12 for 1 T and 1.5 T induction.

1.3.3 Identification of the dynamic property

The determination of the dynamic property Λ is presented in this section. This property depends not only on the induction magnitude, but also on the frequency of excitation [1]. Therefore, the discretized diffusion equation (Eq. 1.10) is used to determine the dynamic property, assumed constant through each measured cycle. It requires the knowledge of the static behavior presented in the inverse Langevin equation (Eq. 1.12). Eq. 1.10 calculates the local magnetic flux density vector **B** from which the average induction is directly derived ($B_{av}(t) = \int_{-\frac{h}{2}}^{\frac{h}{2}} B dz$). The identification of Λ consists in minimizing the error between the cycle's areas that represent the total losses contribution (Strategy 1) or in minimizing the error between the measured and the calculated cycles (Strategy 2).

1. Strategy 1: min $(\int_0^T H(t) dB_{meas}(t) - \int_0^T H(t) dB_{num}(t))$
2. Strategy 2: min $\Sigma(B_{meas}(t) - B_{num}(t))^2$

It appears that strategy 2 gives more accurate fitting and needs less computational time. Therefore, it is adopted to identify the dynamic behavior and a set of properties is obtained for different induction magnitudes and frequencies as shown in Fig. 1.6 and Fig. 1.7. A validation of the model is then performed by solving the direct problem using the identified properties and the results are shown in fig. 1.8 for a reference sample and a laser treated sample. It is shown that the cycles are steeper and thinner for the laser treatement for all inductions and frequencies.

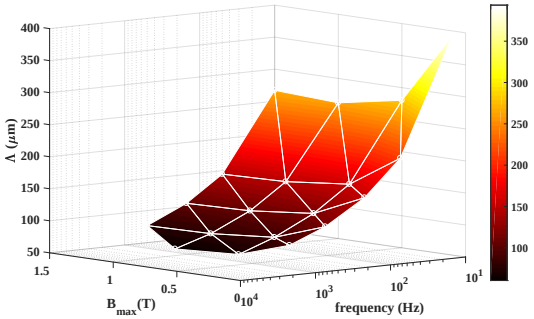

Fig. 1.6 Dynamic property as function of the induction level and the frequency for the reference sample (GO Material).

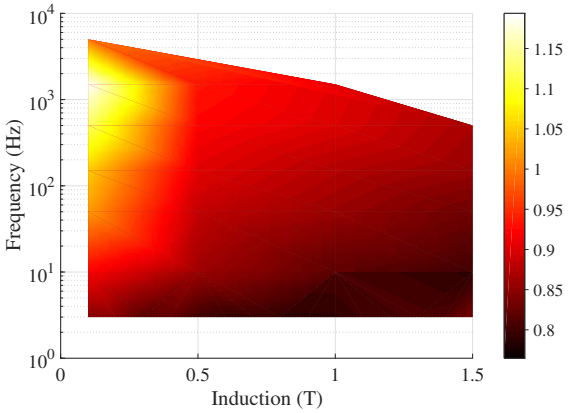

Fig. 1.7 Dynamic property as function of the induction level and the frequency for the reference sample (NGO Material).

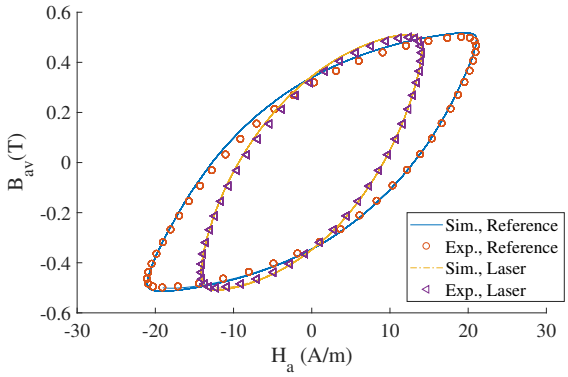

(a) 0.5 T, 50 Hz

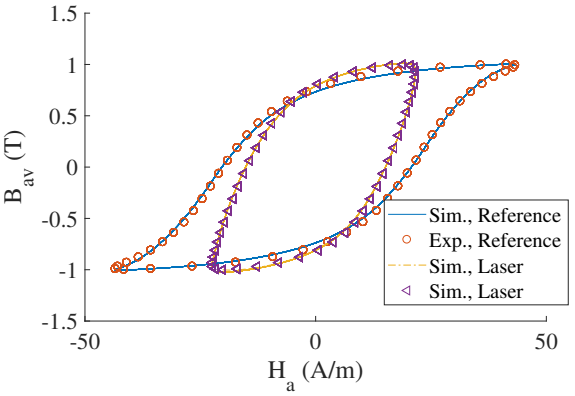

(b) 1 T, 50 Hz

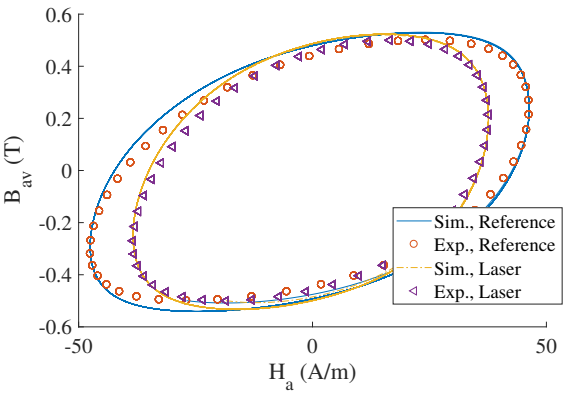

(c) 0.5 T, 500 Hz

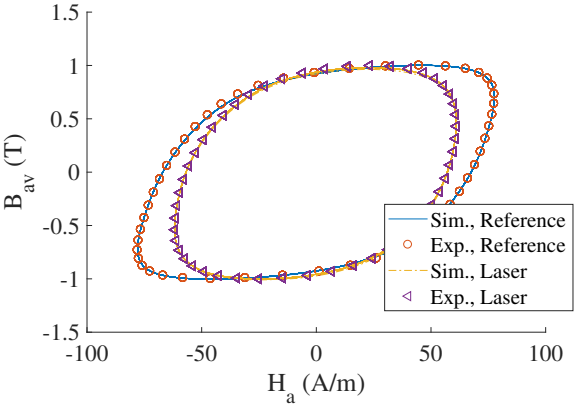

(d) 1 T, 500 Hz

Fig. 1.8 Hysteresis cycles comparison between identified model and measurements

1.4 Sensitivity of the dynamic response to the static and dynamic properties

The transient response of the flux density is calculated for different static μ and dynamic Λ properties using the linear analytical approach developed in section 1.2.4. This parametric study helps to understand the effect of magnetic properties and eventually the effect of the laser treatment sensitive to the magnetic properties. The reference parameters are: thickness $h = 0.23mm$, electrical conductivity $\sigma = 2.10^6(\Omega.m)^{-1}$. The variable parameters are the relative permeability $\mu_r = \mu/\mu_0$ and the dynamic property Λ. The effect of the static property μ_r and the dymanic property Λ in terms of magnitude and delay is observed by comparing the local induction with the average induction with respect to the magnetic field on one hand (Figs. 1.9 and 1.10), and with respect to the average induction on the other hand (Figs. 1.11 and 1.12). The increase of the permeability induces an increase in the dispersion of the flux density profile (skin effect) as shown in Figs. 1.9a and 1.9b. The magnitude and the delay of the induction with respect to the magnetic field increase. On the other hand, the decrease of the dynamic property (domains refinement) leads to an increase in the profile's dispersion with respect to the magnetic field as shown in Figs. 1.10a and 1.10b. The magnitude increases and the induction's delay with respect to the magnetic field decreases when decreasing Λ.
Figs. 1.11 and 1.12 plot the distribution of the magnitude and the angle of the flux density in the cross section for different values of μ_r and Λ and with respect to the average induction. The increase of the permeability induces an increase in the dispersion of the flux density magnitude profile (Fig. 1.11a) and an increase in the dispersion of the flux density phase profile for a limit of $\mu_r = 5000$ then a decrease of the profile dispersion (Fig. 1.11b). On the other hand, the decrease of the dynamic property leads to an increase in the magnitude dispersion with an optimum at Λ=100μm followed by a decrease (Fig. 1.12a). As for the angle between the local and the average induction, its profile is more dispersed when Λ decreases (Fig. 1.12b).

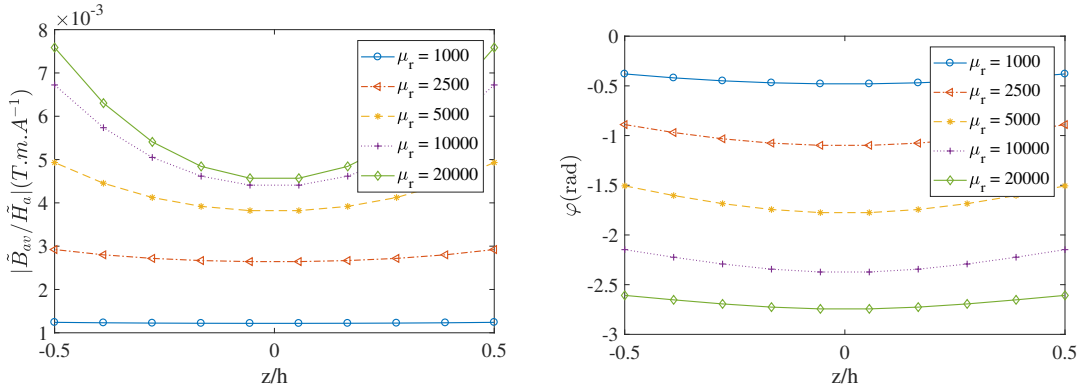

(a) Magnitude distribution **(b)** Delay distribution

Fig. 1.9 Effect of μ_r on the flux density distribution with respect to the applied magnetic field.

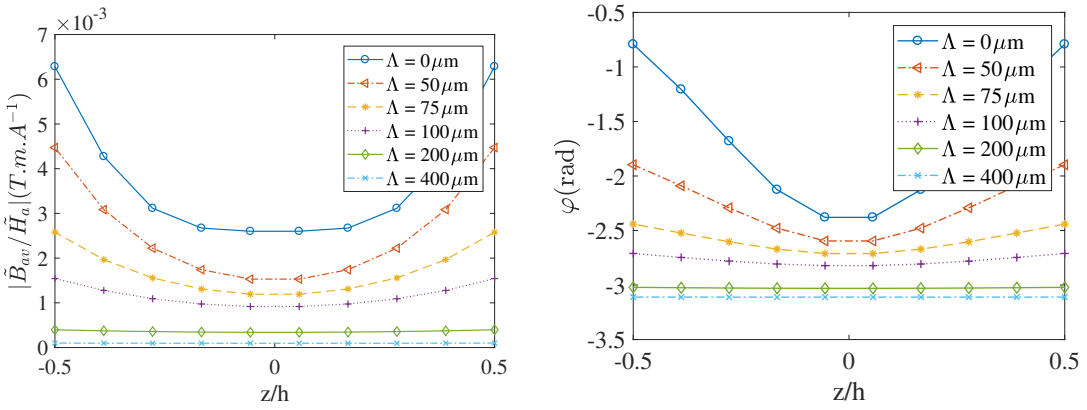

(a) Magnitude distribution **(b)** Delay distribution

Fig. 1.10 Effect of Λ on the flux density distribution with respect the applied magnetic field.

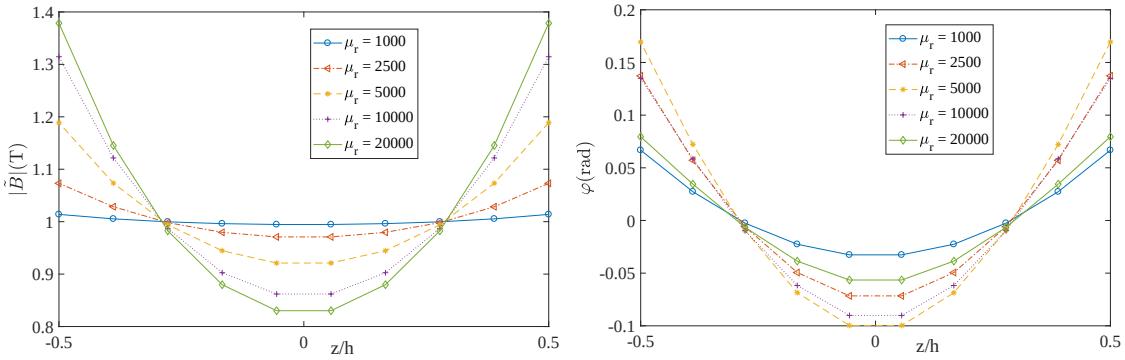

(a) Magnitude distribution (around 1 T) **(b)** Delay distribution (around 0 rad)

Fig. 1.11 Effect of μ_r on the flux density distribution in the cross section.

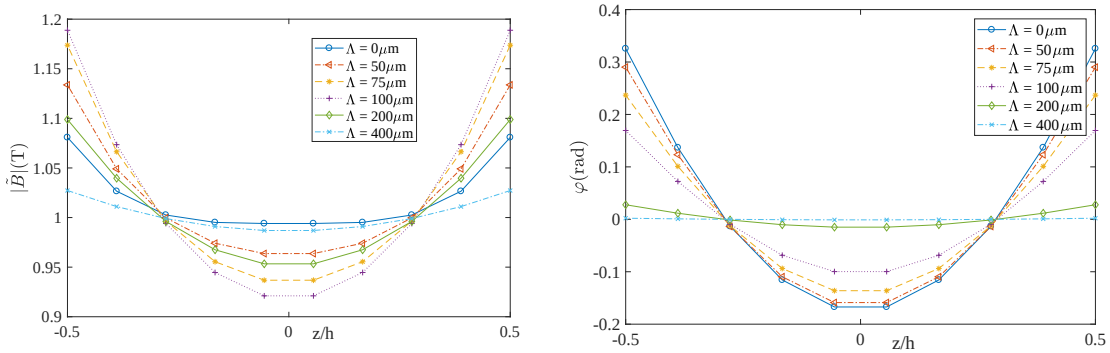

(a) Magnitude distribution (around 1 T) **(b)** Delay distribution (around 0 rad)

Fig. 1.12 Effect of Λ on the flux density distribution in the cross section.

Chapter 2

Mechanical modeling and identification of mechanical loads

2.1 Presentation

Loads are generated inside the SST due to the electromagnetic and magnetostrictive efforts resulting from the magnetization process. In this chapter, these loads are identifed and estimated inside the SST using several techniques. The aim of this study is to identify the effect of laser treatment on these loads, and eventually on the creation of noise and vibration in electrical machines. A correlation between the magnetic properties identified in chapter 1 and the magnetic loads must be determined for this purpose. Hence, the mechanical identification is performed in the same apparatus (the SST) where a 1-D magnetization is considered.

2.1.1 Magnetic stresses generated in the magnetized structure

The magnetic stresses and forces generated in the SST are presented in this section using the beam's theory. The stress components corresponding to an infinitesimal volume in the beam are the normal stresses σ_{xx} and σ_{zz} in x and z directions respectively, and the shear stress σ_{xz} in the plane xz. For a magnetically isotropic material subjected to a magnetization process in the SST, the shear stress component vanishes. As for the beam, the longitudinal component σ_{xx} is more effective than the transverse component σ_{zz} due to the geometric considerations (the length of the plate is much larger than its thickness). Therefore, main magnetic stresses due to either magnetostriction or Maxwell forces are the longitudinal stresses ($\sigma_{mag} = \sigma_{xx}$). In fact, magnetostriction is a phenomenon where the deformation of the elastic medium appears in the presence of the magnetic field. Therefore, a strain tensor is created and the rigid contact between the two yokes and the corners of the sheet prevents the latter from expansion. In fact, the clamps at the corners of the sheet induce a support force that generates a uniform stress distribution through the length of the plate. Meanwhile, the magnetic stresses resulting from Maxwell's forces are also found due to the electromagnetic interaction with the same effect obtained by the magnetostriction.

The total magnetic axial effort $N_{mag}(t)$ that includes both Maxwell and magnetostriction loads is assumed to be proportional to the square of the mean magnetic flux density $B(t)$, considering no external mechanical stresses applied on the structure.

$$N_{mag}(t) = \int_{-\frac{h}{2}}^{-\frac{h}{2}} \sigma_{mag} dz = \int_{-\frac{h}{2}}^{-\frac{h}{2}} \alpha B^2(z,t) dz \tag{2.1}$$

2.1.2 Magnetic Maxwell's Forces in SST

Mechanical volume forces resulting from the distribution of the mechanical stresses in the geometry of the structure are related as follows [5]:

$$f = \begin{pmatrix} \frac{\partial \sigma_{xx}}{\partial x} + \frac{\partial \sigma_{xz}}{\partial z} \\ \frac{\partial \sigma_{xz}}{\partial x} + \frac{\partial \sigma_{zz}}{\partial z} \end{pmatrix} \tag{2.2}$$

The generated efforts through the whole thickness of a plate are given by:

$$N = \begin{pmatrix} N_x \\ M_x \\ Q_x \end{pmatrix} = \int_{-\frac{h}{2}}^{\frac{h}{2}} \begin{pmatrix} \sigma_{xx} \\ z\sigma_{xx} \\ \sigma_{xz} \end{pmatrix} dz \tag{2.3}$$

The shear stress σ_{xz} and the shear effort Q_x vanish and the components m_y and M_x are removed due to the symmetry. The structure is only subjected to vertical forces f_z:

$$f_x = \frac{\partial N_x}{\partial x} = 0 \tag{2.4}$$

$$f_z = \sigma_{zz}(\frac{h}{2}) - \sigma_{zz}(-\frac{h}{2}) \tag{2.5}$$

Similarly to the strategy adopted in Section 2.1, the magnetic surface Maxwell forces generated in the beam are simulated with Altair Flux2D. These forces are the combination of the body forces resulting from the vertical stress gradient and surface forces generated in the material-air interface. Figure 2.1 shows their vertical uniform distribution resulting from the distribution of H and B. The magnitude of these forces is negligible in comparison with the axial forces and their effect on the frequency swift explained in Section 2.2.3.

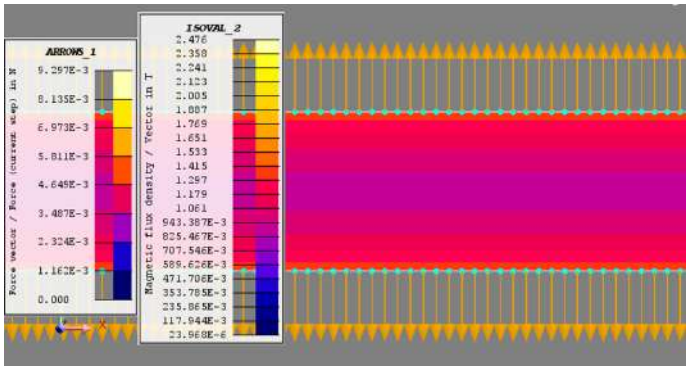

Fig. 2.1 Uniform distribution of Maxwell forces (arrows) on the upper and the lower surfaces of the magnetic sample with a symmetry around the mid-axis

2.2 Transverse Vibration Modeling

A clamped beam of length L, width b and thickness h is considered for modeling the magnetic sheet's mechanical setup. It has a Young's Modulus E, a Poisson ratio ν and a density ρ. The beam is subjected to an axial uniform and cycling magnetic load and two opposite normal forces (Maxwell forces). The dynamic mechanical modeling of the magnetic sheet is developed using the Hamilton's principle. Figure 2.2 illustrates the magneto-mechanical conditions

applied on the magnetic sheet in the SST and Figure 2.3 describes the magnetic loads applied on the sheet due to the magnetostriction.

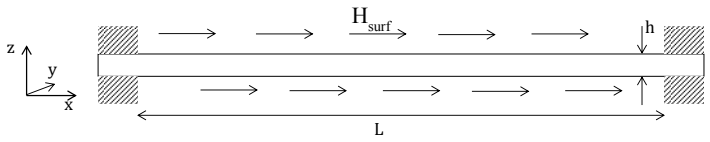

Fig. 2.2 A simple representation of the magneto-mechanical conditions applied on the magnetic sheet inserted in the SST

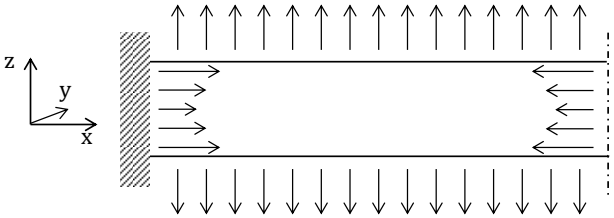

Fig. 2.3 A representation of the magnetic efforts generated in the sheet

2.2.1 Strain and Displacement Components

A thin beam is considered where the shear components are neglected. The in-plane dimensions (length and width) are much larger than the thickness; only in-plane strains and stresses are considered. In addition, the length is relatively larger than the width; the beam theory along the length of the structure is considered. Hence, we only consider the axial strain ε_x^0 and the bending κ_x, and the total strain on a position (x, z) is expressed as follows [6]:

$$\varepsilon_x = \varepsilon_x^0 + z\kappa_x \tag{2.6}$$

where ε_x^0 is the strain component at the mid-axis ($z = 0$) and ε_x is the strain component at a z distance from the mid-axis and κ_x, the bending component is:

$$\kappa_x = -\frac{\partial^2 w}{\partial x^2} \tag{2.7}$$

Considering the finite deformation theory, the axial deformation on the mid-axis is related to the axial displacement u^0 and the vertical displacement w with the following expression:[6]

$$\varepsilon_x^0 = \frac{\partial u^0}{\partial x} + \frac{1}{2}\left(\frac{\partial w}{\partial x}\right)^2 \tag{2.8}$$

The axial strain at a specific position z becomes:

$$\varepsilon_x = \frac{\partial u^0}{\partial x} + \frac{1}{2}\left(\frac{\partial w}{\partial x}\right)^2 - z\frac{\partial^2 w}{\partial x^2} \tag{2.9}$$

2.2.2 Modeling with Hamilton's Principle

The strain energy of the plate is given by:

$$U = \frac{1}{2}\frac{E}{1-\nu^2}b\int_0^L\int_{-\frac{h}{2}}^{\frac{h}{2}}\varepsilon_x^2 dzdx = \frac{1}{2}Eb\int_0^L\left[h\left(\frac{\partial u^0}{\partial x}\right)^2 + \frac{h^3}{12}\left(\frac{\partial^2 w}{\partial x^2}\right)^2 + \frac{h}{4}\left(\frac{\partial w}{\partial x}\right)^4 + h\frac{\partial u^0}{\partial x}\left(\frac{\partial w}{\partial x}\right)^2\right]dx \tag{2.10}$$

The kinetic energy of the magnetic sheet is expressed by [6]:

$$T = \frac{1}{2}\rho b\int_0^L\int_{-\frac{h}{2}}^{\frac{h}{2}}\left[\left(\frac{\partial u_0}{\partial t} - z\frac{\partial^2 w}{\partial x \partial t}\right)^2 + \left(\frac{\partial w}{\partial t}\right)^2\right]dzdx \simeq \frac{1}{2}\rho bh\int_0^L\left[\left(\frac{\partial u_0}{\partial t}\right)^2 + \left(\frac{\partial w}{\partial t}\right)^2\right]dx \tag{2.11}$$

The work done by the in-plane axial uniform load is:

$$W_1 = \frac{1}{2}b\int_0^L\int_{-\frac{h}{2}}^{\frac{h}{2}}\sigma_{mag}(z,t)\left(\frac{\partial w}{\partial x}\right)^2 dzdx = \frac{1}{2}bh\int_0^L N_{mag}(t)\left(\frac{\partial w}{\partial x}\right)^2 dx \tag{2.12}$$

$N_{mag}(t)$ is the membrane load applied on a section of the plate due to the magnetization process; in this study, $N_{mag}(t)$ is uniform through the length and is expressed by:

$$N_{mag}(t) = \int_{\frac{-h}{2}}^{\frac{h}{2}}\sigma_{mag}(z,t)dz \tag{2.13}$$

$\sigma_{mag}(z,t)$ is the longitudinal stress developed in the material including the magnetostrictive and Maxwell effects described in Section 2.1.1.

Applying Hamilton's principle $\delta\int_{t_1}^{t_2}(T-U-W_1)dt = 0$ on the different energy terms of Equations 2.10, 2.11 and 2.12 with respect to the transverse displacement $w(x,t)$, a transverse vibration equation is obtained[7],

$$\rho h\frac{\partial^2 w}{\partial t^2} + E\frac{h^3}{12}\frac{\partial^4 w}{\partial x^4} - N_{mag}(t)\frac{\partial^2 w}{\partial x^2} = 0 \tag{2.14}$$

with the following boundary conditions

$$w_{(x=0)} = 0, w_{(x=L)} = 0, \frac{\partial w}{\partial x}_{(x=0)} = 0, \frac{\partial w}{\partial x}_{(x=L)} = 0, \tag{2.15}$$

Equation 2.14 is time and position dependent (x,t). The position dependence in the x-direction is modeled with a mode shape function applied on the first mode of vibration. The shape function $\phi(x)$ is calculated in a way to include the developed model (Equation 2.14) and the boundary conditions (Equation 2.15). It allows a variable separation between space x and time t on the displacement $w(x,t)$:

$$w(x,t) = w_0(t)\phi(x) \tag{2.16}$$

Replacing Equation 2.16 in Equation 2.14, we obtain:

$$\rho h\phi(x)\frac{\partial^2 w_0(t)}{\partial t^2} + E\frac{h^3}{12}\frac{\partial^4 \phi(x)}{\partial x^4}w_0(t) - N_{mag}(t)\frac{\partial^2 \phi(x)}{\partial x^2}w_0(t) = 0 \tag{2.17}$$

A non-linear equation with linear terms is obtained. Multiplying Equation 2.17 by $\phi(x)$ and integrating on the magnetized length of the sheet we obtain:

$$m\frac{\partial^2 w_0(t)}{\partial t^2} + [k + cN_x(t)]w_0(t) = 0 \tag{2.18}$$

where $m = \rho h \int_0^L \phi^2(x)dx$, $k = \frac{Eh^3}{12}\int_0^L \frac{\partial^4\phi(x)}{\partial x^4}\phi(x)dx$ and $c = -\int_0^L \frac{\partial^2\phi(x)}{\partial x^2}\phi(x)dx$. m, k and c are positive values that depend on the mechanical and geometric configurations of the structure.

Equation 2.18 is the mechanical dynamic equation that models the motion the behavior in deflection for the magnetic plate inserted in the SST.

2.2.3 Axial Effort Calculation Using the Modal Analysis Approach

A simple and specific method for calculating of the magnetic load is presented using the modal analysis approach. In fact, modal analysis consists of determining the natural frequencies and the mode shapes of vibration of the magnetic sheet. It corresponds to the exciting frequency that creates resonance on the sample. The analysis is based on Equation 2.18 by applying the Fourier Transformation.

It can be noticed from the measurements that the acceleration (and eventually the displacement $w_0(t)$) oscillates with the frequencies f, $2f$, ..., nf, where f is twice as much as the magnetic exciting frequency ($f = 2f_{mag}$) and possesses the higher contribution in amplitude (fundamental frequency). At resonance, the oscillating frequency f reaches the natural frequency of vibration f_0 and the secondary frequency have negligible amplitudes as shown in Figure 2.5. The displacement $w_0(t)$ can be expressed as follows :

$$w_0(t) = W_0 \cos(2\pi f t + \varphi_1) \tag{2.19}$$

where W_0 is the amplitude of the signal that appears in the frequency spectrum and φ_1 is the phase shift.
$B(z,t)$ is a sinusoidal signal with a frequency equal to half of the displacement's frequency ($f_{mag} = \frac{f}{2}$), therefore:

$$B(t) = B_{max}\cos(\frac{2\pi f}{2}t + \varphi_2) \tag{2.20}$$

where φ_2 is the phase shift of the flux density's signal.
Combining Equations 2.1 and 2.20 one gets,

$$N_{mag}(t) = \alpha B_{max}^2 \cos^2(\frac{2\pi f}{2}t + \varphi_2) = \frac{N_{max}}{2}[1 + \cos(2\pi f t + 2\varphi_2)] \tag{2.21}$$

where N_{max} is the amplitude of $N_x(t)$ and φ_2 its phase shift. Replacing Equations 2.19 and 2.21 in Equation 2.18 and applying a Fourier transformation on Equation 2.18, a spectral analysis is performed at the resonance frequency ($f = f_0$) that corresponds to the peak amplitude obtained by performing the frequency sweep explained in Section 2.2.4. The following equation is obtained at the resonance frequency:

$$-\omega_0^2 m + k + c\frac{N_{max}}{2} = 0 \tag{2.22}$$

$$N_{max} = \frac{8\pi^2 m}{c}(f_0^2 - f_n^2) \tag{2.23}$$

where $f_n = \frac{1}{2\pi}\sqrt{\frac{k}{m}}$ is the natural frequency of the structure without magnetization. The magnitude of the generated magnetic axial load can be easily determined by measuring the resonance frequency f_0.
It can be noticed from Equation 2.23 that an increase in the resonance frequency ($f_0 > f_n$) corresponds to a tensile load and a decrease in the resonance frequency corresponds to a compressive load.

2.2.4 Frequency Sweep Around the Natural Frequency

The determination of the fundamental resonance frequency f_0 of the structure is performed using a sweep of the magnetic frequency f_{mag} of the magnetic flux density that equals half of the vibrating frequency of the sample. A convergence study is performed in order to determine the resonance frequency corresponding to a peak amplitude in the frequency spectrum. The natural frequency f_n is calculated analytically using the model described above and measured by exciting the sample without magnetization. Figures 2.4 and 2.5 show respectively the transient and the frequency responses measured using the accelerometer at resonance frequency for a maximum induction of 0.9T. As shown in Figure 2.5 the dominant peak is found at the resonance frequency that corresponds to double the applied induction's frequency. Once the resonance frequency is experimentally identified, it is compared to the natural frequency without magnetization and the maximal axial effort is identified using Equation 2.23.

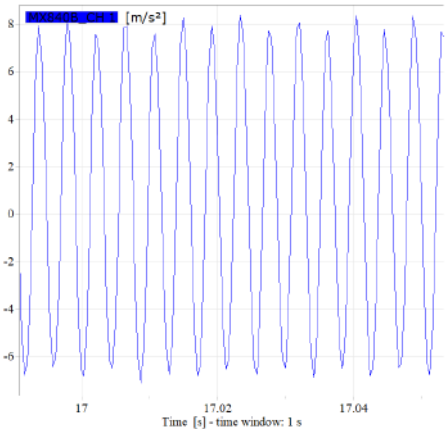

Fig. 2.4 Acceleration's transient response at the resonance frequency

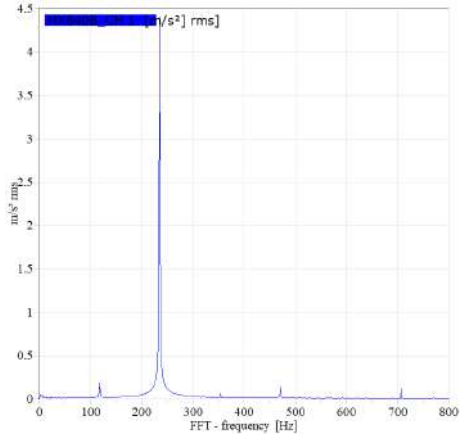

Fig. 2.5 Fast Fourier Transform (FFT) of the measured acceleration at the resonance frequency

2.2.5 Limitations of the transverse modeling

This developed estimates in a very simple way the magnitude of the induced magnetic loads. However, several limitations are observed using this method. First, the frequency sweep requires a compromise between the precision and the time measurement consumption, because a the frequency sweep searches for the resonance frequency that corresponds to a peak amplitude. On the other hand, the transverse model does not give a synchronous measurement between the magnetic signals (induction and magnetic field) and the mechanical load because the latter is determined using a modal analysis technique and not a classic vibration input/output model. Finally, this technique can be limited by the generation of surfaces stresses, due to the transverse vibration, that modify the global dynamic behavior.

2.3 Longitudinal Vibration Modeling

2.3.1 Dynamic equation

Taking into consideration the transverse model's limitations, a more simple approach for the identification of magnetostrictive behavior issued from the magnetization process is considered. In fact, the cover of the SST is removed and the magnetic sheet is clamped at one end and free at the other end as shown in Fig. 2.6. A piezoelectric accelerometer is placed at the free end of the sheet and measures the acceleration in the sheet's longitudinal direction. Due to the magnetization process in the SST, the sheet is only magnetized in a specific region (Fig. 2.6) and a local magnetostrictive strain ε_{ms} is created in this zone, depending on the induction, the Young's modulus, magneto-elastic coupling properties and the internal mechanical stresses. Considering a thin beam with a cross section A and a Young's modulus E, the 1-D longitudinal dynamic behavior is described in Eq. 2.24, where the longitudinal displacement is considered $u(x,t)$.

$$\int_0^L \rho A \frac{\partial^2 u}{\partial t^2} dx + \int_0^L f\left(\frac{du}{dt}\right) dx \int_0^L EA \frac{\partial^2 u}{\partial x^2} dx = \int_0^L f dx = \int_0^L EA \frac{\varepsilon_{ms}}{L_{mag}} dx \tag{2.24}$$

The longitudinal equation 2.24 is discretized with the finite element method, including the boundary condition (fixed-free). A discretized displacement vector$\{u\}$ is obtained with mass $\mathbf{M}$, damping $\mathbf{C}$ and stiffness $\mathbf{K}$ matrices and a discretized force vector $\{f_e\}$; the dynamic equation becomes:

$$\mathbf{M}\{\ddot{u}\} + \mathbf{C}\{\dot{u}\} + \mathbf{K}\{u\} = \{f_e\} \tag{2.25}$$

Vector $\{f_e\}$ contains the magnetostriction strain coefficient ε_{ms}, the Young's modulus E and the cross section A. The force is only applied on the magnetized zone.

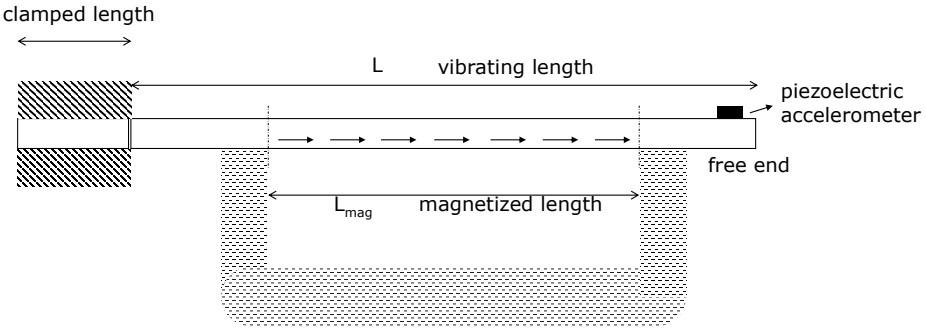

Fig. 2.6 Schematic representation of the longitudinal deformation due to the magnetization process in the SST for a fixed-clamped sheet.

2.3.2 Identification for identification of the Magnetostrictive Coefficient

The identification of the magnetostrictive coefficient ε_{ms} can be perfomed by inversing the Eq. 2.25. In fact, the degree of freedom is equal to a certain value n, Eq. 2.25 contains n unknown values in the discretized displacement vector $\{u\}$ and one unknown in the force vector ε_{ms} that must be identified. The problem is indeterminate since it has more unknown $(n+1)$ than equations (n). Therefore, a measurement of only one displacement component reduces the total number of unknowns and makes the problem solvable. The measurement technique requires the use of a piezoelectric accelerometer at the free end of the structure; the measured acceleration is integrated twice to obtain the free end displacement component. The magnetostrictive coefficient $\varepsilon_{ms}(t)$ is finally determined is parallel with the measured magnetic flux denisty $B_{av}(t)$ and the applied magnetic field $H_a(t)$.

2.3.3 Magneto-mechanical model identification

A correlation between the mechanical signal ε_{ms} and the magnetic signal $B_{av}(t)$ is developed. Many studies have modeled a relation between magnetostriction and the induction at different scales. Some models assume an anhysteretic behavior [8, 9, 10], including the dependence of the magnetostriction on the induction and the present stresses; a direct relation between the magnetostriction and the square of the induction is proposed. The obtained quadratic relationship results from the rotation of the loal magnetization with respect to the crystal's axis [11]. In fact, at this scale, the local magnetization is constant in magnitude but the orientation varies with the applied magnetic field that tends to lead the magnetization in its direction with an energy minimization strategy.
On the other hand, other researches take into account the hysteresis effect between the magnetostriction and the induction [12]. In fact, each domain is deformed due to the application of the magnetic field and the rotation of the magnetic moments. The latter is locally delayed with respect to the applied magnetic field (approach modeled by the dynamic property Λ in chapter 1). In addition, the presence of eddy currents delays the response of the induction with respect to the magnetic field [13]. Therefore, the deformation is also delayed and an hysterestic behavior is observed between the magnetic and the mechanical signals.
An empirical first order modeling approach is proposed:

$$\tau \frac{d\varepsilon_{ms}}{dt} + \varepsilon_{ms}(t) = \frac{1}{P} \frac{B_{av}^2(t)}{2\mu_0} \tag{2.26}$$

τ includes the hysteresis and P is a magneto-elastic property that includes the Young's modulus, the applied stress effect and a magneto-elastic coupling behavior. The identified properties τ and P are defined at the macroscopic scale, considering the observed variables. The comprehension of the physical meaning of these properties requires a transition to the mesoscopic scale where Eq. 2.26 is locally studied using the magnetic analysis developed in chapter 1:

$$\int_{-\frac{h}{2}}^{\frac{h}{2}} \tau \frac{d\varepsilon_{ms}}{dt} dz + \int_{-\frac{h}{2}}^{\frac{h}{2}} \varepsilon_{ms}(t) dz = \int_{-\frac{h}{2}}^{\frac{h}{2}} \frac{B^2(z,t)}{2P\mu_0} dz \tag{2.27}$$

This approach includes the local dynamic behavior and the eddy current losses and the nonlinearty of the magnetic properties that generate harmonics in the dynamic response. This technique helps to clarify the meaning of the identified magneto-elastic properties and to obtain a magneto-mechanical model. The sensitivity to laser treatment will be analyzed, illustrating the effect of different laser configurations on the magneto-elastic behavior. The selection of the optimal laser treatment is based on different strategies:
- Reduction of the harmonics by obtaining linear magnetic properties.
- Reduction of the static magneto-elastic coefficient $\frac{1}{P}$ (magnitude) and increase of the damping coefficient τ.
- Consideration of a properties gradient instead of homogeneous properties.

Bibliography

[1] O. Maloberti, G. Meunier, and A. Kedous Lebouc. On hysteresis of soft materials inside formulations: Delayed diffusion equations, fields coupling, and nonlinear properties. *IEEE Transactions on Magnetics*, 44(6):914–917, 2008. 6, 9

[2] Nicusor Pop and Ovidiu Caltun. Jiles-atherton model in fitting hysteresis curves of magnetic materials. *Journal of Optoelectronics and Advanced Materials*, 13:537–543, 05 2011. 8

[3] Radosław Jedynak. Approximation of the inverse langevin function revisited. *Rheologica Acta*, 54(1):29–39, Jan 2015. 8

[4] J. Szczyglowski. Influence of eddy currents on magnetic hysteresis loops in soft magnetic materials. *Journal of Magnetism and Magnetic materials*, 320(1):97–102, January 2001. 8

[5] S. Timoshenko and S. Woinowky-Krieger. *Theory of plates and shells*. McGraw-Hill book company. 14

[6] "J. M .Berthelot". "*Composite Materials*". "Springer", 1999. 15, 16

[7] Paweł Fritzkowski. Transverse vibrations of a beam under an axial load: minimal model of a triangular frame. *Archive of Applied Mechanics*, 87(5):881–892, May 2017. 16

[8] U. Aydin, P. Rasilo, D. Singh, A. Lehikoinen, A. Belahcen, and A. Arkkio. Coupled Magneto-Mechanical Analysis of Iron Sheets Under Biaxial Stress. *IEEE Transactions on Magnetics*, 52(3), 2015. 20

[9] Anouar Belahcen, Katarzyna Fonteyn, Antti Hannukainen, and Reijo Kouhia. On numerical modeling of coupled magnetoelastic problem. pages 203–206, 2008. 20

[10] Katarzyna Fonteyn, Anouar Belahcen, Reijo Kouhi, Paavo Rasilo, and Antero Arkkio. FEM for Directly Coupled Magneto-Mechanical Phenomena in Electrical Machines. *IEEE Transactions on magnetics*, 46(8):2923–2926, 2010. 20

[11] S. S. Mbengue. *Etude des déformations induites par l'aimantation des dispositifs électrotechniques: développement d'un modèle magnéto-élastique macroscopique.* PhD thesis, Université de Technologie de Compiègne, 2016. 20

[12] Sakda Somkun, Anthony J. Moses, and Philip I. Anderson. Measurement and Modeling of 2-D Magnetostriction of Nonoriented Electrical Steel. *IEEE Transactions on Magnetics*, 48(2):711–714, 2012. 20

[13] A. Belahcen P. Rasilo, D. Singh and A. Arkkio. Iron losses, magnetoelasticity and magnetostriction in ferromagnetic steel laminations. *IEEE Transactions on Magnetics*, 49(5):2041–2044, May 2013. 20

Deliverable D 3.3
Magneto-mechanical dynamic modeling

WP3: Physical studies
Date of Delivery: 30/11/2018 (1st update)
Lead Beneficiary: UPJV - Amiens
Type: Report
Dissemination Level: Public
Version: 2.5

ESSIAL has received funding from the European Union's Horizon 2020 research and innovation program under grant agreement No 766437.

Table of contents (1st update)

List of Figures

List of Tables

Introduction

This report deals with dynamic magnetic and mechanical modeling of soft magnetic materials subject to laser treatments. First, magnetic direct modeling is performed in order to simulate the magnetic behavior of soft magnetic plates subjected to surface uniform magnetic field. Time response magnetic field and magnetic flux density and hysteresis are calculated, depending on the thickness and the magnetic properties of the materials. An indirect modeling is then performed in order to determine the magnetic properties of the material and its magnetic behavior law as a function of laser treatment and the dependent magnetic structure. It might have an impact on the magnetic sources of vibration and the vibro-mechanical properties as well.
Next, a mechanical dynamic analysis is performed; stresses, efforts and forces through the thickness of the plate are defined and modal analysis of the structure is developed in order to determine the mode shapes and natural frequencies of vibrations.
Different solving tools are used; for magnetic modeling, finite element discretization on MATLAB is performed, followed by time simulation with SIMULINK using Maxwell Equations, and numerical modeling with Flux2D software on the other hand. For mechanical modeling, finite element discretization on MATLAB and time simulation on SIMULINK are developed using Hamilton principle, and numerical validation is obtain with HyperWorks Software.

Chapter 1

Magnetic modeling

1.1 Defining the problem

The experimental setup chosen in this thesis is a SST bench. It consists of a closed magnetic circuit that generates a uniform, horizontal and symmetric magnetic field through both surfaces of the soft magnetic plate inserted in the closed circuit. Fig. 1.1 illustrates the plate model to be solved.
The magnetic direct modeling consists in defining the magnetic flux density gradient in the geometry of the structure with time dependency, given the different magnetic properties involved in the magnetic behavior law of the material. However, the procedure here involves an indirect problem solving. In fact, once the magnetic transient responses of the mean flux density and the surface magnetic field are measured, the magnetic properties can be calculated. The latter allows to define the material behavior law that will be used later on for magneto-mechanical coupling, so that the effect of magnetic properties affected by laser treatments on the mechanical response will be analysed and interpreted.

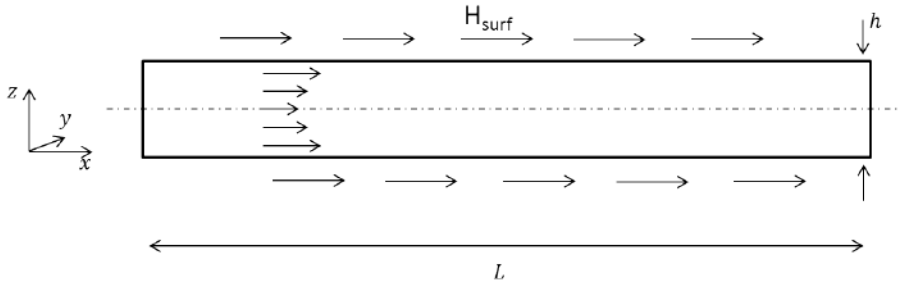

Fig. 1.1 Magnetic plate surrounded by uniform magnetic field as obtained in the SST frame

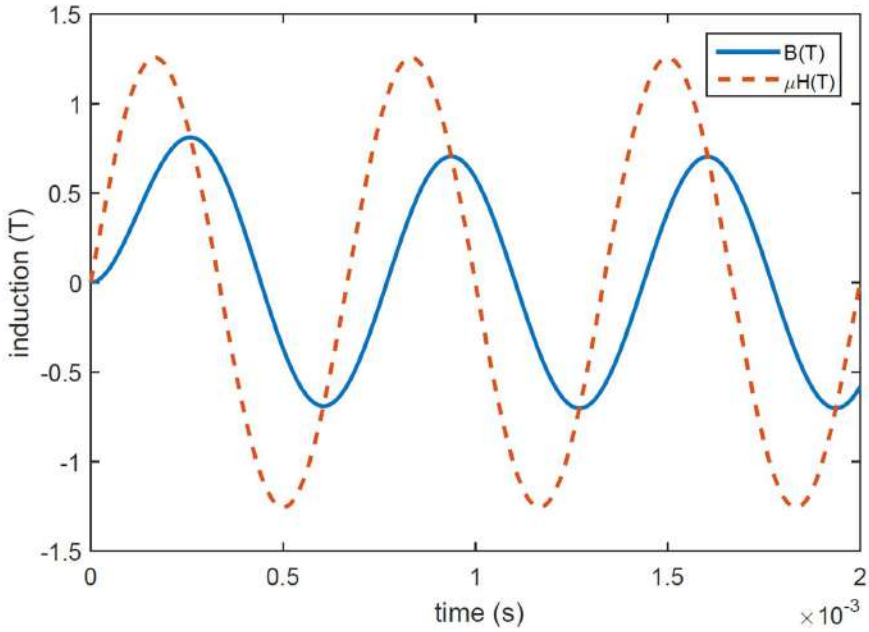

Fig. 1.2 Flux density response with and without consideration of the dynamic property $\Lambda = 250\mu m$ with magnetic field $H = 1000A/m$, frequency $f = 1500Hz$, relative permeability $\mu_r = 1000$ and electrical conductivity $\sigma = 2MS/m$

1.2 Model description

1.2.1 Magnetic behavior law

The behavior law of soft magnetic material can be defined as the relation between the magnetic field and the flux density at a specific time and a specific point of the structure, including static and dynamic parts as defined in Eq. 1.1 [1, 2].

$$\boldsymbol{H}(z) = \frac{1}{\mu(\boldsymbol{B}(z))}\boldsymbol{B}(z) + \sigma\Lambda^2(\boldsymbol{B}(z), \frac{d\boldsymbol{B}(z)}{dt})\frac{d\boldsymbol{B}(z)}{dt} \tag{1.1}$$

where z is the coordinate defined in the thickness h of the plate varying from $\frac{h}{2}$ and $-\frac{h}{2}$, $\boldsymbol{B}$ is the magnetic flux density at position z, $\boldsymbol{H}$ is the magnetic field at position z, μ is the absolute static permeability of the material depending on $\boldsymbol{B}$, σ is the electrical conductivity considered known and constant, and Λ is the dynamic magnetic property that includes all the variations with time. In fact, reference to Eq. 1.1, the magnetic field generated in the plate is seperated into two parts: a static, conservative part affected by the permeability μ and not dependent on the time variation and a dynamic, dissipative part affected by the dynamic property Λ that depends on time or frequency. Fig.1.2 shows the effect of the magnetic dynamic property Λ on the time response of the flux density for a material subjected to a specific magnetic field. In fact, mesoscopic magnetic property μ presents the ability of the material to magnetize in the presence of magnetic field; the higher the static permeability is, the higher the magnetization is. On the other hand, the dynamic property Λ presents the magnetic walls density and mobility; the higher Λ is, the lower the walls mobility or density is, leading to a more delayed response in magnetization as presented in Fig. 1.2 and a more dissipation of magnetic

energy. Maloberti et al. [1] has presented, described and identified this dynamic property in soft magnetic materials [1].

1.2.2 Diffusion equation

The magnetic modeling consists in determining the time response of the gradient of magnetic flux density $B(\Omega, t)$, knowing the time response of the surface magnetic field $H_a(t)$. In fact the modeling consists in using the Maxwell equations that can be reduced in the SST frame to a one-dimensional dependent magnetic flux density. The Maxwell equations can be summarized through the thickness h of the sample, varying from $-\frac{h}{2}$ and $\frac{h}{2}$, to the following equation [3, 4].

$$\sigma \frac{dB}{dt} = \frac{\partial^2 H}{\partial z^2} \tag{1.2}$$

where σ is the electrical conductivity of the material and H is the gradient of the magnetic field through the thickness. Using Eq. 1.2 with limit conditions imposed by the surface magnetic field $H(\frac{e}{2}) = H(-\frac{e}{2}) = H_a(t)$, the magnetic flux density and the magnetic field can be obtained if the relation between both variables is well known and defined, constituting the material behvior law. Combining the diffusion equation Eq. 1.2 with the magnetic law behavior in Eq. 1.1 and the boundary condition, and performing a finite element discretization one can get the following first order equation [4]:

$$A(\mu, z)B + C1(\sigma)\frac{\partial B}{\partial t} + C2(\Lambda, \mu, z)\frac{\partial B}{\partial t} = g \tag{1.3}$$

Where A, $C1$ and $C2$ are matrices derived from Eq. 1.2, depending on the number of elements, the thickness and the different electromagnetic properties, and g represents the excitation vector depending on the boundary conditions. Matrices and vectors presented in Eq. 1.2 are well explained and defined in the previous report. Next, Eq. 1.3 is integrated in SIMULINK for transient resolution of the magnetic flux density varying through the thickness of the sample, and the mean magnetic flux density can be determined with time variation.

1.3 Magnetic properties determination

1.3.1 Permeability law determination

The law of permeability is determined by eliminating the effect of the dynamic part; this can be done for very low frequencies, without taking into account the diffusion effect and the Maxwell equation described in Eq. 1.2 because we are dealing with a static problem where we assume that the magnetic flux density and magnetic field remain the same everywhere in the geometry; the choice of the low frequency consists in compromising between the speed and the precision of the measurements; in fact, the lower the frequency is, the slower the measurement is or will be. On the other hand, at a certain level, the decrease of the frequency becomes useless because the dynamic effect becomes negligible. That's why, in our measurements, $3Hz$ is the frequency considered for grain-oriented materials (GO) as static excitation, and $5Hz$ is considered for non-oriented grain materials (NGO).

The determination of the permeability is derived from the mid anhysteretic magnetization curve obtained seperately on each low induction cycle as shown in Fig. 1.3; in fact, different curves are obtained for different induction levels because the permeability depends not only on the magnetic field and flux density, but on their variation with respect to each other, with an independence on the frequency of the exciting magnetic field or any time variation. An idea of the permeability can also be given by determining the initial magnetization curve of each material as shown in Fig.1.4, and by selecting the minima and maxima couples (H_{max}, B_{max} of

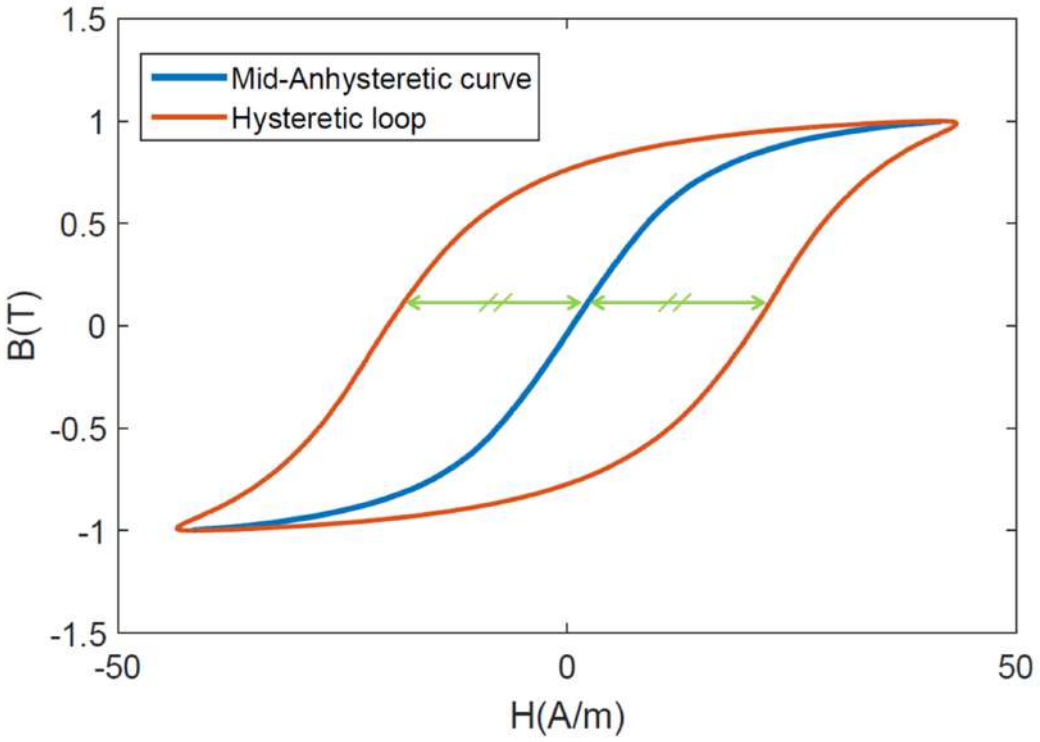

Fig. 1.3 Hysteretic and mid-anhysteretic curves for a $B_{max} = 1T$ induction and a frequency of $50Hz$ for a non-laser treated grain-oriented material (GO)

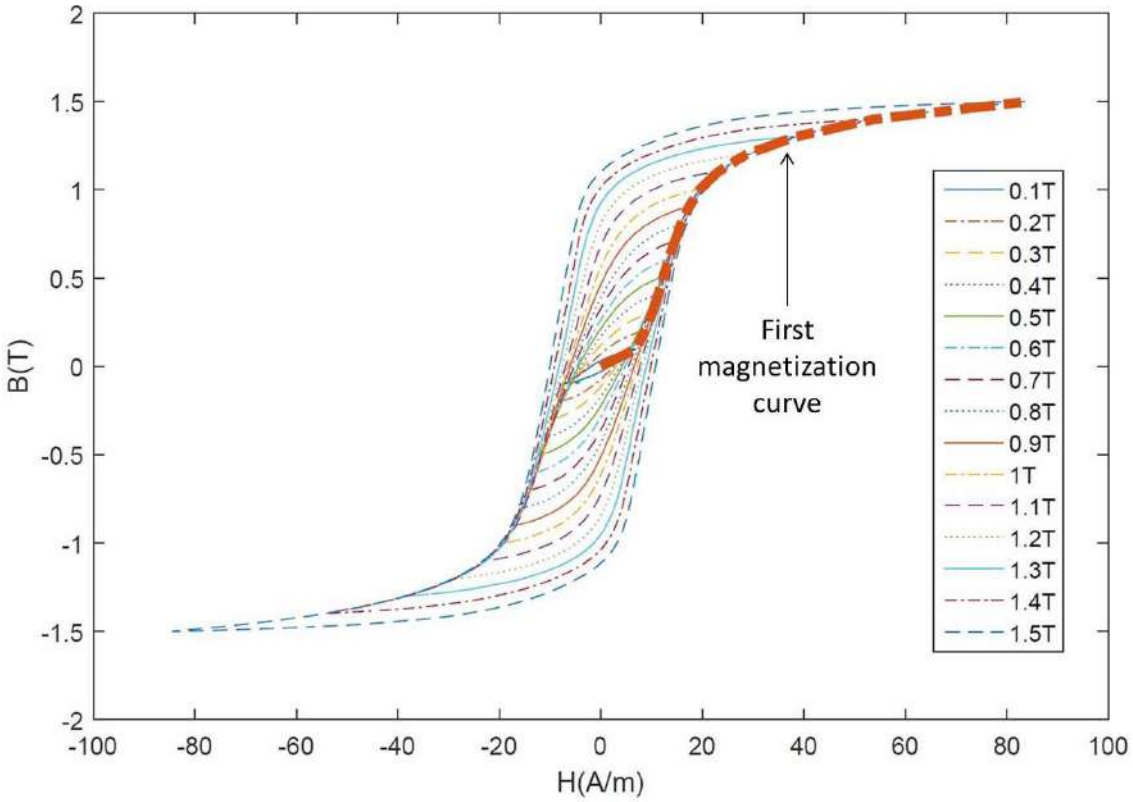

Fig. 1.4 Hysteresis loop at 3Hz for a grain-oriented material with different induction levels with initial magnetization curve (in bold) obtained from maxima couples (H_{max}, B_{max}) obtained from each induction level

each induction level to obtain a unique characteristic curve of the material.

1.3.2 Dynamic property law determination

The determination of the dynamic property with respect to the induction and the frequency is more complicated than the determination of the permeability, because it considers the dynamic behavior and the diffusion effect of the magnetic flux density and the magnetic field through the thickness of the structure. Hence, Eq. 1.1 cannot be directly implemented and the Maxwell diffusion equation must be taken into consideration. Calculation of the dynamic property can follow two steps. The first one considers that the dynamic property is constant through the cycle, and an optimisation of the error between the area of the cycles for measurement and simulation is considered as shown in Fig. 1.5. This strategy gives an average dynamic property within the cycle and can help us compare the value obtained for different laser treatments and analyze the effect of the laser treatment for this property. Next, for a more specific study, the determination of the dynamic property as function of the flux density and its time derivative is performed; Fig. 1.6 shows the mathematical optimization diagram that determines the dynamic property Λ by an iteration method, starting with an initial guess.

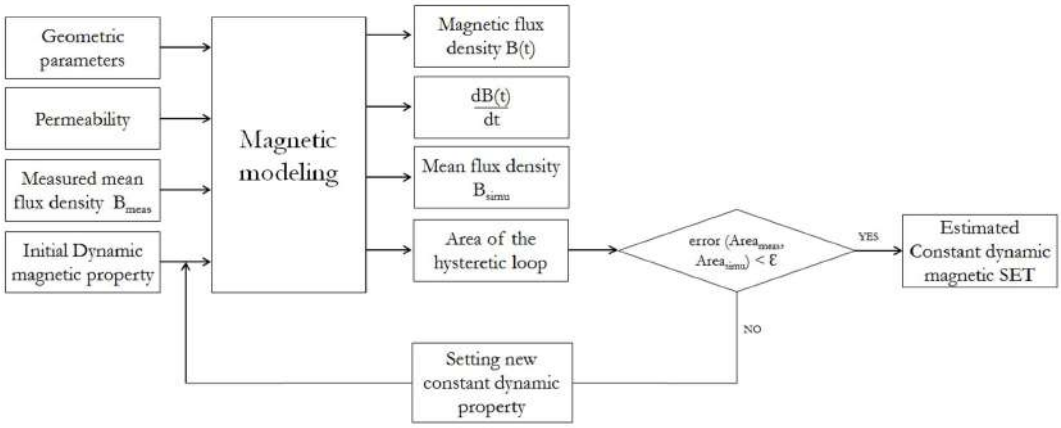

Fig. 1.5 Numerical strategy for determination of the mean magnetic dynamic property Λ through a cycle of specific maximum induction and specific frequency

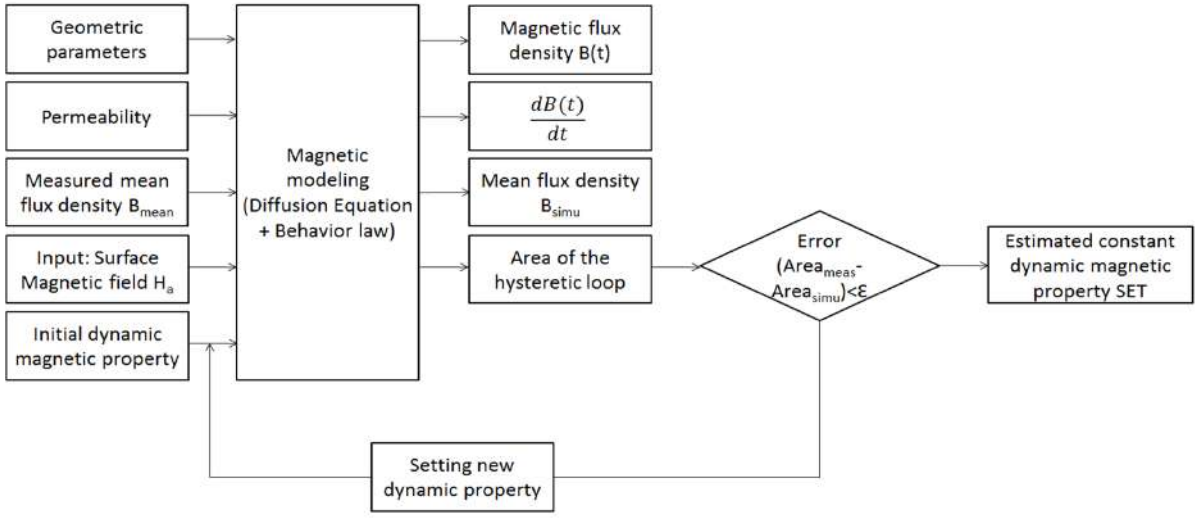

Fig. 1.6 Numerical strategy for determination of the magnetic dynamic property Λ law

Chapter 2

Mechanical modeling

2.1 Brief description of the dynamic mechanical model developed

The soft magnetic plate considered for magnetic measurements has also pure mechanical properties that define its dynamic behavior and its mode shapes and natural frequencies. In this part, the mechanical model of vibration is presented on its own without considering the magneto-mechanical coupling at first. The latter has been introduced during the first period and will be developed during the next period, including the impact of the magnetic properties on both the stiffness and damping matrices and on the excitation input vector. Using the Hamilton's principle that is based on energy formulation and conservation, one can derive using the finite element discretization method, the mass matrix $\boldsymbol{M}$, the stiffness matrix $\boldsymbol{K}$ and the damping matrix $\boldsymbol{C}$, using a modal analysis strategy by deterimining the eigenvalues and the eigenvectors of the eigenproblem formulated by the Hamilton's principle.

$$(-\omega^2 \boldsymbol{M} + \boldsymbol{K})\boldsymbol{\Delta} = \boldsymbol{0} \tag{2.1}$$

where ω^2 is the eigenvalue and Δ is the eigenvector. Once the different matrices are developed from the modal analysis, a time response equation is set and solved using SIMULINK.

$$\boldsymbol{M}\frac{d^2\boldsymbol{U}}{dt^2} + \boldsymbol{C}\frac{d\boldsymbol{U}}{dt} + \boldsymbol{K}\boldsymbol{U} = \boldsymbol{f} \tag{2.2}$$

where $\boldsymbol{f}$ is the excitation input vector and $\boldsymbol{U}$ is the displacement output vector. The modeling is performed on SIMULINK by transforming the second order equation to a first order one by setting a new equation [5]:

$$\boldsymbol{Z} = \begin{pmatrix} \boldsymbol{U} \\ \frac{d\boldsymbol{U}}{dt} \end{pmatrix} \tag{2.3}$$

$$\frac{d\boldsymbol{Z}}{dt} = \begin{pmatrix} \boldsymbol{0} & \boldsymbol{I} \\ -\boldsymbol{M}^{-1}\boldsymbol{K} & -\boldsymbol{M}^{-1}\boldsymbol{C} \end{pmatrix} \boldsymbol{Z} + \begin{pmatrix} \boldsymbol{0} \\ \boldsymbol{f} \end{pmatrix} = \boldsymbol{A}\boldsymbol{Z} + \boldsymbol{B} \tag{2.4}$$

Matrix $\boldsymbol{A}$ contains the modal analysis matrices (mass $\boldsymbol{M}$, stiffness $\boldsymbol{K}$ and damping $\boldsymbol{C}$ matrices) and matrix $\boldsymbol{B}$ contains the excitation input. $\boldsymbol{B}$ is equal to zero when no external excitation is applied Fig. 2.1 plots the displacement response of a fixed-free plate subject to an initial displacement at the free end with no external excitation, simulated by the model developed on SIMULINK as shown in Fig. 2.2.

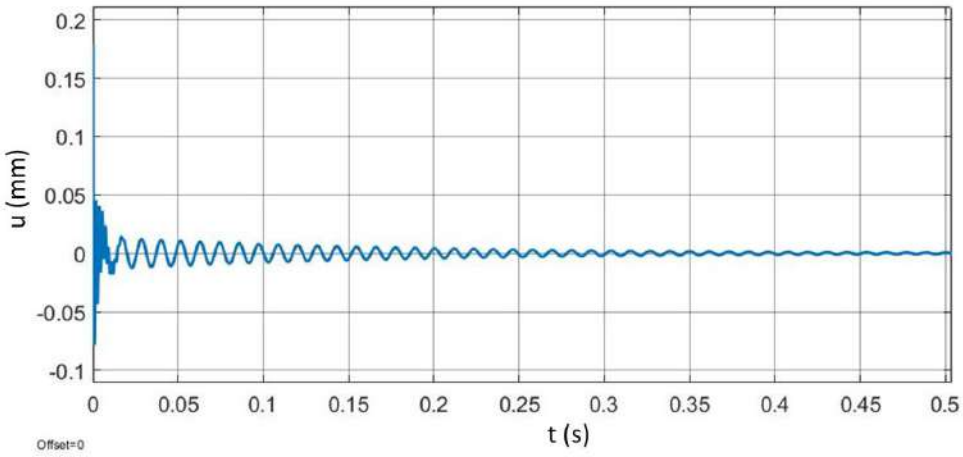

Fig. 2.1 Displacement time response of the free end of a plate with thickness of $1mm$, length of $100mm$, Young modulus of $210GPa$, Poisson Ratio equal to 0.3, density of $7,850Kg/m^3$

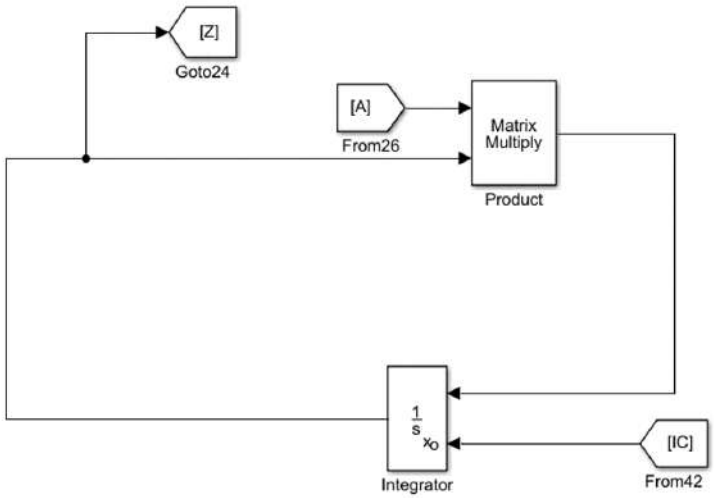

Fig. 2.2 Dynamic mechanical response modeling on SIMULINK

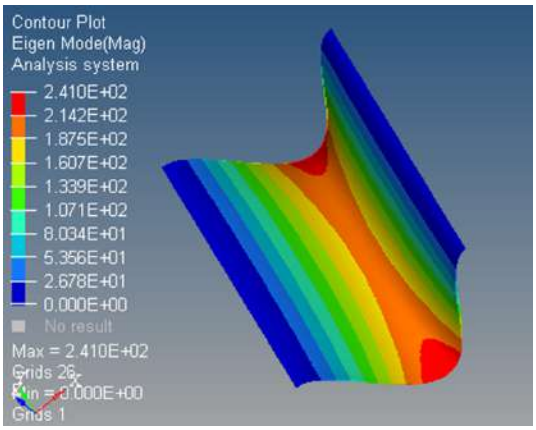

Fig. 2.3 Mode Shape for fixed-fixed magnetic plate in Mode 1

2.2 Modal analysis and experimental strategies

In order to select the position of sensors and exciters on the top of the plate when exposed to a uniform magnetic field, modal analysis of the plate must be performed; natural frequencies of vibration and mode shapes for different vibrational modes. The calculation are performed with two calculations methods; the first one must be calculated based on energy formulation and Hamilton's principle that derives mass and stiffness matrices of the structure for 2D geometry in (xOz) plane and using Matlab and Simulink as numerical solving powers, and the second one using directly HyperWorks from Altair Engineering Software for 3D geometry in (xyz) space. A fixed-fixed plate is considered with geometric properties: length $L = 100mm$, width $w = 150mm$ and thickness $h = 0.5mm$ and mechanical properties: density $\gamma = 7650Kg/m^3$, Young Modulus $E = 210GPa$ and Poisson Ratio $\upsilon = 0.3$. Results for both methods are compared in Table 2.1. Both models are compatible on modes 1, 5 and 12 that correspond to bending in vertical plane xOz. Other modes correspond to vibration out of plane. Mode Shapes are also obtained, Figs. 2.3, 2.4 and 2.4 illustrate the mode shapes corresponding to flexural modes 1, 5 and 12.

Modes	HyperWorks Model	SALLOUM 2D Model	Relative Error
1	277.05	279.9	1.03%
2	301.55		
3	394.17		
4	582.28		
5	764.92	775.8	1.42%
6	798.36		
7	883.88		
8	914.62		
9	1118.23		
10	1301.9		
11	1419.96		
12	1502.45	1532	1.97%

Table 2.1 Natural frequencies(Hz) comparison between numerical simulation with HyperWorks and 2D energy model

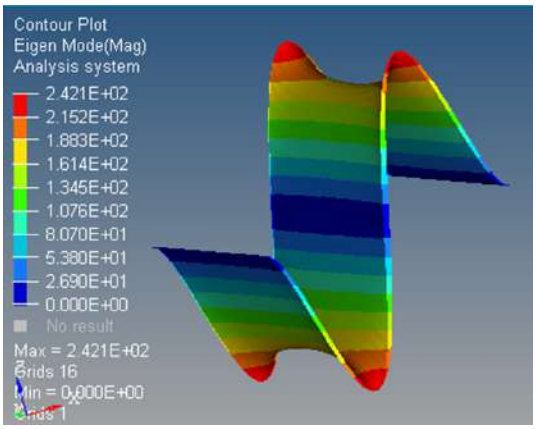

Fig. 2.4 Mode Shape for fixed-fixed magnetic plate in Mode 5

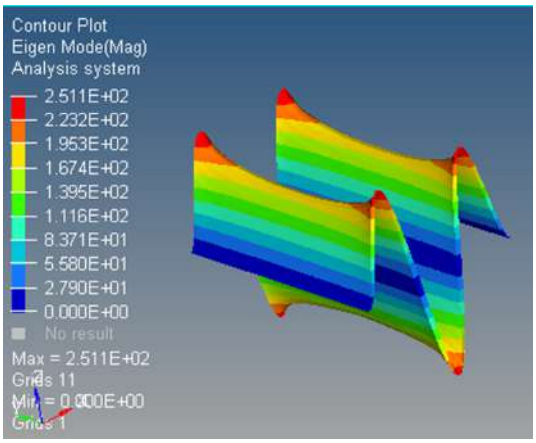

Fig. 2.5 Mode Shape for fixed-fixed magnetic plate in Mode 12

2.3 Stresses, efforts and forces in plates

In this section, a theoretical approach is presented, contributing to the design of the test bench. This approach is mainly based on the theory of plates in order to identify the distribution of plate's stresses and forces that are derived from the magnetization of the specimen in the SST frame.
A plate is a three dimensional structure where the thickness is very small compared to other dimensions.

The general stress tensor corresponding to an infinitesimal volume in a structure is:

$$[\sigma] = \begin{pmatrix} \sigma_{xx} & \sigma_{xy} & \sigma_{xz} \\ \sigma_{xy} & \sigma_{yy} & \sigma_{yz} \\ \sigma_{xz} & \sigma_{yz} & \sigma_{zz} \end{pmatrix} \tag{2.5}$$

where σ_{xx} and σ_{yy} is the normal stresses in the x and y directions σ_{xy}, σ_{xz} and σ_{yz} are the shear stresses in the planes xy, xz and yz.
Mechanical volumic forces are generated from the distribution of the mechanical stresses in the geometry of the structure, and are related as follows [6]:

$$f = div[\sigma] = \begin{pmatrix} \frac{\partial \sigma_{xx}}{\partial x} + \frac{\partial \sigma_{xy}}{\partial y} + \frac{\partial \sigma_{xz}}{\partial z} \\ \frac{\partial \sigma_{xy}}{\partial x} + \frac{\partial \sigma_{yy}}{\partial y} + \frac{\partial \sigma_{yz}}{\partial z} \\ \frac{\partial \sigma_{xz}}{\partial x} + \frac{\partial \sigma_{yz}}{\partial y} + \frac{\partial \sigma_{zz}}{\partial z} \end{pmatrix} \tag{2.6}$$

The generated efforts through the whole thickness of a plate are given by:

$$N = \begin{pmatrix} N_x \\ M_x \\ N_y \\ M_y \\ N_{xy} \\ M_{xy} \\ Q_x \\ Q_y \end{pmatrix} = \int_{-\frac{h}{2}}^{\frac{h}{2}} \begin{pmatrix} \sigma_{xx} \\ z\sigma_{xx} \\ \sigma_{yy} \\ z\sigma_{yy} \\ \sigma_{xy} \\ z\sigma_{xy} \\ \sigma_{xz} \\ \sigma_{yz} \end{pmatrix} dz \tag{2.7}$$

Hence, the equivalent surface forces and moments are obtained:

$$f_x = \frac{\partial N_x}{\partial x} + \frac{\partial N_{xy}}{\partial y} + \sigma_{xz}(\frac{h}{2}) - \sigma_{xz}(-\frac{h}{2}) \tag{2.8}$$

$$f_y = \frac{\partial N_{xy}}{\partial x} + \frac{\partial N_y}{\partial y} + \sigma_{yz}(\frac{h}{2}) - \sigma_{yz}(-\frac{h}{2}) \tag{2.9}$$

$$f_z = \frac{\partial Q_x}{\partial x} + \frac{\partial Q_y}{\partial y} + \sigma_{zz} \tag{2.10}$$

$$m_y = \frac{\partial M_x}{\partial x} + \frac{\partial M_{xy}}{\partial y} + \frac{h}{2}\sigma_{xz}(\frac{h}{2}) + \frac{h}{2}\sigma_{xz}(-\frac{h}{2}) - Q_x \tag{2.11}$$

$$m_x = \frac{\partial M_{xy}}{\partial x} + \frac{\partial M_y}{\partial y} + \frac{h}{2}\sigma_{yz}(\frac{h}{2}) + \frac{h}{2}\sigma_{yz}(-\frac{h}{2}) - Q_y \tag{2.12}$$

2.4 Interpretation of the force balance for an SST frame

In the previous section, the presentation of all the possible force that can act on the volume of the plate was performed in order to identify their impact on the vibration. In fact, the forces can affect the structure in two perspectives; one considering the force as an external source of excitation and its direction of application does not vary with the dynamic of the plate, and the other considered as a displacement dependant force, affecting the stiffness, the natural frequencies and mode shapes of the plate.
In this section, all the possibilities that we can possibly confront in the experimental measurements are offered; the aim of this theoretical interprepation leeds to the right path in the design of the mechanical experimental bench.

2.4.1 Case of isotropic magnetic material

An isotropic material is considered, with a straight plate and a symmetric uniform magnetic field distribution on both surfaces, respecting the setup of the SST bench adopted for magnetic experiment. Based on Maxwell's equations, the magnetic flux density is only z-component dependent and directed in the x-direction; hence, the only magnetic stresses derived from Maxwell and magnetostrictive origins are σ_{xx} and σ_{zz} and the only effort generated in the plate is N_x. The forces applied on the structure due to the SST bench setup is f_x and f_z.

$$f_x = \frac{\partial N_x}{\partial x} \tag{2.13}$$

$$f_z = \sigma_{zz}(\frac{h}{2}) - \sigma_{zz}(-\frac{h}{2}) = 0 \tag{2.14}$$

Theses forces only produce longitudinal vibration, with very high resonance frequencies. Therefore, vibration will not be generated in flexural or torsional modes.
On the other hand, when the structure is excited in flexural or torsional mode, displacement-dependent efforts are generated and affect the vibrational properties of the structure (natural frequency, mode shapes, damping, speed, error...). In order to perceive its effect, an excitation is present and the vibrational response can be obtained and analyzed as a function of the magnetic properties induced by laser scribing.
In a SST frame with isotropic magnetic material, as shown in a previous report, shear stresses σ_{xz} and σ_{yz} are generated depending on the vibration of the structure and displacement-dependent forces are generated from excitation of the structure:

$$m_y = h\sigma_{xz}(\frac{h}{2}) - Q_x \tag{2.15}$$

$$m_x = h\sigma_{yz}(\frac{h}{2}) - Q_y \tag{2.16}$$

and

$$f_z = \frac{\partial Q_x}{\partial x} + \frac{\partial Q_y}{\partial y} \tag{2.17}$$

2.4.2 Excitation of the specimen inside the SST frame

Till now, the vibration of the plate is not achieved because no excitation source is defined theoretically; only displacement-dependent forces are observed. But in reality, vibration of the plate in the SST frame can be observed and a source of excitation is present and must be identified and analyzed. Different assumptions are presented in the upcoming sections.

Case of initial deformation

As shown in section 2.1, the excitation of the structure is not limited to application of forces and moments, but also on applying an initial displacement, similar to the excitation of a mass-spring system by an initial displacement of the mass. This initial displacement is due to the imperfection in the disposition of the plate inside the frame specially for flexible plates.

Case of anisotropic magnetic material

The effect of magnetic anisotropy of the soft magnetic structure is usually included, specially when dealing with grain oriented magnetic materials. In fact, when the material is magnetized with a uniform horizontal magnetic field, the magnetic flux density is not necessarily oriented in the same direction; other components can be generated due to the orientation of the magnetic domains of the structure. Even in non-oriented magnetic materials, a light anisotropy can often appear. As a result, stresses, efforts and forces can be created in other directions, constituting a source of vibration of the structure. In these non-oriented materials, the magnitude of the forces produced by the anisotropy is usually low in comparison with any force that can be applied externally, like a mechanical excitation or air gap effect.

Effect of the air gap between the plate and the core of the SST frame

A source of vibration can be generated by the presence of the air gap lack between the plate and the core of the bench that is used to measure the magnetic parameters. In fact, the presence of a very thin layer of air creates an interface (iron/air/iron), and the Maxwell magnetic force generated can be important, generating a vibration of the plate. However, in the SST, no external mechanical excitation are used and no displacement should be allowed at the air-gaps (fix-fix conditions).

Case of dissymmetry in the magnetic field generated by the SST frame

Another assumption can be treated, regarding the dissymmetry of the surface magnetic field distribution between both sides of the plate. In fact, this dissymmetry generates a disymmetry in the distribution of the magnetic flux density in the thickness of the plate and reference to section 2.3, moments around y axis, and forces in the z axis are created, presenting an excitation of the structure.

2.5 Conclusion and forthcoming steps

This report presents magnetic and mechanical modeling tools needed to determine the effect of laser treatment on the mechanical dynamic response of soft magnetic materials. In the upcoming studies, magneto-mechanical coupling model needs to be developed in order to connect the magnetic and mechanical tools developed in this report. On the other hand, the determination and the analysis of excitation sources derived from magnetic origins must be treated based on the different assumptions presented in section 2.4.2. This study is followed by experimental measurements for vibration. The target of all this procedure is to study and optimize the effect of the gradient of the identified magnetic properties induced by laser

scribing on the mechanical response of the structure. Later on, more complex cases will be treated, including a number of superposed sheets and a technique must be adopted to homogenize the magneto-mechanical properties for these cases.

Bibliography

[1] O. Maloberti, A. Kedous Lebouc, G. Meunier, and V. Mazauric. Field diffusion-like representation and experimental identification of a dynamic magnetization property. *Journal of Magnetism and Magnetic Materials*, 304:507–509, 2006. 7, 8

[2] O. Maloberti, G. Meunier, and A. Kedous Lebouc. On hysteresis of soft materials inside formulations: Delayed diffusion equations, fields coupling, and nonlinear properties. *IEEE Transactions on Magnetics*, 44(6):914–917, 2008. 7

[3] E. Fallah and V. Badeli. A New Approach for Modeling of Hysteresis in 2-D Time-Transient Analysis of Eddy Current Using FEM. *IEEE Transactions on Magnetics*, 53(7):7402714, 2017. 8

[4] M. A. Raulet, B. Ducharne, J. P. Masson, and G. Bayada. The Magnetic Field Diffusion Equation Including Dynamic Hysteresis: A Linear Formulation of the Problem. *IEEE Transactions on Magnetics*, 40(2):872–875, 2004. 8

[5] André Preumont. *Vibration Control of Active Structures, An introduction,* 3^{rd} *Edition*. 12

[6] S. Timoshenko and S. Woinowky-Krieger. *Theory of plates and shells*. McGraw-Hill book company. 16

ESSIAL

Deliverable D 3.3
Magneto-mechanical dynamic modeling

WP3: Physical studies
Date of Delivery: 30/04/2018
Lead Beneficiary: UPJV
Type: Report
Dissemination Level: Public
Version: 1.5

ESSIAL has received funding from the European Union's Horizon 2020 research and innovation program under grant agreement No 766437.

Table of contents (Initial deliverable)

List of Tables

List of Symbols

$\boldsymbol{u}$	Displacement vector
$\boldsymbol{\varepsilon}$	Strain vector
$\boldsymbol{\lambda}$	Magnetostriction strain coefficient vector
(u^0, w, ψ_x)	Displacement components in xz plane
$(\varepsilon_x^0, \kappa_x^0, \gamma_{xz})$	Strain components in xz plane
(x, y, z)	Physical coordinates
(τ, n)	Tangential and normal coordinates
(ξ, η)	Local coordinates
$\boldsymbol{n}$	Surface normal vector
N_i	Shape function
J	Jacobian linking local to physical coordinates
Ω	Volume
S	Surface
t	Time
ω	Angular frequency
I_n	n-dimensional identity matrix
$0_{m,n}$	Null matrix of $n \times n$ dimensions
s	Complex variable of the laplace transform
e	Plate's thickness
b_m	Plate's width
L	Plate's length
E	Young's modulus
υ	Poisson ratio
ρ	Material's density
α, β	Rayleigh parameters
$[M]$	Mass matrix
$[K]$	Stiffness matrix
$[C]$	Damping matrix
$\boldsymbol{f}$	Force vector
$\boldsymbol{\sigma}$	Stress vector

ω_i^2	Eigenvalue of the i^{th} mode
$\boldsymbol{\Phi}$	Eigenvectors matrix
Π	Energy functional
$\boldsymbol{B}$	Magnetic flux density vector
$\boldsymbol{H}$	Magnetic field vector
$\boldsymbol{M}$	Magnetization vector
$\boldsymbol{J}$	Induced current density vector
$\boldsymbol{J_S}$	Source current density vector
$\boldsymbol{E}$	Induced electrical field vector
$\boldsymbol{D}$	Electric flux density vector
$\boldsymbol{A}$	Magnetic potential vector
H_a	Applied longitudinal magnetic field on the surface
μ_0	Magnetic permeability in vaccum
μ_m	Magnetic permeability in magnetic material
μ_m^D	Dynamic magnetic permeability in magnetic material
μ_r	Relative magnetic permeability in magnetic material
μ_r^D	Relative dynamic magnetic permeability in magnetic material
χ_m	Magnetic suspectibilty
χ_m^D	Dynamic magnetic suspectibilty
σ	Electrical conductivity
Λ	Magnetic dynamic property
^{em}	Superscript corresponding to electromagnetic forces
^{ms}	Superscript corresponding to magnetostrictive forces
FEM	Finite Element Method

Chapter 1

State Of Art

1.1 Introduction

This report introduces the state of art of the thesis entitled **Modeling of magnetic and mechanical behavior with property gradients by laser scribing in non-oriented soft magnetic materials**. First, general definitions related to non-oriented ferromagnetic materials are presented and a special focus is concentrated on magnetic domains and walls movement. Next, researches about magnetic modeling and behavior are introduced, followed by a presentation of the intervening electromagnetic forces and their coupling with mechanical behavior. Finally, the influence of laser scribing on the magnetic structure is presented to target the goal of the thesis.

1.2 Non-Oriented ferromagnetic materials

1.2.1 Generalities

Soft magnetic materials received their name in regard their low hardness and their easiness to reverse their magnetization. They have the capacity to concentrate the magnetic flux in different parts of the magnetic circuits. In the low frequencies domain (e.g. the industrial frequency) high permeability and magnetization at saturation and low coercitivities are required so that the hysteresis loop becomes as narrow as possible [3]. Non-oriented materials are soft materials that have low anisotropy; when magnetic field is applied, the material can be easily magnetized in almost any direction and the characteristics are almost equivalent in all space directions. Non-oriented soft magnetic metal sheets are soft, crystalline, conducting, inexpensive materials, used for low frequency applications in electrical machines [4]. The Fe-Si alloy can definitely be considered the most representative material for this class.

1.2.2 Magnetic domains

The existence of magnetic domains and wall movement must be considered when studying the dynamic behavior of soft magnetic materials. In fact, the arrangement of the localized magnetic moments is determined by various kinds of energies: the exchange energy, the magnetostatic energy, the magnetocrystalline anisotropy and the magnetoelastic energy [5]. Magnetic domains are created in a way to minimize the magnetic energy of the material. In addition, one must consider the limit between each domain where sudden transition from one direction to another needs a big amount of exchange energy to be accomplished; a moving wall constituted of atomic planes is created between two domains in order to allow a grad-

ual transition of the magnetization direction between them. Bloch wall is one well-known wall studied by F. Bloch in 1932; at each part of the wall, the density of magnetocrystalline anisotropy energy is equal to the density of exchange energy. Hence, if the anisotropy tends to zero, rotation of the atomic moment is too slow and the Bloch wall will invade all the crystal. Otherwise, the moments will rotate fast and the wall will be thin.
Several methods have been developed to observe magnetic domains and magnetization orientation based on optic principles. These methods need an exceptionally clean surface and free of any constraint. Technically, a light bleam interacts with the magnetic medium leading to the rotation of light polarization plane (Kerr effect). Alves and Barrué [6] visualized on microscopic scale the magnetic domains in soft ferromagnetic materials. This gives information about the permeability and the electromagnetic losses. Furthermore, the structure in domain is influenced by many factors; first, annealing where the structure is affected by the cooling speed, then the mechanical stresses that refine the domains, and finally the magnetic excitations that affect the hysteresis cycle and different derived characteristics (permeability, iron losses, remanent induction).

1.3 Magnetic modeling and behavior

1.3.1 Magnetic model

Differential equations of the scalar and vector potentials $(\mathbf{A}, \phi)$ are derived from Maxwell's equations in order to model the magnetic process. This aims to determine the gradient of the magnetic flux density $\mathbf{B}(x, y, z, t)$ in the studied medium [7]. At frequencies encountered in electrical machines, the system is supposed to be quasi-static, where the rate of change of the electric flux density is negligible in front of the current density $(\frac{\partial \mathbf{D}}{\partial t} \ll \mathbf{J})$. Since the analytical resolution of Maxwell's equations is often difficult, it is preferred to use numerical methods. Arkkio [7] has developed a 2D finite element model for calculation of the potential $\mathbf{A}$ and eventually the magnetic flux density $\mathbf{B}$ that equals $\nabla \times \mathbf{A}$ at each point of the medium. The time-dependence of the problem is solved with a step-by-step time discretization using the Crank-Nicholson method. As the solution is frequency dependant $(\tilde{\mathbf{B}}(x, y, z, \omega))$, a frequence domain approach can also be adopted with a Fourier transformation.

1.3.2 Magnetic behavior in soft magnetic materials

Magnetic modeling presented in section 1.3.1 cannot be possible without the knowledge of the electromagnetic behavior of the ferromagnetic material. Hallal [8], Pellerey [9] and Rossi and Le Besnerais [10] considered a linear relation between the magnetic flux density and the magnetic field with a constant permeability where $(\mathbf{B} = \mu \mathbf{H})$. The non-linearity of the permeability and its dependance with the magnetic field $(\mu(\mathbf{H}))$ has to be considered when the applied magnetic field becomes less capable of magnetizing the material, the permeability decreases in this case and a magnetic saturation can be observed when the magnetic field reaches a certain level. In addition, hysteresis is an irreversible phenomenon that also affect the non-linearity. Arkkio [7] has considered the non-linearity in this thesis and solved the magnetic problem using the Newton-Raphson iterative method; in this case, the magnetic behavior law of the material $\mu(H)$ must be well defined. In addition, the magnetic domains and the walls movement presented in 1.2.2 have an important impact on the magnetization of the material generating eddy currents around moving domain walls. The integration of these effects considers different microscopic properties and modeling becomes more complicated; an homogenized magnetization property $\Lambda(\mathbf{B}, \partial_t \mathbf{B})$ is introduced to take into consideration the microscopic phenomenon (Fig.1.1) [11]. This property is a contribution of different microscopic

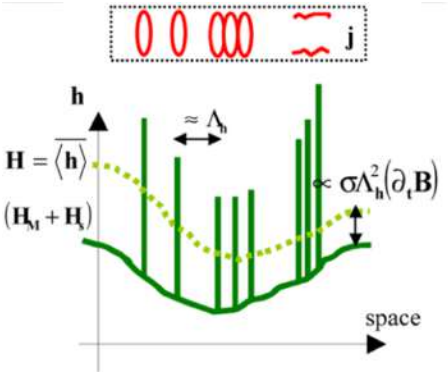

Fig. 1.1 1D scheme to introduce microscopic current and its consequence in terms of mesoscopic dynamic properties [12]

property and constitutes a transition between microscopic and mesoscopic scales and it is expressed as follows:

$$\Lambda = \sqrt{\frac{1}{2\sigma\vartheta J_S n_w m_w S_w}} \tag{1.1}$$

where σ, J_S, n_w, m_w and S_w are respectively the electrical conductivity, the saturation magnetic polarization, the walls volume density, the walls average mobility, the walls mean surface.

The identification of the homogenized property is well carried out and discussed by Maloberti et al. [12] with a 1D test case; a Gauss-Lorentz model which describes evolutions of walls population and mobility is then considered. The 1D model is adopted for the diffusion equation solving through a cross section sheet of an Epstein frame. The assumptions are: unidirectional and homogeneous surface excitation field (according to the depth of the sheet) [13]. Eq. 1.2 has to be solved giving a set of value of **H** varying in the thickness of the Epstein plate, and with the time ($\tilde{\mathbf{H}}(z, \omega)$). The resuts are plotted in Fig.1.2.

Hence, a general diffusion equation is obtained:

$$\nabla \times (\sigma^{-1}\nabla \times ((1 + \sigma\Lambda^2\mu\partial_t .)\mathbf{H}_M)) + \mu\partial_t \mathbf{H}_M = 0 \tag{1.2}$$

where $\mathbf{H}_M$ is the anhysteretic magnetic field.

1.4 Excitation forces

The identification of different forces occuring in electrical machines is necessary to understand the vibro-acoustic phenomena. These forces are mainly the Maxwell forces and the magnetostrictive forces. Several methods have been developed for the determination of these forces. Among these methods, the virtual work method is one precise method but it needs numerical power for solving. This leads by discretization to the obtention of nodal forces that are later on integrated in the mechanical model by coupling the magnetic problem with the mechanical one. Finite element discretization and nodal forces derivation using the virtual work method is explained in details by Belahcen [14].

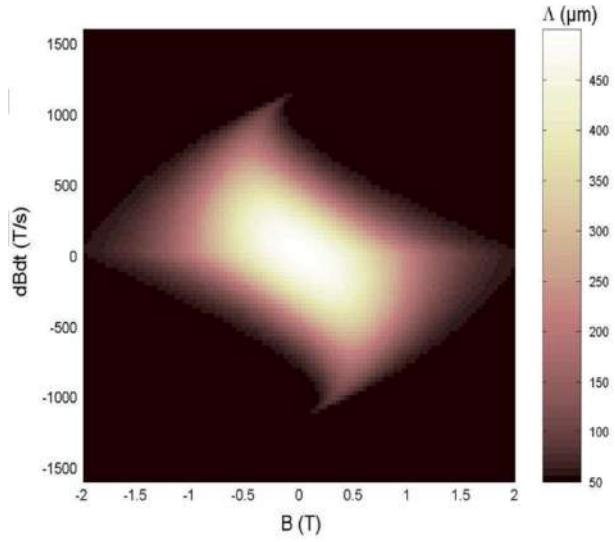

Fig. 1.2 Identification of the dynamic magnetic property Λ [12]

1.4.1 Magnetic forces

Magnetic force is the variation of magnetic energy when the medium is undergoing an incremental displacement for specific magnetic excitation [15]. It can be expressed as:

$$\mathbf{F} = -\frac{\partial}{\partial \mathbf{B}^2}\left(\int_0^{\mathbf{B}} \mathbf{H} d\mathbf{B}\right)\frac{\partial \mathbf{B}^2}{\partial u} - \frac{\partial}{\partial \sigma}\left(\int_0^{\mathbf{B}} \mathbf{H} d\mathbf{B}\right)\frac{\partial \sigma}{\partial u} \tag{1.3}$$

The first term of Eq.1.3 considers the effect of flux density. The second term is omitted when no mechanical stress is applied. This equation in the way it is expressed is valid in a volume bounded by a surface where there is no permeability variation. In the case where the surface is an interface between a material and air with different permeabilities, in addition to volumic forces, surface forces are also considered at the interface between the material and air. Zhou et al. [16, 17, 18, 19] derived a generalized magnetic forces expression, considering surface and body forces using the derivation of the total magnetic energy with respect displacement; the magnetic energy considers energy inside, accross and outside the volume. In the case of vibration of ferromagnetic plates subjected to magnetic field, Wei et al. [1, 20, 21] presented a modified magnetoelastic theory that considered magnetic surface traction forces generated in opposite directions on the upper and the lower surfaces where permeability variation occurs between air and the material. These two opposite surface forces create a couple as shown in Fig. 1.3. The dependance of this couple on the transverse displacement affects the stiffness of the material and eventually its natural frequency and it is shown that the increase in the applied magnetic field increases the natural frequency (Fig. 1.4).

Maxwell forces are the origin of a combination of isotropic pressure and tension along the field lines and they are derived from Lorentz forces. They are generally considered in the case of existence of airgap enclosed by magnetic materials, like in a rotating machine or an inductor, where a very high magnetic energy density is present and generates a highly concentrated magnetic pressure in the airgap (Fig.1.7) [10]. In a rotating machine, radial and tangential components are considered, seen that a closed surface is chosen as a cylinder integrated in the airgap [14]. In the case of inductors, magnetic flux in the airgap is perpendicular to the airgap and the Maxwell stress results in a magnetic pressure along x direction, leading to trac-

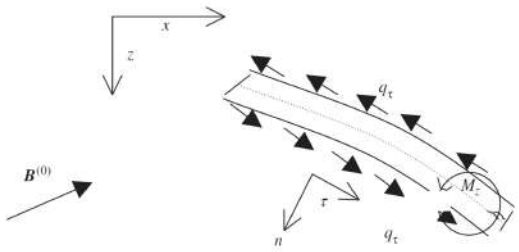

Fig. 1.3 The equivalent force of magnetic traction on the plate [1]

$B^{(0)}$ (mT)	Angle α			
	0	30	45	60
0	1.00	1.000	1.00	1.00
20				
25	1.07	1.004		0.966
40			1.03	
50	1.07	1.016		1.000
75	1.13			1.011
80		1.039	1.03	
100	1.13			1.079
120		1.047	1.06	
125	1.20			1.079
150	1.20			1.202
160	—	1.071	1.06	
175	1.20			1.157
200	1.20	1.097	1.10	1.292
225	1.27			1.315
240		1.124	1.10	
250	1.27			1.337
275	1.27			
280		1.115		

Fig. 1.4 Frequency dependance on external magnetic field applied on a plate [1]

tion/compression stress and in vertical vibration of the core of the transformer [10].

1.4.2 Magnetostrictive forces

Magnetostriction is a phenomenon present in magnetic materials where strain is caused in the presence of the magnetic field. In microscopic point of view, it results from the interaction between the magnetization direction and crystal lattices deformations where magnetoelastic energy is generated [5]. Therefore, in the macroscopic scale, a strain tensor results when a magnetic field is applied to a ferromagnetic material. A stress tensor can result from the strain tensor generating mechanical forces and causing in many applications the vibration of the structure.
The magnetostrictive strain tensor depends not only on the applied magnetic field, but also on the stress distribution and orientation [22, 23, 24, 14, 25, 26]. An inverse phenomenon also occurs, the Villari effect, where the magnetic properties change with mechanical stresses applied on the body (Fig.1.5). The consideration of the inverse magnetostriction depends on the problem; in vibration applications, low stress field is considered and the inverse effect can be neglected [27].

Many studies have considered the magnetostriction effect and specially the importance of the magnetostrictive forces on the vibration that occurs on magnetic materials in electrical machines. First, the determination of the magnetostrictive strain coefficient λ in the direction of the flux density is considered in order to obtain the strain tensor in arbitrary direction of the magnetic flux density as shown in Eq.1.4 for isochoric magnetostriction [23], where the transformation occurs with unchanged volume; this case is obtained for low and medium magnetic field. On the other hand, at very high magnetic fields, volumic magnetostriction occurs consisting of variation of volume [28].

$$\varepsilon^{ms} = \frac{\lambda}{2B^2}(3B_iB_j - \delta_{ij}B^2) \tag{1.4}$$

From Eq. 1.4, when the flux density vector is directed along x, the strain tensor becomes:

$$\begin{bmatrix} \lambda & 0 & 0 \\ 0 & -\frac{\lambda}{2} & 0 \\ 0 & 0 & -\frac{\lambda}{2} \end{bmatrix} \tag{1.5}$$

Magnetostriction in electrical steel laminations is widely accepted as an important source of deformation and vibration in rotating machines and transformer cores. As mentioned before, the main parameter to define is the magnetostrictive strain λ that depends on the magnetization of the material. Delince et al. [28] and Kloos [29] give a linear relationship between the strain and the magnetization depending on the strain and magnetization on saturation:

$$\lambda = \lambda_S \frac{M}{M_S} \tag{1.6}$$

where the indice S corresponds to the saturation.
This linear equation is adopted for modeling, but it doesn't give accurate representation of the magnetostrictive behavior; other references adopted a non-linear formula representing the variation of the strain coefficient with the magnetic flux density [30, 16]. Others use experimental measurements to model the magnetostrictive behavior; Belahcen [14] has calculated the magnetostrictive forces using directly measured stress versus magnetic flux density and

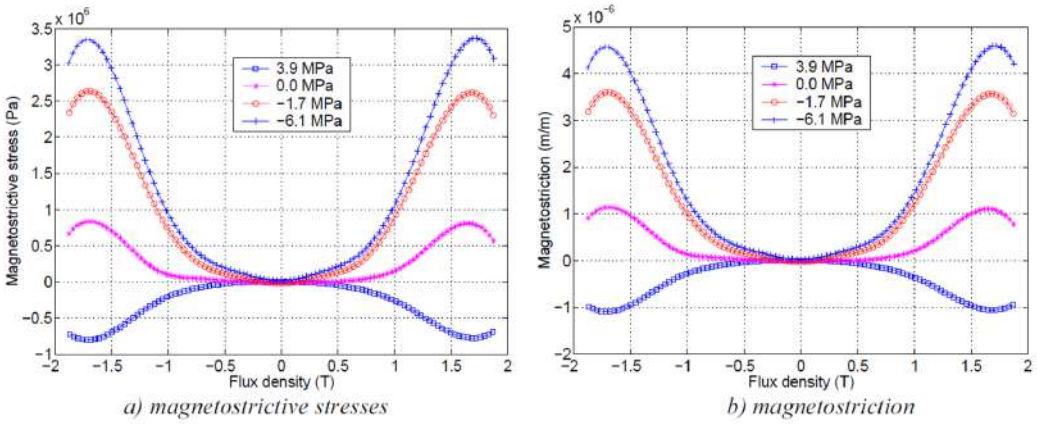

Fig. 1.5 Magnetostriction with external stress applied [14]

applied mechanical stress, using a modified Epstein frame. Results are plotted in Fig.1.5 showing that magnetostriction depends on flux density and the mechanical stress present in the structure. Another experimental approach that models this phenomenon is adopted; a model based on Helmholtz free energy in which the strain tensor and the magnetic flux density vector are the basic variables is developed [22, 24, 31]. Different parameters are identified experimentally and are adopted as behavior parameters of the material: the Maxwell forces, the magnetostriction, the magnetization M and the magnetic field H versus the magnetic flux density. This method is not only applicable for magnetostrictive stresses, but it also expresses the Maxwell stresses and the magnetic field as function of the flux density vector and the strain tensor. Different functions are derived in details in the thesis of Fonteyn [31]. The limitation of this method is that hysteresis is not included in the modeling; another approach has been considered by Hilgert et al. [32], it uses neural networks to model hysteresis under sinusoidal magnetization and it has shown that the inclusion of hysteresis in the magnetostriction model has a significant impact on the calculated results for the vibration in the case of transformers (Fig. 1.6).

1.4.3 Contribution of acting forces on vibration in electrical machines

Different studies on transfomers and electrical machines have been carried out to determine the forces' effects on the vibration of the structure. The contribution of the Maxwell forces and magnetostriction has been carried out in vibration studies. In fact, Maxwell forces inside the material are neglected, but Maxwell forces on the interface between air and the material are important due to the high variation of magnetization between air and the magnetic material [14]. Maxwell forces are specially effective with the presence of airgaps in electrical machines. For transformers, where closed circuit is considered, the effect of Maxwell forces compared with magnetostriction is neglected because no airgap is considered. Rossi and Le Besnerais [10] have analyzed in the case of a inductor with airgap the cancellation effects of the overall magnetic forces due to magnetostriction and Maxwell forces and have developed a model to better understand how to compensate Maxwell and magnetostrictive forces and reduce vibrations. They also showed that there is no general rule regarding the contribution of magnetostriction and Maxwell forces. The contribution of each force on the vibration is presented in Fig.1.8. In the case of rotating machines, the Maxwell forces are mainly dominant in the iron-air interface where rigid body displacements and elastic deformations of the structure

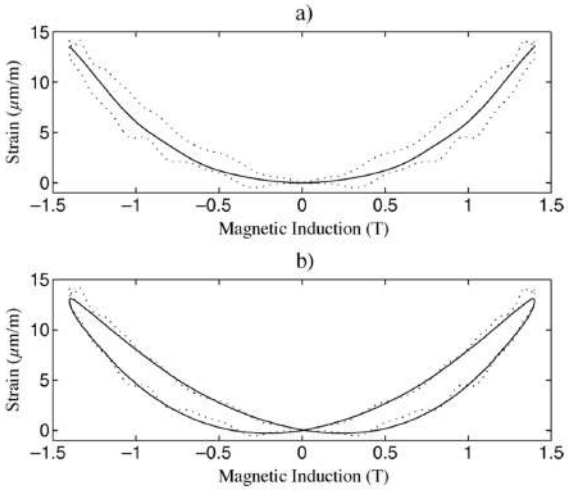

Fig. 1.6 Magnetostriction representation (a)Without hysteresis consideration (b)With hysteresis consideration [32]

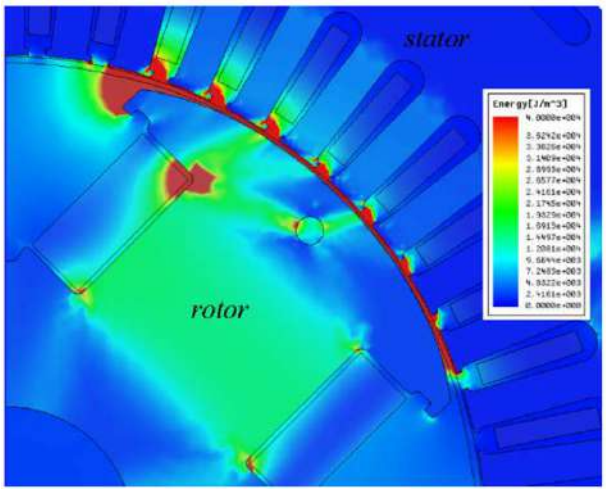

Fig. 1.7 FE magnetic energy density distribution in a rotating motor showing the concentration of magnetic energy at the airgap between the stator and the rotor [9]

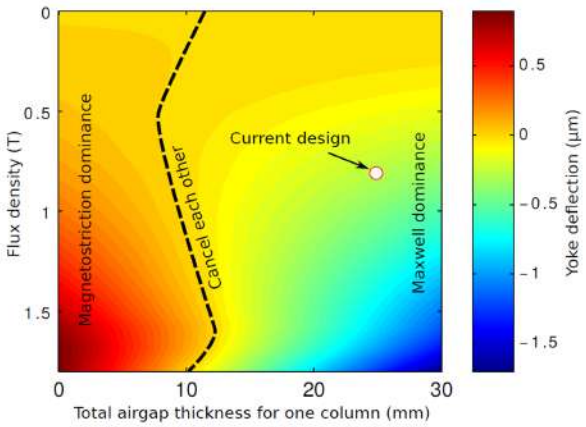

Fig. 1.8 Contribution of magnetostriction and Maxwell forces in yoke deflection of inductor [10]

occur at the same time, as for magnetostriction, only deformation of the structure's material occurs. Pellerey [9] and Hallal [8] neglected the effect of magnetostriction on the vibration of rotating machines in front of the Maxwell forces that were treated carefully.

1.5 Magneto-mechanical modeling

1.5.1 Mechanical vibration of materials

Energy coming from magnetic sources is integrated in the mechanical structure generating rigid body motion and dynamic displacement inside the structure that leads to mechanical vibration due to inertial and elastic properties characterizing the structure. Nowadays, solving techniques are becoming standard due to the presence of a large variety of potential mechanical solvers that are used to model the vibrational behavior by deriving mass, damping and stiffness matrices [8]. In the case where magnetic forces are the source of excitation of the structure, the challenge appears in coupling the magnetic effect with the mechanical response. The mechanical equation $-\omega^2[M]\mathbf{U}(\omega) + \omega[C]\mathbf{U}(\omega) + [K]\mathbf{U}(\omega) = \mathbf{F}(\omega)$ models the Fourier transform input/output relationship between the exciting force $\mathbf{F}$ and the resuting displacement $\mathbf{U}$, where $[M]$, $[C]$ and $[K]$ are the mass, damping and stiffness matrices characterizing the material. Many studies focused on optimizing the mechanical displacement response in order to minimize the noise generated in the machine [8, 9, 14, 10].

1.5.2 Magneto-Mechanical coupling

Coupling between magnetic and mechanical models is needed to link magnetic to mechanical phenomena and it has been carefully considered in previous studied [33, 34]. Weak coupling has been widely adopted; it considers only the effect that magnetic field has on the elastic field through magnetic forces without affecting the properties of the material. On the other hand, strong coupling, where the magnetic behavior is affected by mechanical stresses, can be considered when magnetostriction is considered. Belahcen [14] integrated the magnetostriction effect for both weak and strong coupling by considering the effect of mechanical stresses on the magnetic behavior. For simpler problem and depending on the situation considered, weak coupling is commonly used in vibrational analysis where stress generated is low enough and do not affect the magnetic properties [8, 27, 10]. Different kinds of magneto-mechanical

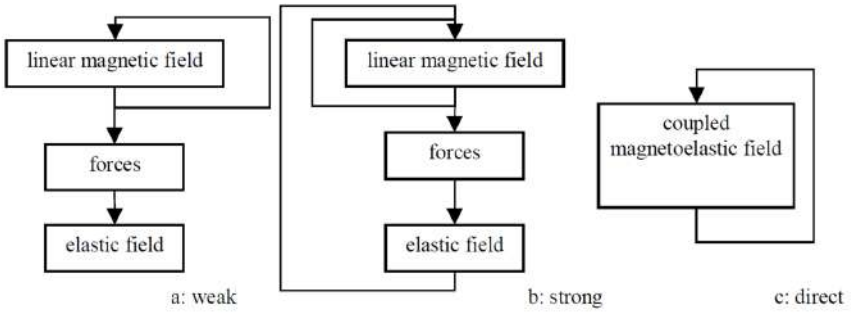

Fig. 1.9 Flowchart of different kinds of coupling [14]

couplings mentioned in litterature are illustrated in Fig.1.9. The coupling can be resumed by the following form:

$$\begin{bmatrix} S & D \\ C & K \end{bmatrix} \begin{bmatrix} \mathbf{A} \\ \mathbf{u} \end{bmatrix} = \begin{bmatrix} J \\ F \end{bmatrix} \tag{1.7}$$

A and **u** are respectively the magnetic potential and the structure displacement that characterize the solution of magnetic and mechanical problems. For weak coupling, $D = 0$ and the only coupling term C presents the magneto-mechanical connection and is replaced with the electromagnetic force F_{rel} where $F_{rel} = -CA$.

1.6 Laser scribing

Laser have been extensively used for materials processing applications since their invention. One of these is scribing of materials where only surface properties are modified. Laser scribing refers to the removal of a thin layer of material from the surface [35]. The factors that are affected the most are: size of grains, purity of the material, degree of refinement of the magnetic domains, surface tension and internal strains. Many studies have concentrated there research on the effect that have each of these factors, specially domain refinement and wall movement, on the core loss of the ferromagnetic material.
The enhancement of magnetic properties (hysteresis loss, total core loss, coercivity, remanence, permeability and saturation induction) of 3% silicon steel laminations using three different lasers for scribing was studied by Patri et al. [35]. The improvement of the material's softness by the laser treatment is explained by three mechanisms: domain refinement, relaxation of internal stress and inhibition of domain wall movement. In fact, the high concentration of laser energy deforms plastically the substrate forming a localized zone of compressive stress creating subdomains that tend to decrease the magnetoelastic energy and refine the magnetic domain. This mechanism leads to breakage of bonds, internal stress relaxation and domain wall movement during magnetizing and demagnetizing cycles, decreasing the total core loss. The domain refinement concept has been illustrated by Kajiwara and Enokizono [36] using a parametric study where iron loss decreases for transerve and rolling direction of laser scratches. But when both scratches are applied simultaneously, the iron loss decreases much more. Iron loss decrease is also improved by applying smaller pitches of laser scratches. Different results collected by Kajiwara are displayed in Fig.1.10. Johnson et al. [37] revealed the importance of laser surface scribing with optimum parameters (scribe speed, scribe spacing, power and pulse frequency) on core losses reduction in amorphous metallic ribbons based on domain refinement.

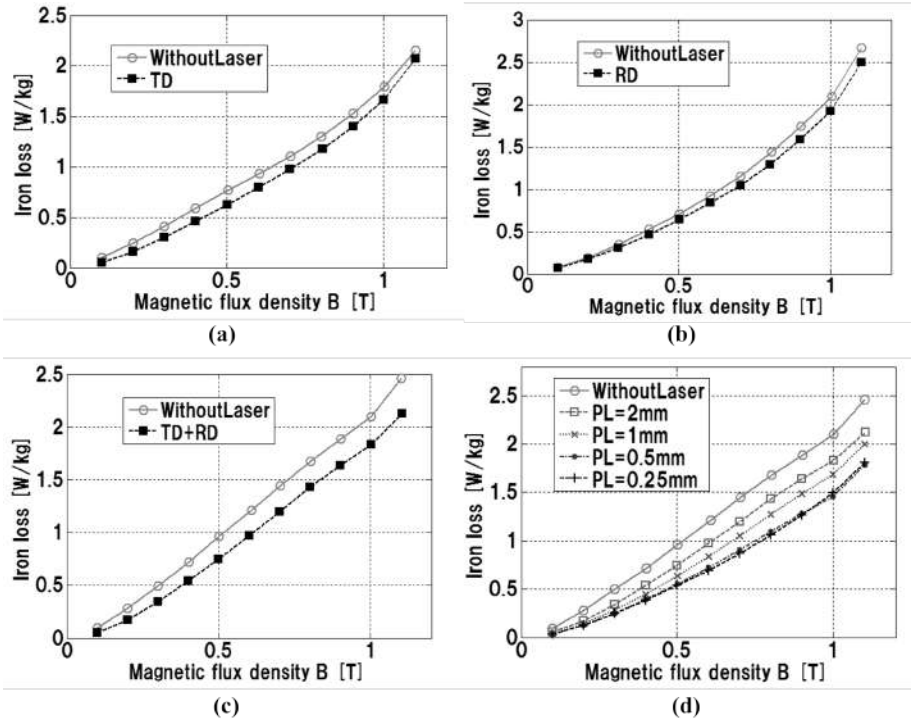

Fig. 1.10 Comparison between case without laser and with laser for iron losses with diferent configurations (a) TD (b) RD (c) TD + RD (d) irradiation pitch PL variation [36]

The influence of dotted lines produced by laser scribing on the domain structure and shape of the hysteresis loops has been described by Zeleňáková et al. [38]. It was shown that the hysteresis loop is steeper for samples with small density of dotted lines than for non-treated samples. This is due to the fact that magnetic polarization vector rotates much narrower and the number of movable domain walls is larger. For high density dots, a wavy hysteresis curve is generated; the domain wall displacement and the rotation of the spontaneous magnetic polarization vector happen simultaneously. Zeleňáková et al. also revealed the impact of laser treatment on the coercivity that increases with the increase of the dots density. Different results are plotted in Fig.1.11.

As mentioned before, previous studies mainly focus on the importance of laser treatment on magnetic losses and the improvement of softness in magnetic materials. Very few consider the effect of lasers on the vibration and the noise behavior that is generated from magnetic forces induced in the magnetic materials. This approach next to losses analysis, have been considered by Lahn et al. [39] and have been studied on grain oriented electrical steel present in three-phase transformer cores. The main source of transformer noise taken into account is the magnetostriction; it gives a rough indication but it is not the final indicator of the behavior of the real cores. Optimized laser parameters are generated so that the noise behavior is improved by laser domain refinement as shown in Fig.1.12. Otherwise, non-optimal characteristics will increase the magnetostriction and the generated noise.

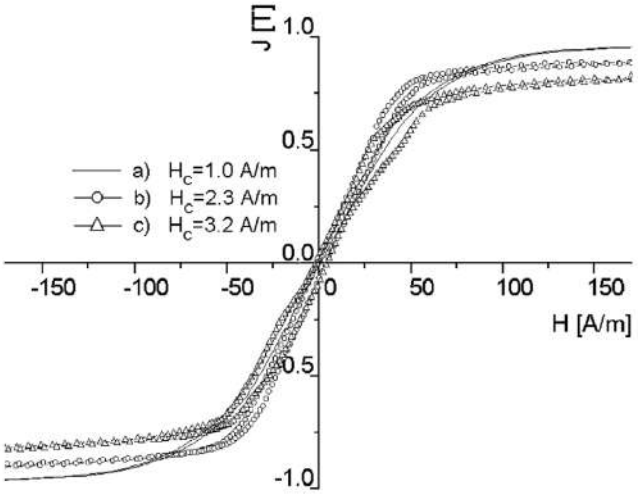

Fig. 1.11 Hysteresis loops of Finemet: a) Non-treated sample b) Laser treated sample with small density dotted lines c) Laser treated sample with high density dotted lines [38]

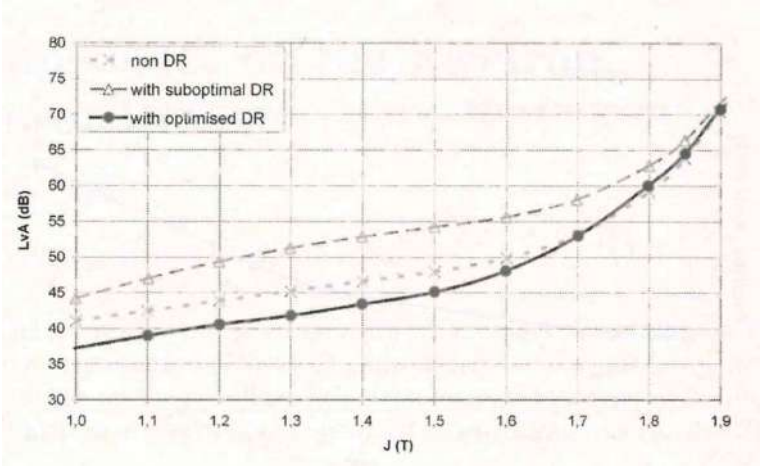

Fig. 1.12 Calculated noise on basis of magnetostriction by considering laser domain refinement (DR)[39]

1.7 Study orientation

The originality of the project is to model and eventually optimize mechanical vibration and acoustic noise responses using laser surface texturizing technique while preserving high mechanical and thermal resistance. First, a magnetic modeling that considers magnetic domains and walls movement is a needed to identify the magnetic flux density gradient through the structure, including the magnetic dynamic property introduced by Maloberti et al. [11, 12, 40, 41]. Next, the determination and the identification of magnetic body and surface forces affecting the vibrational behavior of the structure is carried out by considering magnetic forces and magnetostriction, and taking into account the interaction between the structure and air and the domains and the walls motion. The forces identification allows a magneto-mechanical coupling and connects the magnetic model to the mechanical model. Then, a mechanical-vibrational modeling has to be done to identify natural characteristics and vibrational response resulting from magnetic forces excitation. Once the direct magneto-mechanical model is set, the importance of laser scribing appears and a parametric study related to the effect of magnetic dynamic properties is presented in details permitting the optimisation of the scribing versus the vibration and the noise generation. Different challenges occur: the knowledge of the magnetic behavior laws of the chosen material by considering the accurate dynamic property, the selection and the calculation of the magnetic forces, the experimental challenges and the choice of test bench that is adapt the most with the model developed by choosing specific sensor and measurement equipments. All these challenges will let us select the optimal properties that can be obtained by laser scribing with specific optimized laser parameters.

Chapter 2

Theoretical study

2.1 Problem Setup

We consider a soft magnetic fixed plate subjected to a longitudinal magnetic field H_a represented in Figs. 2.1 and 2.2. This chapter aims to present a theorical approach of the equations leading to the calculation of the vibration of this plate. First, to simplify the problem, different assumptions have to be considered:

For mechanical modeling:
1- The material is homogeneous and linearly elastic; the mechanical problem is purely linear.
2- Isotropic material is considered with only mechanical properties E and ν.
3- Rayleigh damping model is adopted with α and β parameters.
4- The problem is reduced to two dimensions analysis in x and z directions.
5- For vibration analysis, small displacements are considered.
6- Geometric parameters are the thickness e and the length L of the plate; any variation in the width will not be treated.
7- The plate is fixed: all displacement components are locally equal to zero at fixed points: $u(x = 0, z, t) = 0$.

For magnetic modeling:
8- A quasi-static problem where the electrical displacements of the beam are assumed to be small compared with the conductive currents ($\frac{\partial \mathbf{D}}{\partial t} \ll \mathbf{J}$).
9- The considered soft non-oriented material is magnetically isotropic and the magnetization process occurs in the direction imposed by the applied magnetic field because there is no dominant magnetization direction to the detriment of another.

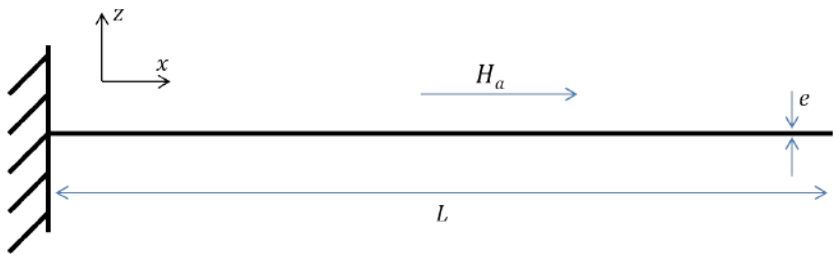

Fig. 2.1 A soft ferromagnetic plate subjected to a longitudinal magnetic field

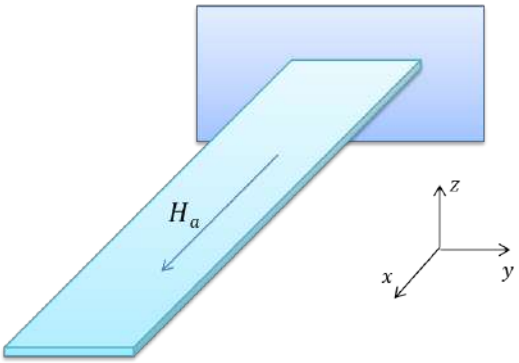

Fig. 2.2 A 3D presentation of the ferromagnetic plate

10- The magnetic permeability μ and the dynamic magnetic property Λ are considered constant and unique due to the isotropy.
11- The electrical conductivity σ is constant.
12- The only magnetic source is the longitudinal magnetic field applied on both surfaces of the beam: this source is time dependent but it is uniform on the whole plate's surface: $H(x, z = \pm\frac{e}{2}, t) = H_a(t)$.
13- The magnetic field is generally dependent on the stress field applied on the material. In this study, no pre-stress is applied and the generated stress from the vibrational problem is neglected. The magnetic problem is independent from mechanical problem; a weak coupling model will be adopted.

2.2 1D Magnetic problem formulation

The magnetic problem consists on defining the gradient of the magnetic flux density vector $\mathbf{B}(x, z, t)$ or of the magnetic potential vector $\mathbf{A}(x, z, t)$ for every point in the material and at every time. The magnetization of the structure is only possible if it exists a source of magnetization. In this case, the considered source is an external magnetic field applied on the beam's surfaces in longitudinal direction with a uniform distribution as mentioned in assumption 12.
The magnetic problem is modeled using Maxwell equations presented below, considering assumption 8:

$$rot\ \mathbf{E} = -\frac{\partial \mathbf{B}}{\partial t} \tag{2.1}$$

$$rot\ \mathbf{H} = \mathbf{J} + \mathbf{J}_S \tag{2.2}$$

$$div\ \mathbf{B} = 0 \tag{2.3}$$

These equations combine magnetic and electrical variables. To solve this problem, the magnetic and electrical behaviors must be well defined. The current density and the electric field are proportional (Eq. 2.5) as shown in assumption 11. The relation between the flux density and the magnetic field is shown in Eq. 2.4.

$$\mathbf{H} = \frac{1}{\mu_m}\mathbf{B} + \sigma\Lambda^2\frac{\partial}{\partial t}\mathbf{B} = (\frac{1}{\mu_m} + \sigma\Lambda^2\frac{\partial}{\partial t})\mathbf{B} \tag{2.4}$$

$$\mathbf{J} = \sigma\mathbf{E} \tag{2.5}$$

Eqs. 2.1, 2.2, 2.3, 2.4, 2.5 become:

$$\sigma s\mathbf{B}(s) = \begin{bmatrix} \frac{\partial^2}{\partial z^2} + \frac{\partial^2}{\partial y^2} & -\frac{\partial^2}{\partial x \partial y} & -\frac{\partial^2}{\partial x \partial z} \\ -\frac{\partial^2}{\partial x \partial y} & \frac{\partial^2}{\partial x^2} + \frac{\partial^2}{\partial z^2} & -\frac{\partial^2}{\partial y \partial z} \\ -\frac{\partial^2}{\partial x \partial z} & -\frac{\partial^2}{\partial y \partial z} & \frac{\partial^2}{\partial x^2} + \frac{\partial^2}{\partial y^2} \end{bmatrix} (\frac{1}{\mu_m} + \sigma\Lambda^2 s)\mathbf{B}(s) = \Delta((\frac{1}{\mu_m} + \sigma\Lambda^2 s)\mathbf{B}(s)) \quad (2.6)$$

In this problem, considering assumtion 4 and the uniformity of the applied magnetic field in assumption 12, Eq. 2.6 becomes:

$$\begin{aligned} \sigma s B_x(z,s) &= \frac{\partial^2}{\partial z^2}(\frac{1}{\mu_m} + \sigma\Lambda^2 s)B_x(z,s) \\ B_x(\pm\frac{e}{2}, s) &= B_a(s) \end{aligned} \quad (2.7)$$

where $B_a(s) = \frac{\mu_m}{1+\sigma\Lambda^2\mu_m s} H_a(s)$

The equation above can be solved analytically for a second order linear equation with respect to z, or using the finite element technique in the z dimension.

Analytically, the solution is:

$$B(z,s) = B_a(s)[c_1 e^{\sqrt{\frac{b}{a}}z} + c_2 e^{-\sqrt{\frac{b}{a}}z}] \quad (2.8)$$

where $a = 1 + \mu_m\sigma\Lambda^2 s$ and $b = \sigma\mu_m s$.

For the finite element solving technique for 1D case, a quadratic element is considered, due to the convergence power that it can reach. Returning to Eq. 2.7, by multipling the differential equation by a test function $v(z)$, and by integrating through the thickness we get:

$$\int_{-\frac{e}{2}}^{\frac{e}{2}} bB(z)v(z)dz - \int_{-\frac{e}{2}}^{\frac{e}{2}} a\frac{\partial^2 B(z)}{\partial z^2}v(z)dz = 0 \quad (2.9)$$

Using the part integration, we get:

$$\int_{-\frac{e}{2}}^{\frac{e}{2}} bB(z)v(z)dz + \int_{-\frac{e}{2}}^{\frac{e}{2}} a\frac{\partial B(z)}{\partial z}\frac{\partial v(z)}{\partial z}dz = 0 \quad (2.10)$$

By transforming the physical coordinate z to local coordinates η with -1,1 boundaries for quadratic element, we get:

$$\int_{-1}^{1} b\sum_{1}^{3} N_i(\eta)\tilde{B}_i(s)N_j(\eta)det(J)d\eta + \int_{-1}^{1} a\sum_{1}^{3}\frac{\partial N_i(\eta)}{\partial\eta}\frac{d\eta}{dz}\tilde{B}_i(s)\frac{\partial N_j(\eta)}{\partial\eta}\frac{d\eta}{dz}det(J)d\eta = 0 \quad (2.11)$$

Using the FEM, the problem consists of solving a system of linear equations in the form:

$$[K_{mag}]\tilde{B}(s) = b_a(s) \quad (2.12)$$

$[K_{mag}]$ is the magnetic stiffness matrice and $b_a(s)$ is the source, in this case it corresponds to the boundary conditions applied on the surfaces of the beam and it can be expressed as:

$$b_a(s) = \begin{bmatrix} B_a(s) & 0 & 0 & \dots & 0 & 0 & B_a(s) \end{bmatrix}^T \quad (2.13)$$

A magnetic flux profile function of z is obtained through the thickness of the beam.

2.3 Mechanical modeling

2.3.1 Boundary Conditions

The boundary conditions of the fixed beam are considered as equality constraints to the free vibration problem as follows

$$u(x=0,t)=0 \tag{2.14}$$

where $u(x,t)=[u^0,w,\psi_x]^T$ is the displacement vector at any point in the plane (x,z) at time t, with 3 displacement components: 2 linear and 1 angular: u^0 is the mid-plane linear displacement component along x, w is the linear displacement component along z, and ψ_x is the angular displacement component about y axis and through the xz plane.

2.3.2 Energy formulation

One of the most used and most practical approaches used in magneto-mechanical coupling is the energy approach. Using Hamilton's principle, an energy conservation formulation is obtained:

$$\sum \frac{\partial \Pi}{\partial u}=0 \tag{2.15}$$

Strain Energy Π^K

The strain vector of the beam ε is expressed as follows,

$$\varepsilon^T=\begin{bmatrix}\varepsilon_x^0 & \kappa_x & \gamma_{xz}\end{bmatrix} \tag{2.16}$$

Where ε_x^0 is the axial strain component along x axis, κ_x is the twisting strain component through xz plane and about y axis, and γ_{xz} is the shear strain component along the plane (xz). The strain vector is related to the displacement vector defined in Eq. 2.16 as follows,

$$\varepsilon=\begin{pmatrix}\varepsilon_x^0\\ \kappa_x^0\\ \gamma_{xz}\end{pmatrix}=\begin{pmatrix}\frac{\partial}{\partial x} & 0 & 0\\ 0 & 0 & \frac{\partial}{\partial x}\\ 0 & \frac{\partial}{\partial x} & 1\end{pmatrix}\begin{pmatrix}u^0\\ w\\ \psi_x\end{pmatrix}=[B_u^x]\mathbf{u} \tag{2.17}$$

We define the following stiffness matrix,

$$[C]=\begin{pmatrix}A_{11} & B_{11} & 0\\ B_{11} & D_{11} & 0\\ 0 & 0 & A_{44}\end{pmatrix} \tag{2.18}$$

Where the constants (A_{jk},B_{jk},D_{jk}) are defined as

$$(A_{jk},B_{jk},D_{jk})=\sum_{m=1}^{n}\int_{z_{m-1}}^{z_m}Q_{jk}^m(1,z,z^2)dz \qquad j,k=1,2,6 \tag{2.19}$$

$$A_{jk}=\sum_{m=1}^{n}\int_{z_{m-1}}^{z_m}KQ_{jk}^m dz \qquad j,k=4,5 \text{ and } K=\frac{5}{6} \tag{2.20}$$

where

$$[Q]=\frac{E}{1-\upsilon^2}\begin{pmatrix}1 & \upsilon & 0\\ \upsilon & 1 & 0\\ 0 & 0 & \frac{1-\upsilon}{2}\end{pmatrix} \tag{2.21}$$

Hence, the strain energy of the beam is expressed as follows:

$$\Pi^K = \frac{1}{2} b_m \int_0^L \mathbf{u}^T [B_u^x]^T [C][B_u^x]\mathbf{u} dx \tag{2.22}$$

And the variation of the strain energy with respect to the displacement becomes

$$\frac{\partial \Pi^K}{\partial \boldsymbol{u}} = b_m \int_0^L [B_u^x]^T [C][B_u^x]\mathbf{u} dx \tag{2.23}$$

Kinetic Energy Π^M

Including the inertia effect, the mass moment of inertia of half of the beam segment about each end shall be computed and included at the diagonal locations corresponding to the rotational degrees of freedom. The kinetic energy of a beam is expressed as follows:

$$\Pi^M = \frac{1}{2}\rho b_m \int_0^L [e(\dot{u}^2 + \dot{w}^2) + \frac{e^3}{12}\dot{\psi_x}^2] dx \tag{2.24}$$

$$\Pi^M = \frac{1}{2}\rho b_m \int_0^L \begin{pmatrix} \dot{u} & \dot{w} & \dot{\psi_x} \end{pmatrix} \begin{pmatrix} e & 0 & 0 \\ 0 & e & 0 \\ 0 & 0 & \frac{e^3}{12} \end{pmatrix} \begin{pmatrix} \dot{u} \\ \dot{w} \\ \dot{\psi_x} \end{pmatrix} dx = \frac{1}{2}\rho b_m \int_0^L \dot{u}^T [m] \dot{u} dx \tag{2.25}$$

$$\frac{\partial \Pi^M}{\partial \boldsymbol{u}} = \rho b_m \int_0^L [m] \ddot{u} dx \tag{2.26}$$

2.3.3 Finite element discretization

The problem described in the continuous domain is now discretized; the system is divided into isoparametric, 3-noded quadratic elements with first order shear deformation for each beam, using the finite element method (FEM), by transforming the physical coordinate (x) into local coordinate (ξ). Shape functions developed for 3-noded quadratic elements are used to discretize the domain. Hence, a variable u can be expressed using the nodal relationship.

$$u = \sum_{k=1}^{3} N_k u_k \tag{2.27}$$

where u_k is the variable's value at node k. Hence, the nodal relationship is applied to the displacement components as follows, $u^0 = \sum_{k=1}^{3} N_k u_k^0$, $w = \sum_{k=1}^{3} N_k w_k$, $\psi_x = \sum_{k=1}^{3} N_k \psi_{xk}$. Then, adopting the Gaussian quadrature formulas, mass and stiffness matrices can be derived for each element. Later, the global mass and stiffness matrices shall be obtained by assembling the elementary matrices with respect to the nodes displacement components, in order to calculate the natural frequencies corresponding to each mode in the discretized domain.

Beam Stiffness Matrix

To derive the stiffness matrix, one must first adopt the Gaussian quadrature formula by expressing the potential energy in the following form

$$\Pi^K = \frac{1}{2} u^T [K] u \tag{2.28}$$

Then, using the nodal displacement relationship in Eq. 2.27 applied on strain-displacement relation in Eq. 2.17, Eq. 2.23 is discretized as follows

$$\Pi^K = \frac{1}{2} \mathbf{u}^T \left(b_m \int_{-1}^{1} [B_u^\xi]^T [C] [B_u^\xi] [J] d\xi \right) \mathbf{u} \tag{2.29}$$

Where J is the Jacobian matrix which is used to transform the physical coordinate (x) to the curvilinear coordinate (ξ) and $[B]$ is constructed using the shape functions for 3-nodes quadratic element. Hence, the stiffness matrix of the beam can be expressed as,

$$[K] = b_m \int_{-1}^{1} [B_u^\xi]^T [C] [B_u^\xi] det[J] d\xi \tag{2.30}$$

Beam Mass Matrix

To derive the mass matrix, we must also adopt the Gaussian quadrature formula by expressing the kinetic energy expressed in Eq.2.25 in the following form

$$\Pi^M = \frac{1}{2} \dot{u}^T [M] \dot{u} \tag{2.31}$$

Thus, using the Gaussian quadrature formula Eq.2.31 in Eq. 2.25 and including the inertia effect, we get

$$[M] = \rho b_m \int_{-1}^{1} [F]^T [m] [F] det[J] d\xi \tag{2.32}$$

Where $[F]$ is a matrix function of the shape functions and

$$[m] = \begin{pmatrix} e & 0 & 0 \\ 0 & e & 0 \\ 0 & 0 & \frac{e^3}{12} \end{pmatrix} \tag{2.33}$$

Assembly

Once the elementary mass and stiffness matrices are set for each element, their assembly will be made in global mass and stiffness matrices in order to take into consideration the whole displacements nodes in the structure. The assembly technique consists on combining all the elements contributions and considering the commun nodes between two consecutive elements.

2.3.4 Eigen problem resolution

Once the global symmetric mass and stiffness matrices are obtained, where $[K]$ is positive semi definite and $[M]$ is positive definite, the following Eigen-equation corresponding to the free vibration problem can be solved for determining the natural frequencies ω_i and the eigenvectors ϕ_i that corresponds to the mode shapes.

$$(-\omega_i^2[M]+[K])\{\phi_i\}=0 \tag{2.34}$$

The modes classification corresponds to the natural frequencies obtained in ascending order, from the lowest to the highest. The number of natural frequencies depends on the mesh size, and it is equal to the degree of freedom of the system. But the frequencies analyzed are the ones corresponding to the first 10 modes classified from the lowest (fundamental) to the highest.

2.4 Dynamic approach

2.4.1 Dynamic flexibility matrix

Using Hamilton's principle in Eq. 2.15, the general form of motion modeling the vibrational behavior of the beam or any mechanical structure, considering the inertia, elastic, damping and external force acting on the structure with a finite number n degree of freedom is:

$$[M]\ddot{\mathbf{u}}(t)+[C]\dot{\mathbf{u}}(t)+[K]\mathbf{u}(t)=f(t) \tag{2.35}$$

Here, the mass matrix $[M]$ and the stiffness matrix $[K]$ are derived from the eigen problem. The damping matrix $[C]$ represents the different dissipations in the structure. A simple representation of these losses is given by a Rayleigh damping assumption:

$$[C]=\alpha[M]+\beta[K] \tag{2.36}$$

The coefficients α and β are selected to fit to the response of the structure. Eq. can be written using the laplace transform:

$$G(s)\mathbf{F}(s)=\mathbf{U}(s)=([M]s^2+[C]s+[K])^{-1}\mathbf{F}(s) \tag{2.37}$$

A transfer function $G(s)$ matrix connecting the external forces to the structure displacement vector is generated. It resumes the whole vibration process at each node of the structure. The element i,j of $G(s)$ give the impact of i^{th} force on the j^{th} displacement component. $G(s)$ is also known as the dynamic flexibility matrix.

2.4.2 Modal decomposition

The determination of $G(s)$ as expressed in Eq. 2.37 takes a very large resolution time and becomes almost impossible when the degree of freedom increases. Hence, a modal decomposition is developed and aims to express the transfer function with the eigenvalues and the eigenvectors derived from the eigenproblem. Let us perform a change of variables from physical coordinates u to modal coordinates v [42]:

$$\boldsymbol{u}=\boldsymbol{\Phi v} \tag{2.38}$$

Substituting in Eq. 2.35 we get:

$$\boldsymbol{\Phi}^T[M]\boldsymbol{\Phi}\ddot{\boldsymbol{v}}+\boldsymbol{\Phi}^T[C]\boldsymbol{\Phi}\dot{\boldsymbol{v}}+\boldsymbol{\Phi}^T[K]\boldsymbol{\Phi v}=\boldsymbol{\Phi}^T\boldsymbol{f} \tag{2.39}$$

The obtained matrices $\Phi^T[M]\Phi$, $\Phi^T[C]\Phi$ and $\Phi^T[K]\Phi$ are diagonal and can be derived using Eq. 2.34.

$$\Phi_j^T[K]\Phi_i = \omega_i^2 \Phi_j^T[K]\Phi_i \tag{2.40}$$

$$\Phi_i^T[K]\Phi_j = \omega_j^2 \Phi_i^T[K]\Phi_j \tag{2.41}$$

Substracting Eq. 2.41 from 2.40, and considering that $[K]$ and $[M]$ are symetric, we get:

$$(\omega_i^2 - \omega_j^2)\Phi_j^T[M]\Phi_i = 0 \tag{2.42}$$

This equation gives the following:

$$\Phi_j^T[M]\Phi_i = 0 \text{ when } \omega_i \neq \omega_j \tag{2.43}$$

This leads to the following:

$$\Phi^T[M]\Phi = diag(\mu_i) \tag{2.44}$$

$$\Phi^T[K]\Phi = diag(\mu_i\omega_i^2) \tag{2.45}$$

$$\Phi^T[C]\Phi = diag(2\xi_i\mu_i\omega_i) \tag{2.46}$$

where

$$\xi_i = \frac{1}{2}(\frac{\alpha}{\omega_i} + \beta\omega_i) \tag{2.47}$$

Returning to the modal decomposition, Eq. 2.39 can be written as:

$$\ddot{v} + 2\xi\Omega\dot{v} + \Omega^2 v = \mu_i^{-1}\Phi^T f \tag{2.48}$$

with the notations:

$$\begin{aligned} \xi &= diag(\xi_i) \\ \Omega &= diag(\omega_i) \\ \mu &= diag(\mu_i) \end{aligned} \tag{2.49}$$

From Eq. 2.48 one can express the dynamic flexibility derived in Eq. 2.37 as follows:

$$[G(s)]\mathbf{F}(s) = \mathbf{U}(s) = \Phi\mathbf{V}(s) = \Phi diag\{\frac{1}{\mu_i(s^2 + 2\xi_i\omega_i s + \omega_i^2)}\}\Phi^T\mathbf{F}(s) \tag{2.50}$$

The expansion of this equation gives the following:

$$[G(s)] = \sum_1^n \frac{\Phi_i\Phi_i^T}{\mu_i(s^2 + 2\xi_i\omega_i s + \omega_i^2)} \tag{2.51}$$

The vibrational response vector $\mathbf{U}(s)$ can be now determined once the excitation vector $\mathbf{F}(s)$ is known; the results for any component of vector $\mathbf{U}(s)$ can be illustrated using bode diagram.

2.5 Forces acting on the structure

One main challenge of the study is to identify the excitation vector at each node. Let us return to the energy concept to formulate the energy resulting applied forces. The mechanical fields in a volume Ω with boundary S are expressed as follows [43]:

$$\Pi_\Omega = -\int_\Omega \int_u f_\Omega^T \delta u d\Omega \tag{2.52}$$

$$\Pi_S = -\int_S \int_u n.f_S^T \delta u dS \tag{2.53}$$

Eqs. 2.52 and 2.53 correspond to body and surface forces respectively. These forces have there origin from different sources: mechanical forces and moments, thermal forces, electromagnetic forces. In this study, only electromagnetic forces are considered and their effect on the vibrational response is well carried out.

2.5.1 Origin of electromagnetic forces

Kloos et al. [29] has revealed the macroscopic magnetic forces acting on mechanical structures. The main forces are the Lorentz force and the magnetostrictive force. Other forces resulting from the non-colinearity between the magnetic field, the magnetic flux density and the forces resulting from the inhomogenities in the magnetic permeability are also explained. Before we derive an explicit form of the acting forces, we will present the total magnetic stresses that define these forces. They are expressed in a tensor as:

$$[\sigma] = [T] + [\sigma_{ms}] \tag{2.54}$$

where $[T]$ is the Maxwell tensor derived from the Lorentz force, and $[\sigma_{ms}]$ is the magnetostriction stress tensor. The total force resulting from the stresses is the sum of electromagnetic (Maxwell) and magnetostrictive forces:

$$f = div[\sigma] = f^{em} + f^{ms} \tag{2.55}$$

2.5.2 Generalized Magnetic Forces Expression for a constant surface magnetic field

The Maxwell forces acting on the structure are explained. The functional of the energy of the magnetoelastic interaction for the deformable magnetic medium, taking into consideration the presence of the air interface, for a uniform time-independent magnetic field applied on surface of the sample, can be written as [16]

$$\Pi^{em} = \int_{\Omega^+(u)} \int_0^{B^+} H^+ dB^+ d\Omega^+ + \frac{1}{2}\int_{\Omega^-(u)} \mu_0 (H^-)^2 d\Omega^- \tag{2.56}$$

Superscripts + and − correspond respectively to the beam and air media. Considering the interface conditions of magnetic field in boundary S:

$$B_n^+ = B_n^-, H_\tau^+ = H_\tau^- \tag{2.57}$$

$$(H^+)^2 = (H_n^+)^2 + (H_\tau^+)^2, (H^-)^2 = (H_n^-)^2 + (H_\tau^-)^2 \tag{2.58}$$

The magnetic force F acting on the body and the surface of the structure is the change rate of the magnetic energy with respect to the structure displacement when the magnetic medium

is undergoing an incremental displacement with the magnetic excitation held fixed, and it can be expressed as follows:

$$\boldsymbol{F}^T = -\frac{\delta \Pi^{em}}{\delta \boldsymbol{u}} \tag{2.59}$$

We will calculate the variation of the total magnetic energy to displacement:

$$\begin{aligned}\delta_{\boldsymbol{u}} \Pi^{em}\{\boldsymbol{u}\} = &\left(\int_{\Omega^+(\boldsymbol{u}+\delta\boldsymbol{u})} - \int_{\Omega^+(\boldsymbol{u})}\right)\int_0^{B^+} \boldsymbol{H}^+ d\boldsymbol{B}^+ dv \\ &+\frac{1}{2}\left(\int_{\Omega^-(\boldsymbol{u}+\delta\boldsymbol{u})} - \int_{\Omega^-(\boldsymbol{u})}\right)\mu_0(\boldsymbol{H}^-)^2 dv\end{aligned} \tag{2.60}$$

$$\delta_{\boldsymbol{u}} \Pi^{em}\{\boldsymbol{u}\} = \int_S \left[\int_0^{B^+} \boldsymbol{H}^+ d\boldsymbol{B}^+ - \frac{1}{2}\mu_0(\boldsymbol{H}^-)^2\right] \boldsymbol{n}^+ . \delta \boldsymbol{u} dS \tag{2.61}$$

$$\delta_{\boldsymbol{u}} \Pi^{em}\{\boldsymbol{u}\} = \int_S \left[\int_0^{B^+} \boldsymbol{H}^+ d\boldsymbol{B}^+ - \frac{1}{2}\mu_0[\frac{(\mu_m)^2}{\mu_0^2}(H_n^+)^2 + (H_\tau^+)^2]\right] \boldsymbol{n}^+ . \delta \boldsymbol{u} dS \tag{2.62}$$

$$\begin{aligned}\delta_{\boldsymbol{u}} \Pi^{em}\{\boldsymbol{u}\} = &-\int_{\Omega^+} \nabla[\frac{\mu_m^2}{2\mu_0}(\boldsymbol{H}^+)^2 - \int_0^{B^+} \boldsymbol{H}^+ d\boldsymbol{B}^+]\delta \boldsymbol{u} dv \\ &-\int_S [-\frac{1}{2\mu_0}((\mu_m)^2 - \mu_0^2)(H_\tau^+)^2]\boldsymbol{n}^+ \delta \boldsymbol{u} dS\end{aligned} \tag{2.63}$$

Using Gauss integral formula, Zhou et al. [16] have deduced volume and surface magnetic forces:

$$f_\Omega^{em} = \nabla[\frac{\mu_m^2}{2\mu_0}(\boldsymbol{H}^+)^2 - \int_0^{B^+} \boldsymbol{H}^+ d\boldsymbol{B}^+] \tag{2.64}$$

$$f_S^{em} = [-\frac{1}{2\mu_0}(\mu_m^2 - \mu_0^2)(H_\tau^+)^2]\boldsymbol{n}^+ \tag{2.65}$$

Both volume and surface forces can be reformulated as one equivalent force surface force using Eq. 2.62; the distribution of the volume force through the thickness will be considered in the incoming studies:

$$f_S^{eq} = \left[\frac{1}{2}\mu_0[\frac{\mu_m^2}{\mu_0^2}(H_n^+)^2 + (H_\tau^+)^2] - \int_0^{H^+} \boldsymbol{B}^+ d\boldsymbol{H}^+\right] \boldsymbol{n}^+ \tag{2.66}$$

The equivalent surface force expressed in Eq. 2.66 is normal to both surfaces of the plate. When the plate vibrates with small deformation, the normal surface vector $\boldsymbol{n}^+$ forms an angle θ with the z-axis. Hence, the equivalent surface force f_S^{eq} can be projected on the x and z axis. The forces projections on the upper and the lower surfaces of the plate are illustrated in details in Fig. 2.68. Its is shown that the forces in x-direction and z-direction are equal and in opposite direction. The z-direction forces generate a normal stress σ_z that is neglected in the theory of plates due to the low thickness of the plate in front of the width and the length. On the other side, the x-forces create a mechanical moment expressed as:

$$M_x^{em} = f_{xS}^{eq} e \tag{2.67}$$

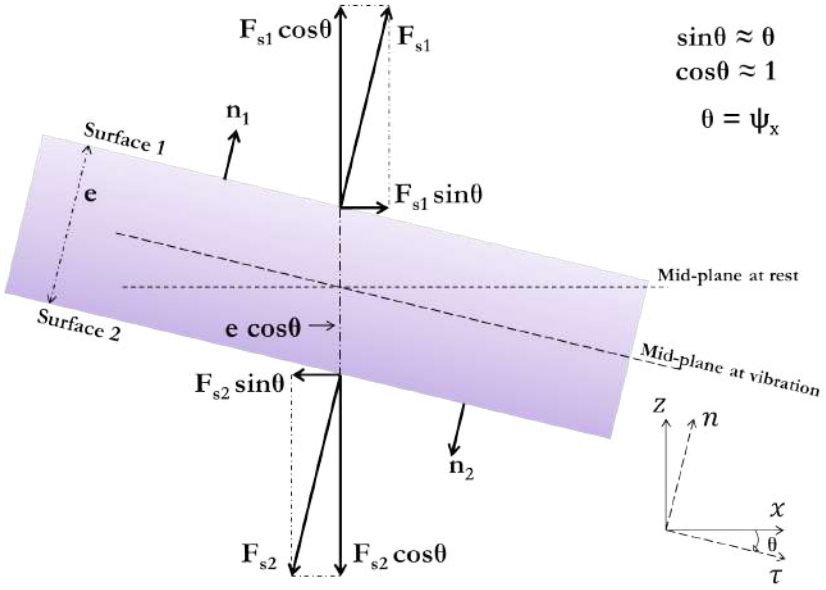

Fig. 2.3 The presentation of the projected total magnetic surface force

$$M_x^{em} = \left[\frac{1}{2}\mu_0[\frac{(\mu_m)^2}{\mu_0^2}(H_n^+)^2 + (H_\tau^+)^2] - \int_0^{B^+} \boldsymbol{H}^+ d\boldsymbol{B}^+\right] e\psi_x \tag{2.68}$$

Based on displacement-dependent moment, one can find new natural frequencies of the magnetic structure with specific magnetic field applied on both surfaces of the plate.

2.5.3 Magnetostrictive forces

Magnetostriction is the process where a deformation of the material is obtained when subjected to a magnetic field. When the material is blocked, magnetostriction generated stress and a force will be applied on the material leading to vibration. Magnetostriction is characterized by a magnetostrictive strain vector λ. For the case of the beam, this vector is only directed with x axis, knowing that the strain in z axis is neglected $\lambda^T = (\lambda, 0, 0)$. it can be related with the induced stress by:

$$\sigma_{ms} = -[Q]\lambda \tag{2.69}$$

The strain energy resulting from the magnetostriction is [30]:

$$\delta\Pi^{ms} = -\int_A \begin{pmatrix} N_\lambda \\ M_\lambda \\ 0 \end{pmatrix}^T \delta\varepsilon dA \tag{2.70}$$

where

$$N_\lambda = \int_{-\frac{e}{2}}^{\frac{e}{2}} [Q]\lambda dz \tag{2.71}$$

$$M_\lambda = \int_{-\frac{e}{2}}^{\frac{e}{2}} [Q]\lambda z dz \tag{2.72}$$

By deriving Eq. 2.70 with respect to the displacement, we obtain a magnetostriction force vector:

$$\boldsymbol{F}^{ms} = b_m \int_0^L [B_u] \begin{pmatrix} N_\lambda \\ M_\lambda \\ 0 \end{pmatrix} det(J) d\xi \tag{2.73}$$

Chapter 3

Applications and simulations

3.1 Introduction

In this chapter, we will discuss the numerical results obtained from simple applications of the theories developed in the previous chapter. First, an electromagnetic modeling is treated, where a magnetic flux density distribution in the structure is obtained, depending on different geometric and magnetic parameters; a special attention will focus on the effect of the dymanic magnetic property considered by Maloberti et al. [11]. Next, a modal analysis is developed, giving the natural frequencies of vibration of the concerned structure. Then, the implementation of the longitudinal magnetic field on the surface will be caried out in order to find its effect on the variation of the natural frequencies.

3.2 Geometric, Magnetic, Mechanical properties

Let us consider a fixed beam subjected to uniform longitudinal applied magnetic field H_a on both surfaces. We consider the different assumption presented in the previous chapter. Tables 3.1 presents the basic geometric, mechanical and magnetic properties that correspond to the studied case and the results obtained later.

Properties	**Symbol**	**Value**
Young's Modulus (GPa)	E	200
Poisson Ratio	υ	0.3
Density (Kg/m^3)	ρ	7850
Thickness (mm)	e	0.5
Length (mm)	L	100
Electrical conductivity (S/m)	σ	2×10^6
Relative permeability	μ_r	1000
Dynamic property (μm)	Λ	50
Applied magnetic field (A/m)	H_a	1000

Table 3.1 Beam's properties

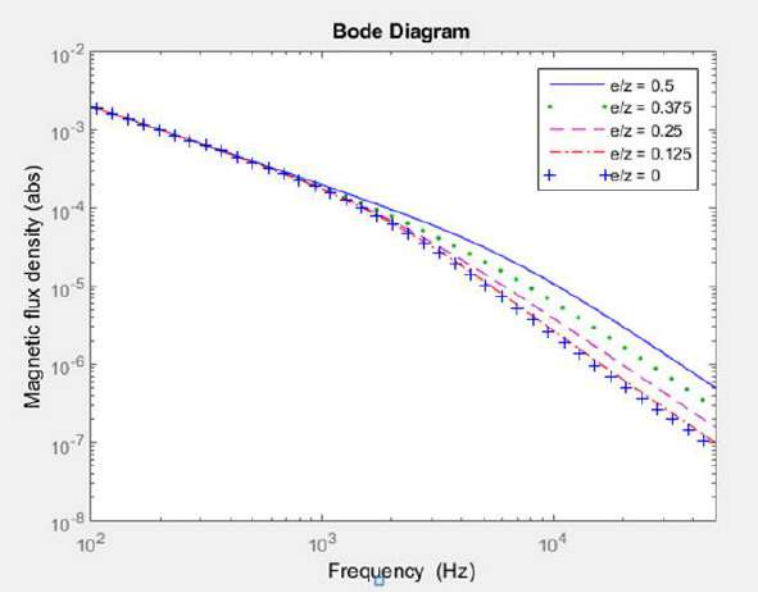

Fig. 3.1 Bode diagram of magnetic flux density distribution in the thickness of the plate with $\Lambda = 100\mu m$

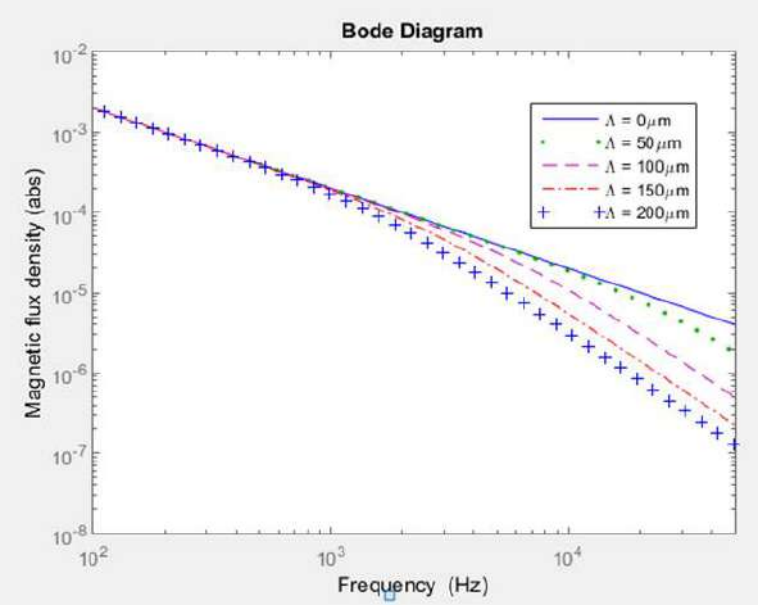

Fig. 3.2 Bode diagram of magnetic flux density variation with different dynamic properties at the surface of the plate

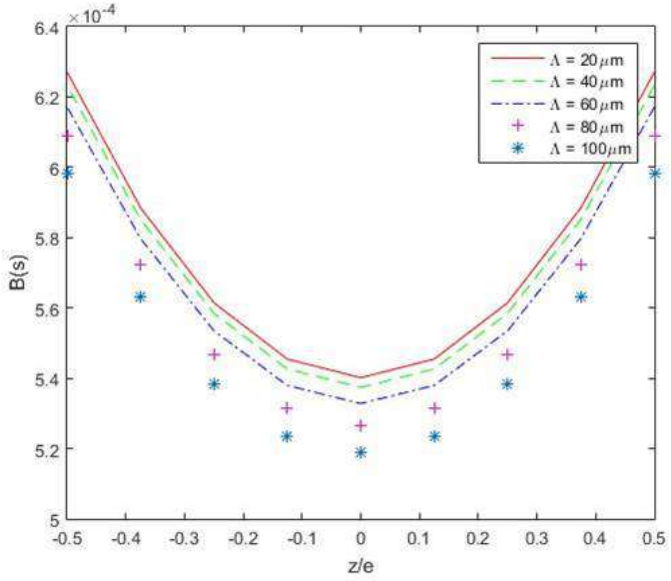

Fig. 3.3 Variation of the magnetic flux density with the thickness of the plate, depending on the magnetization dynamic property Λ at 2000*Hz*

3.3 Magnetic Modeling

The goal of the magnetic modeling is to obtain a distribution of the magnetic flux density in the whole structure. In this case, a longitudinal magnetic field is applied in a uniform way on the surface and though the length of the beam; the only variation of the magnetic flux density happens in the thickness of the beam and is oriented through x axis. The obtained results give a frequency dependance of the flux density. Fig. 3.1 shows the variation of the flux density through the thickness of the plate using a bode diagram illustration. The results show that the magnetic flux density has its maximum on the surfaces where the magnetic field is applied and decreases through the thickness. The same interpretation can be obtained with the result shown in Fig. 3.3 that illustrates the magnetic flux density variation with the thickness of the plate for a frequency of 2000*Hz*.
The impact of the dynamic magnetization property Λ is also revealed. Fig. 3.2 illustrates the effect that this factor has on the frequency response of the magnetic flux density and Fig. 3.3 shows the impact of Λ on the flux density through the thickness with an excitation frequency of 2000*Hz*. It is shown that the magnetic flux density gradient decreases with the increase of Λ. In fact, for smaller magnetic domains, the loss in the magnetic flux density decreases.

3.4 Magneto-Mechanical modeling including the surface magnetic forces

Mechanical study involving a modal analysis applied on the structure is considered using a 1D finite element method. The implementation of derived matrices is obtained using Matlab based on the parameters presented in Table 3.1. Natural frequencies of vibration are resumed and compared in Table 3.2. Two columns of frequencies are obtained: one corresponds to the natural frequencies without any applied magnetic field, and one corresponds to the case where magnetic field H_a is applied. It is shown that the frequency increases when the magnetic field is applied. This is well explained in Eq. 2.68, where the addition of displacement-dependent force will increase the stiffness and the natural frequency, due to the application of a magnetic surface traction force that depends on the deformation of the structure. The effect of the dynamic magnetic property Λ is not considered yet; it will be carefully treated later where a detailed vibrational response is studied and different vibration characteristics will be optimised.

$H_a(A/m)$	0	1000
Mode	**Frequency** (Hz)	
1	42.75	48.29
2	268.51	303.04
3	754.48	851.29
4	1486.13	1676.19
5	2473.28	2788.23
6	3725.58	4197.5
7	5255.63	5917.17
8	7078.97	7963.46
9	9214.37	10355.97
10	11683.95	13117.78

Table 3.2 Natural frequencies derived from modal analysis

3.4.1 Comparison with previous studies

This section presents a comparison with the calculation made using a MATLAB simulation concerning the surface traction force effect on the vibration with previous results obtained by Wei et al. [1] and Takagi et al. [2]. The comparison is based on the variation of the fondamental natural frequency of the plate with the applied magnetic flux density. Different mechanical, geometric and magnetic properties adopted are resumed in Table 3.3 and results are plotted in Fig. 3.4. From the comparison of the observed results in Fig. 3.4, we can

Properties	**Symbol**	**Value**
Young's Modulus (GPa)	E	200
Poisson Ratio	υ	0.3
Density (Kg/m^3)	ρ	7850
Thickness (mm)	e	0.5
Length (mm)	L	100
Relative permeability	μ_r	16

Table 3.3 Different properties adopted by Wei et al. [1] and Takagi et al. [2]

notice that the curve generated by the model developed in this paper is convex. In fact, from

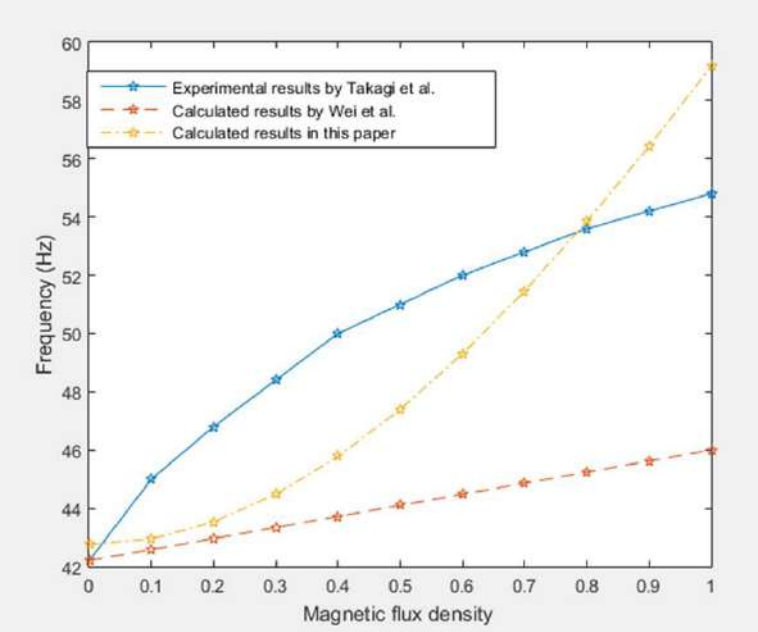

Fig. 3.4 Natural frequency variation with the applied magnetic density results

assumption 10, considering that the magnetic permeability μ_m is constant, we can deduce that the fondamental natural frequency increases with the square of the magnetic flux density and the applied magnetic field. Once the assumption 10 is omitted and the dependence of the magnetic permeability with the flux density is considered, the convexity of the curve will decrease, tending to look like the experimental curve obtained by Takagi et al. [1].

3.5 Incoming studies

In the incoming studies, we will first work on improving the primary model; the variation of the magnetic permeability with the flux density must be taken into account. On the other hand, the distribution of the volume forces through the thickness will be carried out.
Based on the state of art and on the primary generated calculations and simulations, we will next focus on the importance of the homogenized dynamic magnetic property Λ on the natural frequencies of vibration, and on the vibration response of the magnetic structure by incorporating the effect of magnetostrictive forces acting on the body of the structure and by taking into consideration the effect of Λ on the magnetostriction. The importance of this study is to determine in theoretical point of view an optimal presentation of the gradient and the periodicity of Λ that optimizes the vibrational characteristics of the studied system and help to select of the best laser treatment adequate for the optimization.
Once the optimizing procedure is well set and defined, we will focus on a more general study where μ_m and Λ are not constant and vary with the magnetization of the material; more powerful numerical programs shall be developed with specific numerical methods of resolution, either by programming on MATLAB or by the help of engineering software ALTAIR.
On the other hand, experimental studies will be performed where specimens with different laser treatments and different geometries are presented. Mechanical tests and measurements shall be obtained to analyse the vibrational response of the different specimens. Experimental study is a must to verify and validate theory and numerical simulations, and is a powerful tool

to help in the decision of optimal laser treatment.

Bibliography

[1] L. Wei, S. A. Kah, and H. Ruilong. Vibration analysis of a ferromagnetic plate subjected to an inclined magnetic field. *International Journal of Mechanical Sciences*, (49):440–446, 2007. 4, 10, 11, 35, 36

[2] T. Takagi, J. Tani, S. Matsuda, and A. Kawamura. Analysis and experiment of dynamic deflection of a thin plate with a coupling effect. *IEEE Transactions on Magnetics*, 28(2):1259–1262, 1992. 4, 35

[3] H. Gavrila and V. Ionita. Crystalline and amorphous soft magnetic materials and their applications - Status of art and challenges. *Journal of Optoelectronics and Advanced Materials*, 4(2):173–192, 2002. 7

[4] T. Waeckerle. Matériaux magnétiques doux cristallins - Tôles magnétiques fer-silicium non orientées (NO). *Techniques de l'ingénieur*, (D 2 132):1–15, 2015. 7

[5] P. Brissonneau. Les domaines magnétiques. *Revue de physique appliquée*, 9(5):783–792, 1974. 7, 12

[6] F. Alves and R. Barrué. Magnétisme microscopique à l'échelle des domaines magnétiques dans les matériaux ferromagnétiques doux. *J3eA*, 3(6), 2004. 8

[7] A. Arkkio. *Analysis of Induction Motors Based on the Numerical Solution of the Magnetic Field and Circuit Equations*. PhD thesis, Acta Polytechnica Scandinavica, 1987. 8

[8] J. Hallal. *Etudes des vibrations d'origine électromagnétique d'une machine électrique : conception optimisée et variabilité du comportement vibratoire*. PhD thesis, Laboratoire d'Electromécanique de Compiègne, UTC, 2014. 8, 15

[9] P. Pellerey. *Etude et Optimisation du Comportement Vibro-Acoustique des Machines Electriques, Application Au Domaine Automobile.* PhD thesis, Laboratoire d'Electromécanique de Compiègne, UTC, 2012. 8, 14, 15

[10] M. Rossi and Jean Le Besnerais. Vibration Reduction of Inductors Under Magnetostrictive and Maxwell Forces Excitation. *IEEE Transactions on Magnetics*, 51(12), 2015. 8, 10, 12, 13, 15

[11] O. Maloberti, A. Kedous Lebouc, G. Meunier, and V. Mazauric. Field diffusion-like representation and experimental identification of a dynamic magnetization property. *Journal of Magnetism and Magnetic Materials*, 304:507–509, 2006. 8, 19, 32

[12] O. Maloberti, G. Meunier, and A. Kedous Lebouc. On hysteresis of soft materials inside formulations: Delayed diffusion equations, fields coupling, and nonlinear properties. *IEEE Transactions on Magnetics*, 44(6):914–917, 2008. 9, 10, 19

[13] M. A. Raulet, B. Ducharne, J. P. Masson, and G. Bayada. The Magnetic Field Diffusion Equation Including Dynamic Hysteresis: A Linear Formulation of the Problem. *IEEE Transactions on Magnetics*, 40(2):872–875, 2004. 9

[14] A. Belahcen. *Magnetoelasticity, magnetic forces and magnetostriction in electrical machines*. PhD thesis, University of technology Helsinki, 2004. 9, 10, 12, 13, 15, 16

[15] J. R. Melcher. *Continuum Electromechanics*. 1981. 10

[16] H.M. Zhou, Y.H. Zhou, X.J. Zheng, and J. Wei. A General Magnetoelastic Coupling Theory of Deformable Magnetized Medium Including Magnetic Forces and Magnetostriction Effects. *Tech Science Press*, 12(3):237–249, 2009. 10, 12, 28, 29

[17] Y.H. Zhou and X. Zheng. A generalized variational principle and theoretical model for magnetoelastic interaction of ferromagnetic bodies. *Science in China*, 42(6), 1999. 10

[18] Y.H. Zhou and X. Zheng. A general expression of magnetic force for soft ferromagnetic plates in complex magnetic fields. *International Journal of Engineering Science*, 35(15):1405–1417, 1997. 10

[19] Y.H. Pao. *Electromagnetic Forces in Deformable Continua*. 1978. 10

[20] T.N. Golubeva, Yu. S. Korobkov, and V.E. Khromatov. Influence of a Longitudinal Magnetic Field on the Vibration Frequencies of Ferromagnetic Plates. *Russian Electrical Engineering*, 84(3):155–159, 2013. 10

[21] S.A. Mohajerani and M. Nikkhah Bahrami A. Mohammadzadeh. An Exact Solution for Vibration Analysis of Soft Ferromagnetic Rectangular Plates Under the Influence of Magnetic Field with Levy Type Boundary Conditions. *Journal of Solid Mechanics*, 9(1):186–197, 2017. 10

[22] U. Aydin, P. Rasilo, D. Singh, A. Lehikoinen, A. Belahcen, and A. Arkkio. Coupled Magneto-Mechanical Analysis of Iron Sheets Under Biaxial Stress. *IEEE Transactions on Magnetics*, 52(3), 2015. 12, 13

[23] H. Ebrahimi, Y. Gao, A. Kameari, H. Dozono, and K. Muramatsu. Coupled Magneto-Mechanical Analysis Considering Permeability Variation by Stress Due to Both Magnetostriction and Electromagnetism. *IEEE Transactions on Magnetics*, 49(5):1621–1624, 2013. 12

[24] Anouar Belahcen, Katarzyna Fonteyn, Antti Hannukainen, and Reijo Kouhia. On numerical modeling of coupled magnetoelastic problem. pages 203–206, 2008. 12, 13

[25] O. Mohammed, T. Calvert, and R. McConnell. A model for magnetostriction in coupled nonlinear finite element magneto-elastic problems in electrical machines. *IEEE*, pages 728–735, 1999. 12

[26] M. Besbes, Z. Ren, and A. Razek. Finite Element Analysis of Magneto-Mechanical Coupled Phenomena in Magnetostrictive Materials. *IEEE transactions on magnetics*, 32(3):1058–1061, 1996. 12

[27] M. Liu, O. Hubert, X. Mininger, F. Bouillault, and L. Bernard. Modélisation de la déformation de transformateurs de puissance par approche magnéto-mécanique. 2015. 12, 15

[28] F. Delince, A. Genon, J. M. Gillard, H. Hedia, and A. Nicolet W. Legros. Numerical computation of the magnetostriction effect in ferromagnetic materials. *Journal of Applied Physics*, 69(8):5794–5796, 1991. 12

[29] G. Kloos. Magnetostatic Maxwell stresses and magnetostriction. *Electrical Engineering*, (81):77–80, 1998. 12, 28

[30] Y. Zhang, H. Zhou, and Y. Zhou. Vibration Suppression of Cantilever Laminated Composite Plate with Nonlinear Giant Magnetostrictive Material Layers. *Acta Mechanica Solida Sinica*, 28(1):51–61, 2015. 12, 30

[31] K. A. Fonteyn. *Energy-based magneto-mechanical model for electrical steel sheets*. PhD thesis, Aalto University, School of Electronics, Communications and Automation, 2010. 13

[32] T. Hilgert, L. Vandevelde, and J. Melkebeek. Comparison of Magnetostriction Models for Use in Calculations of Vibrations in Magnetic Cores. *IEEE Transactions on Magnetics*, 44(6):874–877, 2008. 13, 14

[33] K. Delaere, R. Belmans, K. Hameyer, W. Heylen, and P. Sas. Coupling of magnetic and vibrational modal analysis using local forces. *Xth International Symposium on Theoretical Electrical Engineering ISTET'99, Magdeburg, Germany*, pages 417–422, 1999. 15

[34] L.b. Xin and Z.d. Hu. Free Vibration of Fixed Supported and Multilayered Magneto-Electro-Elastic Plates. 23-25 Nov. 2012. 15

[35] S. Patri, R. Gurusamy, P.A. Molian, and M. Govindaraju. Magnetic domain refinement of silicon-steel laminations by laser scribing. *Journal of materials science*, 31(7):1693–1702, 1996. 16

[36] T. Kajiwara and M. Enokizono. Effect of Laser Stress on Vector Magnetic Properties of Electrical Steel Sheets. *IEEE Transactions on Magnetics*, 50(4):2002404, 2014. 16, 17

[37] M. J. Johnson, R. Chen, and D. C. Jiles. Reducing Core Losses in Amorphous $Fe_{80}B_{12}Si_8$ Ribbons by Laser-Induced Domain Refinement. *IEEE Transactions on Magnetics*, 35(5):3865–3867, 1999. 16

[38] A. Zeleňáková, P. Kollár, M. Kuźmiński, M. Kollárová, Z. Vértesy, and W. Riehemann. Magnetic properties and domain structure investigation of laser treated finemet. *Journal of Magnetism and Magnetic Materials*, 254:152–154, 01 2003. 17, 18

[39] L. Lahn, C. Wang, A. Allwardt, T. Belgrand, and J. Blaszkowski. Impoved Transformer Noise Behavior by Optimized Laser Domain Refinement at ThyssenKrupp Electrical Steel. *IEEE Transactions on Magnetics*, 48(4):1453–1456, 2012. 17, 18

[40] O. Maloberti, V. Mazauric, G. Meunier, A. Kedous-Lebouc, P. Wendling, and B. Colin. A magnetic vector potential formulation to deal with dynamic induced losses within 2-d models. *IEEE Transactions on Magnetics*, 43(4):1205–1208, 2007. 19

[41] O. Geoffroy, A. Kedous-Lebouc, O. Maloberti, V. Mazauric, and G. Meunier. Vers une formulation de l'hystérésis Magnétique dynamique vectorielle. *Revue Internationale de Génie Electrique*, pages 515–529, 2006. 19

[42] André Preumont. *Vibration Control of Active Structures, An introduction, 3^{rd} Edition*. 26

[43] Z. Xian, Z. Pengcheng, Y. Qingxin, Z. Lihua, and Z. Xin. Numerical Estimation and Optimization of Vibration Noise due to Magnetostriction and Magnetic Forces for laminated Core Structure. Oct. 22-25, 2014. 28